To the Graduate Council:

I am submitting herewith a thesis written by Dax D. Jolly entitled "Rotating Machinery Misalignment Detection and Prediction Using Motor Power Spectrum". I have examined the final copy of this thesis for form and content and recommend that it be accepted in partial fulfillment of the requirements for the degree of Master of Science, with a major in Nuclear Engineering.

Dr. J. Wesley Hines, Major Professor

We have read this thesis and
recommend its acceptance:

Accepted for the Council:

Associate Vice Chancellor and
Dean of the Graduate School

Rotating Machinery Misalignment Detection and Prediction Using Motor Power Spectrum

A Thesis
Presented for the
Master of Science
Degree
The University of Tennessee, Knoxville

Dax D. Jolly
December 1998

DEDICATION

This Thesis is dedicated to my parents

Mr. Douglas G. Jolly

and

Mrs. Linda E. Jolly

who have supported me and given me
many invaluable educational opportunities
and experiences.

ACKNOWLEDGEMENTS

I would like to show my most sincere gratitude to Dr. J. Wesley Hines, of the University of Tennessee, Department of Nuclear Engineering, for his patience, guidance and assistance in performing the research presented in this thesis. I would also like to personally thank Mr. Don Casada of the ORNL Advanced Motor Testing Facility for answering all my questions and aiding immensely in the digitizing of the data off the digital tapes. I would also like to show my appreciation to my thesis committee members Dr. Robert E. Uhrig and Dr. Belle Upadhyaya. I would also like to thank Stephen Jesse and James Kuropatwinski from the University of Tennessee for performing the bulk of the data acquisition for this research.

I would like to show my utmost appreciation to Dr. H.L. Dodds, Department Head, University of Tennessee Department of Nuclear Engineering, for his encouragement to go on to graduate school and attain a Master's Degree, without his encouragement I'd have never gone to graduate school. I would also like to extend my appreciation to all of the faculty and staff of the Nuclear Engineering Department for answering questions when they were asked.

Also, I would like to give my heart felt gratitude to My parents and Grandparents who put up with my not visiting home as much as they would like while I worked on this thesis. I would also like to thank all my friends who put up with me and encouraged my pursuit.

The Maintenance and Reliability Center in conjunction with Duke Power funded this study in the use of advanced signal processing techniques to predict motor shaft misalignment through The University of Tennessee Department of Nuclear Engineering.

ABSTRACT

This thesis explores methods to detect and predict rotating machinery misalignment using power frequency spectrum data obtained at the Oak Ridge National Laboratory Advanced Motor Testing Facility for a 3-phase 50 horsepower electric motor connected to 150 horsepower dynamometer. Three types of flexible couplings were used to create data for controlled alignment condition observations. An elastomer type flexible coupling, a gear type flexible coupling, and a grid type flexible coupling are used to show that the alignment conditions of a motor system can be predicted from the input power frequency spectrum of an electric motor. Five types of alignment prediction methods are used and they all performed differently for the three types of couplings.

Some of the differences in the mapping procedures are due to the way that the method performs the mapping. The Multiple Linear Regression method simply fits a straight line between the inputs and outputs, so its prediction results will be highly dependent on changes in the motor system and the amount of linearity between the inputs and outputs. The Linear Correlation Coefficient (LCC) Neural Network uses an Artificial Neural Network (ANN) to train on the most highly correlated frequencies to the alignment condition to allow the non-linearities of those frequencies to be fitted. The Principal Component Analysis (PCA) method removes the collinearity from the data by mapping the data to an orthogonal space based on variability of the input data and then trains an ANN based on the important principal components (PC's). The Linear Partial Least Squares (LPLS) method maps the relationship linearly based on PC's that are determined in a supervised manner from the variability of the input and its relationship to the outputs. The Non-Linear Partial Least Squares (NLPLS) method uses an ANN to perform the mapping between the supervised PC's and the alignment condition.

The methods that performed the best for each of the couplings and the alignment conditions were as follows. The method that produced the smallest mean error for the elastomer type coupling to predict the parallel offset misalignment was the LCC Neural Network mapping with an average prediction error of 11.87 mils compared to 25.15 mils for a MLR. The best method for predicting the angular misalignment in the elastomer type coupling was the LPLS method with an average prediction error of 2.92 mils/inch compared to the MLR error of 2.99 mils/inch.

The method that produced the smallest mean error for the gear type coupling to predict the parallel offset misalignment was the PCA Neural Network mapping with an average prediction error of 2.71 mils compared to 7.34 mils for a MLR. The best method for predicting the angular misalignment in the gear type coupling was the LCC Neural Network method with an average prediction error of 0.13 mils/inch compared to the MLR error of 3.97 mils/inch.

The method that produced the smallest mean error for the grid type coupling to predict the parallel offset misalignment was the NLPLS mapping with an average prediction error of 1.59 mils compared to 3.04 mils for a MLR. The best method for predicting the angular misalignment in the grid type coupling was the LCC Neural Network method with an average prediction error of 0.31 mils/inch compared to the MLR error of 0.93 mils/inch.

An online system can be implemented by placing sensors on two of the three phase voltages and currents to determine the total input power to a system. The system would then have to be trained on the operating parameters for each system that it is placed on to be able to more accurately predict the alignment conditions. A combination of these methods could be used as the predictor function, but the most robust method would use the NLPLS techniques with more independent testing and training.

TABLE OF CONTENTS

CHAPTER	PAGE
1.0 INTRODUCTION	1
1.1 MOTIVATION FOR RESEARCH	1
1.2 APPLICATIONS OF RESEARCH	2
1.2.1 Nuclear Industry Applications	2
1.2.2 Other Applications	3
1.3 MAINTENANCE OVERVIEW	3
1.4 SHAFT ALIGNMENT	5
1.4.1 Measurement of Alignment	6
1.4.2 Precision Alignment	7
1.4.3 Benefits of Precision Alignment	7
1.5 PREVIOUS RESEARCH ON ALIGNMENT	8
1.5.1 Misalignment Prediction from Vibration	8
1.5.2 Motor Information from Electrical Signatures	9
1.5.3 Motor Efficiency from Alignment	9
2.0 BACKGROUND	11
2.1 OVERVIEW	11
2.2 FAST FOURIER TRANSFORM	12
2.3 DIMENSIONALITY REDUCTION	13
2.3.1 Linear Correlation Coefficients	14
2.3.2 Principal Component Analysis	14
2.4 MULTIPLE LINEAR REGRESSION	16
2.5 ARTIFICIAL NEURAL NETWORK	18
2.6 PARTIAL LEAST SQUARES	21
2.7 STATISTICAL EVALUATION	23
3.0 METHODOLOGY	24
3.1 PROCEDURE	24
3.2 EXPERIMENTAL SET-UP	26
3.2.1 Mechanical Set-Up of ORNL Test Site	26
3.2.2 Flexible Couplings Used During Testing	28
3.2.3 Data Collection Set-Up	30
3.3 DATA PREPARATION	31
3.3.1 Data Acquisition	31
3.3.2 Signal Processing	33
3.3.3 Frequency Resolution Reduction	36
3.3.4 Data Set Expansion	38
3.3.5 Creation of Training and Testing Sets	38
3.4 MULTIPLE LINEAR REGRESSION	39
3.5 LINEAR CORRELATION COEFFICIENT NEURAL NETWORK	40
3.6 PRINCIPAL COMPONENT NEURAL NETWORK	41
3.7 PARTIAL LEAST SQUARES LINEAR MODEL	42
3.8 PARTIAL LEAST SQUARES NON-LINEAR MODEL	42

CHAPTER PAGE

3.9 STATISTICAL EVALUATION 43

4.0 RESULTS 44

4.1 DATA ANALYSIS 44
4.1.1 Training/Testing Sets for Elastomer Type Coupling 44
4.1.2 Training/Testing Sets for Gear Type Coupling 45
4.1.3 Training/Testing Sets for Grid Type Coupling 46
4.2 RESULTS FROM MULTIPLE LINEAR REGRESSION MODEL 46
4.2.1 Results for Elastomer Type Coupling 47
4.2.2 Results for Gear Type Coupling 48
4.2.3 Results for Grid Type Coupling 49
4.3 RESULTS FROM LINEAR CORRELATION NEURAL NETWORK 50
4.3.1 Results for Elastomer Type Coupling 51
4.3.2 Results for Gear Type Coupling 54
4.3.3 Results for Grid Type Coupling 57
4.4 RESULTS FROM PRINCIPAL COMPONENT NEURAL NETWORK 59
4.4.1 Results for Elastomer Type Coupling 61
4.4.2 Results for Gear Type Coupling 62
4.4.3 Results for Grid Type Coupling 64
4.5 RESULTS FROM PARTIAL LEAST SQUARES LINEAR MODEL 66
4.5.1 Results for Elastomer Type Coupling 67
4.5.2 Results for Gear Type Coupling 71
4.5.3 Results for Grid Type Coupling 75
4.6 RESULTS FROM PARTIAL LEAST SQUARES NON-LINEAR MODEL 79
4.6.1 Results for Elastomer Type Coupling 80
4.6.2 Results for Gear Type Coupling 84
4.6.3 Results for Grid Type Coupling 88
4.7 STATISTICAL EVALUATION REMARKS 91

5.0 CONCLUSIONS 100

5.1 CONCLUSIONS FOR MISALIGNMENT PREDICTION 100
5.2 RECOMMENDATIONS FOR FUTURE WORK 102

LIST OF REFERENCES 104

APPENDICES 107

APPENDIX A: Graphs of the Results 108
APPENDIX B: Actual Test Alignment Conditions with the Predicted Ones 160
APPENDIX C: Non-Linear Partial Least Squares MATLAB Scripts 169

VITA 174

LIST OF FIGURES

Figure 1.1 The Types of Motor Shaft Alignment 5

Figure 2.1 Schematic of a Feed Forward Artificial Neural Network 18
Figure 2.1 Schematic of Artificial Neuron 20

Figure 3.1 Procedure used to determine the best method for predicting motor shaft misalignment from power frequency spectrum. 25
Figure 3.2 Motor and Dynamometer Setup at ORNL 27
Figure 3.3 Plan View of Aluminum Motor Support 27
Figure 3.4 Rexnord Elastomer type coupling 29
Figure 3.5 Dodge Grid Type Coupling 29
Figure 3.6 Zurn Gear Type Coupling 30
Figure 3.7 Typical Three-Phase Currents 33
Figure 3.8 Typical Three-Phase Voltages 34
Figure 3.9 Typical Total Three-Phase Power 35
Figure 3.10 Typical FFT for an Alignment Condition 36
Figure 3.11 Differences in Frequency Spectrum with Alignment condition 37
Figure 3.12 How Frequency Spectrum Changes with Alignment 40

Figure 4.1 MLR Angular Prediction for Elastomer type coupling 48
Figure 4.2 MLR Angular Prediction for Gear type coupling 49
Figure 4.3 MLR Angular Prediction for Grid type coupling 50
Figure 4.4 LCC ANN Angular Prediction for Elastomer type coupling 54
Figure 4.5 LCC ANN Angular Prediction for Gear type coupling 57
Figure 4.6 LCC ANN Angular Prediction for Grid type coupling 61
Figure 4.7 Information Contained in Each PC for Elastomer type coupling 62
Figure 4.8 PCA ANN Angular Prediction for Elastomer type coupling 63
Figure 4.9 Information Contained in Each PC for Gear type coupling 63
Figure 4.10 PCA ANN Angular Prediction for Gear type coupling 65
Figure 4.11 Information Contained in Each PC for Grid type coupling 65
Figure 4.12 PCA ANN Joint Prediction for Grid type coupling 66
Figure 4.13 Information Contained in PLS factors for Elastomer type coupling 67
Figure 4.14 Parallel errors for PLS factors for Elastomer type coupling 68
Figure 4.15 Angular errors for PLS factors for Elastomer type coupling 69
Figure 4.16 Joint errors for PLS factors for Elastomer type coupling 70
Figure 4.17 LPLS Angular Prediction for Elastomer type coupling 71
Figure 4.18 Information Contained in PLS factors for Gear type coupling 72
Figure 4.19 Parallel errors for PLS factors for Gear type coupling 72
Figure 4.20 Angular errors for PLS factors for Gear type coupling 73
Figure 4.21 Joint errors for PLS factors for Gear type coupling 74
Figure 4.22 LPLS Angular Prediction for Gear type coupling 75
Figure 4.23 Information Contained in PLS factors for Grid type coupling 76
Figure 4.24 Parallel errors for PLS factors for Grid type coupling 77
Figure 4.25 Angular errors for PLS factors for Grid type coupling 78
Figure 4.26 Joint errors for PLS factors for Grid type coupling 79
Figure 4.27 LPLS Angular Prediction for Grid type coupling 80
Figure 4.28 Prediction Errors for Different NLPLS Network Architectures 81
Figure 4.29 Parallel errors for NLPLS factors for Elastomer type coupling 82

Figure 4.30 Angular errors for NLPLS factors for Elastomer type coupling 83
Figure 4.31 Joint errors for NLPLS factors for Elastomer type coupling 84
Figure 4.32 NLPLS Angular Prediction for Elastomer type coupling 85
Figure 4.33 Parallel errors for NLPLS factors for Gear type coupling 86
Figure 4.34 Angular errors for NLPLS factors for Gear type coupling 86
Figure 4.35 Joint errors for NLPLS factors for Gear type coupling 87
Figure 4.36 NLPLS Angular Prediction for Gear type coupling 88
Figure 4.37 Parallel errors for NLPLS factors for Grid type coupling 89
Figure 4.38 Angular errors for NLPLS factors for Grid type coupling 90
Figure 4.39 Joint errors for NLPLS factors for Grid type coupling 91
Figure 4.40 NLPLS Angular Prediction for Grid type coupling 92

LIST OF TABLES

Table 3.1 Motor and Dynamometer at ORNL 26
Table 3.2 Couplings Used with the Manufacturer's Tolerances 28
Table 3.3 Tape Events Corresponding to Experimental Alignment Conditions 32

Table 4.1 Alignment Conditions for Rexnord Elastomer type coupling 45
Table 4.2 Alignment Conditions for Zurn Gear type coupling 46
Table 4.3 Alignment Conditions for Dodge Grid type coupling 47
Table 4.4 Parallel Frequencies for Elastomer type coupling 52
Table 4.5 Angular Frequencies for Elastomer type coupling 53
Table 4.6 Parallel Frequencies for Gear type coupling 55
Table 4.7 Angular Frequencies for Gear type coupling 56
Table 4.8 Parallel Frequencies for Grid type coupling 58
Table 4.9 Angular Frequencies for Grid type coupling 60
Table 4.10 Training and Testing Errors for Elastomer Type Coupling 93
Table 4.11 Training and Testing Errors for Gear Type Coupling 94
Table 4.12 Training and Testing Errors for Grid Type Coupling 95
Table 4.13 Parallel Offset Misalignment Prediction Errors for the Elastomer Type Coupling 96
Table 4.14 Angular Offset Misalignment Prediction Errors for the Elastomer Type Coupling 97
Table 4.15 Parallel Offset Misalignment Prediction Errors for the Gear Type Coupling 97
Table 4.16 Angular Offset Misalignment Prediction Errors for the Gear Type Coupling 98
Table 4.17 Parallel Offset Misalignment Prediction Errors for the Grid Type Coupling 99
Table 4.18 Angular Offset Misalignment Prediction Errors for the Grid Type Coupling 99

1.0 INTRODUCTION

This section introduces the motivation for this research along with its applications. It also discusses a basic maintenance overview to give an understanding of how this research would fit into a Maintenance and Reliability Program. It then gives some details on motor shaft alignment techniques and benefits and ends with some of the previous research performed in this area.

1.1 MOTIVATION FOR RESEARCH

The objective of this research is to be able to detect motor shaft misalignment and predict motor shaft alignment from the motor's power spectrum. Electric motors generate a force that turns the motor shaft. Other mechanisms harness the power of the motor by attaching another shaft to the motor shaft through a coupling. Deviations in the motor shaft system cause immediate changes to the input power to the motor. A system based on power changes is more sensitive than one based on vibration changes because the information is immediately transferred instead of having to be passed through the different structures of the motor.

There have been previous studies to determine the relationship between machine misalignment with machine vibration [Casada '97, Hines '97a, Kuropatwinski '97, Nower '96, Piotrowski '95]. These studies showed that this relationship is non-linear and therefore difficult to analyze. Results from a system using this relationship in a neural network [Kuropatwinski '97] to detect and predict the misalignment of a machine were mixed. This study showed more rigid couplings yielded better results than more flexible ones.

There have also been studies to determine the amount of excess power consumed because of machine misalignment as compared to a perfectly aligned machine [Daintith '96, Hines '97a, Ludeca '94, Weiss '91, Xu '93]. The earlier studies proposed that there were huge savings in power consumption to be gained through proper alignment. More recent studies indicate that

there is not a significant change in efficiency related to motor shaft misalignment when the couplings are operated within the manufacturer's recommended alignment range. These studies did indicate that there is a measurable change in the input power frequency spectrum for different alignment conditions.

This thesis will use several advanced signal processing techniques including multiple linear regression, linear correlation analysis, principal component analysis, and partial least squares regression to determine if the motor power spectrum frequency can be used to detect and predict the misalignment of rotating machinery. Each type of machine has a different response to forces applied to them. The type of machine, the structure of the machine, the operating speed of the machine, and many other factors influence these forces. A very stiff mounting surface, for instance, could cause a binding with shaft misalignment causing more power to be utilized. Just the misalignment itself could cause fluctuations in power. The amount of vibration in a system can be determined through modal analysis techniques. The machine itself can cause power fluctuations in the power spectrum. Just changing the operating speed itself can change the total power to a motor. The desired application is a system using these techniques in an online system to give real time alignment data to an operator so that corrections could be made before any damage to the motor system was incurred.

1.2 APPLICATIONS OF RESEARCH

This research has many potential applications in today's industry. Some of the more profitable are in the Power Industry including the Nuclear Power area. There are also many applications not associated with power generation such as anywhere rotating machinery is used such as in a Chemical Process Plant. Some of these industries use many thousands of rotating machines to perform their everyday processes.

1.2.1 Nuclear Industry Applications

All nuclear power plants use electric motor-driven rotating equipment. These motors are used both in the primary reactor loop portion of the plant and in the secondary steam generation loop of the power plant. These motors operate pumps and other mechanical systems that are essential to the daily operations of the power plant. Some of these systems are also used to

maintain fail safe safety devices that operate in the event of a plant malfunction to ensure the safety of the personnel at the plant. Misalignment in these motor systems creates an unnecessary source of wear on the seals, bearings, gears, and other moving parts and stationary parts such as the motor housings in the system. This excess wear can cause the systems to breakdown or quit operating prematurely, in turn producing repair or replacement costs and downtime from the production of electricity. All of these extra costs help to increase the cost of electricity to the consumer.

By creating an on-line system to detect motor shaft misalignment and predict motor shaft alignment in real time, the maintenance and correction of problems could be performed before the condition damaged the system. This would allow the maintenance to be performed at scheduled shutdowns rather than creating an unscheduled one and causing lost power revenues. The previous misalignment detection designs based on vibration spectra are highly dependent on the rigidity of the motor system through which the vibrations must be transferred. The goal of this research is to create a system that is more robust to reduce these dependencies.

1.2.2 Other Applications

Today's competitive industrial climate has a major focus to reduce operating costs and improve product quality. This has created a need for more efficient and cost effective maintenance procedures. Current estimates place maintenance expenses as much as fourteen percent or more of a company's total operating cost [Hines '98, Pardue '96, Upadhyaya '98]. One of the largest portions of this maintenance expense stems from the repair and replacement of machines. This could be reduced through the use of an on-line system to detect and predict motor shaft misalignment along with other types of proactive maintenance programs. The proper maintenance regime could possibly extend the life of a machine indefinitely.

1.3 Maintenance Overview

Industrial organizations throughout the world are re-engineering their maintenance activities to remain competitive in production, reliability, safety, and cost optimization [Upadhyaya '98]. Currently, industrial maintenance costs between four and fifteen percent of the total production costs of an organization. It is estimated that over five hundred billion dollars per

year are spent by United States companies on maintenance activities. Savings of over one hundred billion dollars per year could be realized through the implementation of advanced maintenance and reliability technologies and practices.

There are four types or classes of maintenance in widespread use today. These are reactive maintenance, preventive maintenance, predictive maintenance, and proactive maintenance [Hines '97a, Upadhyaya '98]. One of the most inefficient methods is reactive maintenance. This method involves fixing or replacing the machine only after it has broken. This method requires a company to have a large supply of replacement parts and machines available to minimize the amount of downtime associated with a failure. As one can see, this would be an expensive way to operate.

Preventive maintenance use became widespread with computer technology advancements in the late 1970's. It allowed companies to schedule maintenance activities on a predetermined interval based on type and time of maintenance problems and the life expectancy of a given component in a plant and keep track of all repairs made in a system. Preventive maintenance reduced maintenance costs an average of thirty percent over a reactive maintenance system, making it the most widely used type of maintenance [Emmert '96, Pardue '96]. An inefficiency to this scheme is that sometimes repairs or replacements are performed before they are necessary.

Predictive maintenance techniques monitor a machine's operational variables to determine when to make repairs. This process reduces the amount of over-maintaining caused by preventive maintenance. Some of the variables that can be monitored are machine vibration, temperature, lubricants, motor current, motor flux, and motor power among others. This type of maintenance procedure allows a plant to monitor and schedule maintenance tasks in an efficient manner.

Proactive maintenance philosophies try to find the causes of machine failures and remove the root causes of failures from the machines. Causes of machine failure can be many things such as load imbalance or even motor shaft misalignment. If the root causes can be eliminated the life of the machine can be extended.

An on-line detection and prediction system is part of both predictive and proactive maintenance. The system would monitor the machine in an attempt to mitigate the cause of failure of the equipment. The majority of companies concerned with lowering maintenance costs are pushing towards a proactive maintenance program.

1.4 SHAFT ALIGNMENT

Electric motors generate a force that turns the motor shaft. Other mechanisms harness the power of the motor by attaching another shaft to the motor shaft through a coupling. Shaft misalignment is the deviation of relative shaft position from its collinear axis of rotation at the points of power transmission when equipment is operating normally [Hines '97, Piotrowski '95]. There are two components to shaft misalignment: parallel offset misalignment and angular misalignment. Figure 1.1 shows these two types of alignment conditions for a typical motor system. Parallel offset misalignment is where the centerlines of the two shafts are parallel, but the axis is offset to a certain degree. Angular misalignment is where the centerlines of the two shafts intersect at the power transfer point, but they are not parallel to one another. Perfect alignment of a system is desired, but usually there is a combination of both parallel offset misalignment and angular misalignment evident in a system. Misalignment causes unnecessary wear to a system creating maintenance expenses that could be avoided.

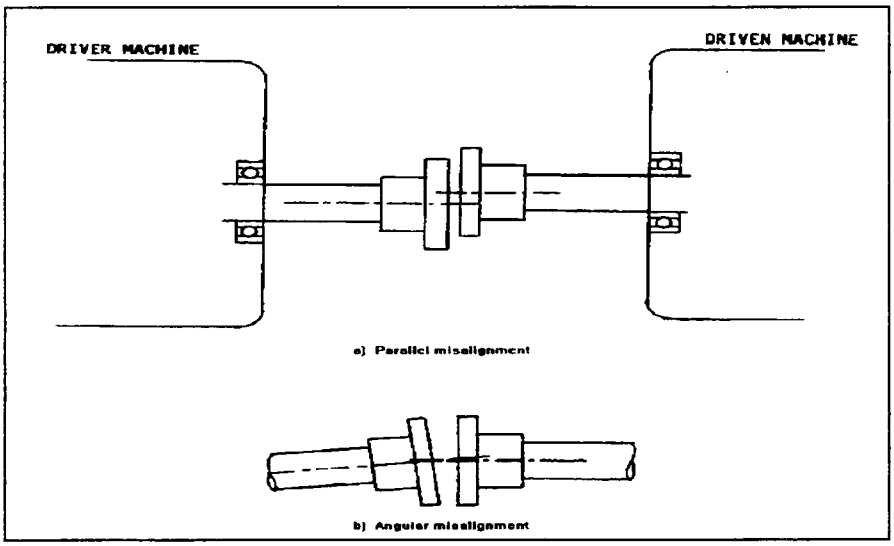


Figure 1.1 The types of motor shaft alignment. a) Parallel offset misalignment and b) Angular misalignment.

1.4.1 Measurement of Alignment

Parallel offset misalignment is commonly measured in units of mils. One mil is defined as one thousandth of an inch. Angular misalignment is usually measured in mils per inch [Kuropatwinski '97, Piotrowski '95, Wowk '91]. Motor shaft misalignment is usually classified into one of four grades: unsafe, poor, acceptable, and excellent [CSI, Hines '97a, Ludeca, Piotrowski '95]. The tolerances used for grading a misalignment condition vary with each coupling and depend on the machine's operating conditions.

An unsafe grade usually means that the alignment is outside the manufacturer's design specification's allowance. A poor grade typically means that the alignment is within the manufacturer's allowances, but outside the machine's recommended limits. An acceptable grade usually means that the alignment is both within the manufacturer's design specification's allowances and within the machine's recommended limits. An excellent grade typically means that the alignment is very near perfectly aligned. These grades get more restrictive the faster the motor shaft is turning.

There are several methods to check and set the alignment of a motor system employed today. The simplest method just uses a tape measure and a straight edge. This method is typically used as a quick field check for unsafe or poor grade alignment. Another alignment-measuring tool is the dial indicator. The dial indicator is more accurate than the tape measure and straight edge. They are widely used because they are easy to operate and inexpensive. Dial indicators measure misalignment by one of two methods: the face and rim method or the reverse indicator method. The face and rim method places perpendicular dial gauges to ensure that the face of one shaft is perpendicular to the rim of the shaft and parallel to the other shaft and determines angular misalignment. The reverse indicator method places one gauge on each shaft. Each gauge measures the difference from the other shaft. The results are used to determine that amount of parallel offset misalignment.

The more precise alignment-measuring tool is the laser alignment system. A laser alignment system utilizes a laser emitter/receiver head and a reflector head. The emitter sends a signal to the reflector, which reflects it back to the receiver. The receiver is connected to a computer that gives accurate alignment measurements as well as directions for aligning the system [CSI, Ludeca].

The more accurately a system is aligned the more the alignment costs. The tradeoff is better operating equipment with less wear weighed against the cost of aligning them.

1.4.2 Precision Alignment

Precision alignment requires sophisticated equipment and personnel with extensive training. The alignment equipment can cost as much as twenty thousand dollars or more. In plants where there are many thousands of rotating machines, the labor cost can be very large to align the equipment. Another problem is how the plant environment effects shaft alignment. Thermal growth due to operating conditions, machine wear, and even building structure changes can misalign a system [Hines '97a, Upadhyaya '98].

Attaining this precision alignment itself can be a difficult and time-consuming task. The machinery could be in hazardous or radioactive environments requiring special protection to the technician performing the alignment. The machinery itself is usually heavy and may be bound by obstructions. The precision alignment procedure could require many hours work. During the alignment process, the motor system is in operable. Again, the more precise the alignment, the more time necessary to complete it therefore causing the trade-off to be used.

1.4.3 Benefits of Precision Alignment

The main benefit to precision alignment is the reduced load on the machine's mechanical components [Hines '97a, Piotrowski '95]. These reduced loads increase the machine's life expectancy by creating less wear on the system's components. If the machines last longer then they will not have to be replaced as often. This could result in large savings to the companies employing these techniques.

Another benefit to precision alignment in some cases is reduced power consumption. However, the major savings in power consumption only appear in the difference between poor and unsafe graded alignment versus excellent alignment. The difference between acceptable and excellent grade is essentially not measurable. Therefore, efficiency is not a major benefit to precision alignment.

This extended life expectancy will result in fewer breakdowns and therefore less downtime for maintenance activities. Once the investment to precision align a system has been

undertaken, it would be desirable to know when the system is misaligned so that it could be realigned before it damaged the machine. An online system could facilitate this knowledge to the maintenance team.

1.5 PREVIOUS RESEARCH ON ALIGNMENT

There has been considerable research performed on alignment. Some of this research focused on using the vibration spectra from the alignment conditions to train a neural network to predict the misalignment conditions of a motor shaft system. Other research focused on motor efficiency versus alignment.

1.5.1 Misalignment Prediction from Vibration

Research performed at the University of Tennessee, Department of Nuclear Engineering in 1997 showed that under certain conditions, vibration spectra could be used to predict the misalignment conditions for a motor system [Hines '97a, Kuropatwinski '97]. The findings of this research showed that an artificial neural network could be trained on certain vibration data from some types of flexible couplings to predict motor misalignment. The data was first run through a principal component analysis to reduce the dimensionality of the data without losing any of the overall significance of the data.

The conclusions of this research showed that the results of the PCA/ANN methodology were highly dependent on the motor system setup conditions such as rigidity of the motor mounts. The type of couplings used to connect the motor to its load was also important in determining the predictability of the system. Typically, the more rigid the coupling connection, the better the network was able to predict the alignment conditions.

Research performed by Turvac Inc. showed that there are several considerations when using vibration analysis for misalignment detection [Piotrowski '97]. These considerations include that there is not a linear relationship between vibration amplitude and the amount of misalignment, the amount of vibration can increase after re-aligning, and that the majority of information is at running speeds.

Other research performed by Computational Systems Incorporated (CSI) showed which operating frequencies showed the most information about misalignment [Nower '94]. These

frequencies showed that the best indicators for misalignment are the one and two times operating speed frequencies. It also showed that the information content varied with different couplings.

1.5.2 Motor Information from Electrical Signatures

Advanced motor-current demodulation techniques have also been used to monitor three-phase gas compressors [Smith '91]. Results from monitoring several variables such as flow characteristics and surges were very similar to those obtained through vibration-sensing techniques. These techniques were also successfully applied to other machinery such as refrigeration compressors, brine pumps, vacuum pumps, fans, and other electric motors to various mechanical and electrical faults. These studies showed that there is considerable information available in the electrical signatures of machinery.

These techniques can be applied with vibration-sensing techniques to form a more robust method of predicting misalignment. This more robust model would then be less dependent on the motor system set-ups and the other factors that are evident in the vibration type systems. The signals are immediately transferred to the input powers without having to be modulated through the motor structure.

Other work has been performed by the Oak Ridge National Laboratory Advanced Motor Testing Facility to compare the use of vibration analysis with the use of electrical signatures for determining the misalignment of a suction pump [Casada '98]. This work showed that the electrical signature information was more sensitive for the alignment detection than the vibration analysis information. It was able to show changes even when the vibration analysis had none.

1.5.3 Motor Efficiency from Alignment

The majority of the current literature related to shaft alignment versus motor efficiency claims that as the misalignment worsens, the efficiency of the motor goes down [Daintith '96, Ludeca '94, Weiss '91]. There are several articles available on research performed by different sources discussing the power savings that resulted from improved alignment. Most of these tests simply compared input power consumption without comparing the amount of power transferred to the system. More recent research at the University of Tennessee, Maintenance Reliability

Center in a controlled environment has cast doubt on some of the previous research's findings [Hines '97a].

In general, the earlier research supported that the proper alignment of rotating machinery improved the systems efficiency. The results of these reports varied greatly as to how much power savings were actually found by the improved alignment. The methods used to calculate these savings did not take into account output power or other critical motor transients. Much of the power savings were determined from motor current instead of current and voltage. In this research the output power was simply assumed to be constant.

The University of Tennessee research performed a more controlled experiment to determine the relationship between motor shaft alignment and motor efficiency. This research measured the three phase voltages and currents and used them to calculate the total motor input power. The motor torque and speed was also measured to calculate the motor output power. These input and output powers were compared to determine the motor efficiency at the misalignment conditions. The conclusions from this research showed that precision alignment produced no significant power savings when compared to operating the tested flexible couplings within their normal manufacturer specified alignment limitations. This research did show that some changes in input power were evident with alignment changes hence the output power must have changed for the efficiency to remain nearly constant.

2.0 BACKGROUND

This section explains the objective of this research and gives an overview of how the objectives will be reached. It then explains the techniques used to accomplish the goals and the methods of comparing the performance of each of the methods.

2.1 OVERVIEW

The purpose of this research is to develop a system to predict electric motor shaft alignment conditions and detect when the motor is misaligned based on the motor's power frequency spectrum. A three-phase electric motor has three currents and three voltages as inputs. These voltages and currents can be directly measured in real time with equipment readily available to maintenance personnel and technicians from companies such as Omega [Omega].

At the Oak Ridge National Laboratory Advanced Motor Test Facility, a floating ground system is used to connect the motor inputs through a control room to the motors. This specific motor set-up allows the instantaneous three phase currents to sum to zero, as well as the instantaneous three phase voltages. By using Ohm's law, the three-phase currents can be multiplied by the corresponding voltages to calculate each phase's power. The three separate three phase powers can then be summed together to get the total input power to the motor. The time domain power can then be transformed to the frequency domain power spectrum through a discrete Fourier transform. Once the power data is in the frequency domain many techniques can be used to map it to the misalignment conditions.

These techniques include Multiple Linear Regression (MLR), Artificial Neural Networks (ANN), and Partial Least Squares (PLS) techniques. MLR simply fits a straight line to map the frequency spectrum to the alignment conditions. ANN's allow nonlinear relationships to be learned between the frequencies and the alignment conditions. PLS techniques create a more

robust generalization between frequency and alignment techniques than MLR methods for limited collinear data [Geladi '85]. There are also several other techniques to perform this mapping, but this research focuses on these methods.

2.2 FAST FOURIER TRANSFORM

The Discrete Fourier Transform (DFT), developed by Gauss in the early nineteenth century, is the primary means for determining the frequency content of a time waveform [Casada '98, Heideman '84, Upadhyaya '98]. Time domain data is usually recorded as the amplitude of a signal versus the sample time of the wave. This data can also be visualized in the frequency domain as an amplitude corresponding to a frequency of the signal. Time waveforms are usually continuous periodic analog signals. The repetitive nature of the waveform is what allows the frequency components to be visualized.

To convert a continuous analog signal to a digital form, it is necessary to sample the analog waveform at discrete points. To acquire a waveform properly, the discrete points must be chosen to sample the continuous signal fast enough to maintain its highest frequency components. According to the Nyquist Sampling Theorem, the sampling frequency must be at least twice as large as the highest Fourier component frequency of the input analog signal to ensure the frequencies are characterized properly [Chapra '88, Simpson '87].

The DFT algorithm is an extremely burdensome process. For a signal with N discrete points in the time sample, the algorithm to transform to the frequency domain would require N^2 complex mathematical operations. This is why the Fast Fourier Transform (FFT) algorithm was developed. The FFT computes the DFT in an economical fashion by using the results from previous computations and the symmetry of the function to compute the transform much faster.

The Fourier analysis theorem states that for any waveform defined from t = 0 to T, where T is the minimum time in which the waveform repeats itself, the waveform can be expressed as a sum of sine and cosine waves [Chapra '88] by the following equations:

$$x(w,t) = \frac{a_o}{2} + \sum_{n=1}^{\infty} a_n \cos(nwt) + \sum_{m=1}^{\infty} b_m \sin(mwt)$$

with the coefficients *a* and *b* defined as

$$a_n = \frac{2}{T}\int_{-T/2}^{T/2} x(t)\cos(n\omega \cdot t)dt$$

$$b_m = \frac{2}{T}\int_{-T/2}^{T/2} x(t)\sin(m\omega \cdot t)dt\,.$$

The finite Fourier transforms of the waveform *x(w,t)* is given by

$$X(f,T) = \int_{0}^{T} x(t)\exp(-i2\pi \cdot f \cdot t)dt$$

and the power spectral density of the Fourier transform *X(f,t)* is defined as

$$S_{xx} = \frac{1}{T}|X(f,T)|^2$$

where the right hand side is divided by the signal period for scaling purposes. As T becomes large, the power spectral density approximation S_{xx} approaches their true values.

An additional concern in digitizing a waveform is signal aliasing [Casada '98,Chapra '88, Upadhyaya '98]. Signal aliasing arises when frequencies of the original waveform exceed half of the sampling frequency, $f_s/2$. The resulting frequency domain signatures will have errors due to frequency overlapping (folding) of these higher frequencies upon the frequencies up to $f_s/2$. This maximum frequency is called the Nyquist folding frequency. To correct for this properly, a low-pass filter with a well-chosen cut-off frequency should be used to attenuate the frequencies above the Nyquist folding frequency or the sampling frequency must be fast enough to compensate for the highest frequency above which there is no power information.

2.3 DIMENSIONALITY REDUCTION

After the FFT's are constructed, the amount of data must be reduced to a manageable amount for the mapping techniques to properly work. This is accomplished using advanced signal processing data extraction techniques. There are two major types of data extraction that are widely used. These are linear correlation coefficient analysis and Principal Component Analysis (PCA). Linear correlation analysis determines how variables change with respect to other variables. PCA is a method used to reduce the dimensionality of data without losing the information contained in the data.

2.3.1 Linear Correlation Coefficients

Linear correlation analysis is one way to extract useful predictors from a multi-variable data set. It can be used to relate each variable in a matrix with every other variable in the matrix and form a correlation coefficient matrix. In other words, it assesses the linear dependence between the variables [Agnew '89]. The coefficients range from negative one to positive one. A positive one correlation coefficient would correspond to the most correlation and would mean that a change of the first value would cause a similar change to the second value. A zero correlation coefficient would correspond to the least correlation showing that a change in the first value would cause no change in the second value. A negative one correlation coefficient means the two values are oppositely correlated, or that a change in the first value would cause the opposite change to occur for the second value.

If the alignment conditions are appended to the end of the frequency data, then the values of the last two columns of a correlation coefficient matrix represent how each frequency element varies with the alignment condition. The less correlated frequencies are then removed from the matrix to reduce the number of frequencies used for the mapping.

2.3.2 Principal Component Analysis

Principal Component Analysis (PCA) is a method used to reduce the dimensionality of an input space without losing a significant amount of information and to remove the collinearity problems from a data set. A lower dimensional input space will usually reduce the time necessary to train a neural network and improve the mapping's generalization [Bishop '95, Joliffe '86, Kuropatwinski '97]. The objective of PCA is to reduce the dimensionality of the data while preserving as much relevant information as possible. PCA can also be thought of as a method to extract the features of the data while removing the collinearity of it.

PCA involves linearly transforming the input space into a space with smaller dimensionality [Bishop '95]. Suppose there are N samples of D-dimensional data forming a matrix NxD. We want to transform these into a dimension M where $M < D$. The input matrix of data will be signified as X and is NxD dimensions while the transformed data is labeled Z and is NxM dimensions. The transform matrix is U, where

$$Z = X \bullet U$$

X can be represented as a linear combination of D orthonormal vectors that make up the matrix U. Each new feature Z_i is a linear combination of the data X and the transformation matrix U:

$$Z_i = X \bullet U_i$$

The feature vectors Z can be transformed back into the original data X without a loss of information as long as the number of features is equal to the dimension of the original space. If D<M is retained, then usually some information lost. The objective is to choose as small a D as possible that does not loose much information. The word information is used to mean the variability in the data. Many times there is variability in the data from random noise sources, but this variability is usually of no concern and by transforming to a lower dimensionality space this noise can sometimes be removed from the data. Important features Z_i and unimportant features B_i are used to transform the Principal Components (PC) space data back into the original space:

$$X = \sum_{i=1}^{M} Z_i U_i^T + \sum_{i=M+1}^{D} B_i U_i^T$$

In the above equation, there are M features that are important and D-M-1 non-important features. It is desired to select the transform so that the first summation contains the useful information and the second summation contains noise [Joliffe '86].

The vectors U_i form the basis in the new PC space. These basis vectors are chosen to minimize the sum of squared errors between the estimate of the data and the original data set and be orthogonal so that PC_1 contains the maximum variance of data:

$$error = X - \sum_{i=1}^{M} Z_i U_i^T$$

It can be shown that the optimal choice for basis vectors satisfies the following relationship [Bishop '95]:

$$\sum U_i = \lambda_i U_i$$

This is recognized as an eigenvalue problem where λ_i and U_i are the eigenvalues and eigenvectors of the covariance matrix. The eigenvectors U_i are termed the principal components. PCA can be performed using Singular Value Decomposition (SVD) [Joliffe '86]. SVD is a method that decomposes the X matrix into a diagonal matrix L of the same dimension as X and a unitary square matrix U, with dimensions number of columns of X, of principle components and

an orthonormal square matrix A, with dimensions number of columns of X of right singular values where:

$$X = A * L * U^T$$

SVD requires the data to be mean centered and contain more samples than variables in the data to allow more information to be explained in the data.

To determine how many of the principal components are important, the diagonal values of L are examined. These values are then squared to convert the singular values to the amount of variance of the data contained in the matrix X. These values can then be associated with the percentage of information that each principal component contains by dividing them by the total variance of the data matrix X. These percentages are analyzed to determine how many of the principal components are necessary for the approximation (M) by finding the break point where the PC's don't contain any useful information.

Another method of determining which PCs to keep is by using them all to form the principal component score matrix (Z) and then determining which ones are linearly correlated with the misalignment conditions. Then by removing the PCs that are not correlated, only the useful ones are retained in Z. Once the number of necessary components is determined and the principal component scores are calculated, the transformation matrix U is retained so that subsequent data can be compressed. These Z_i can be used to regress the response variable. This is called Principle Component Regression (PCR) and has two advantages over MLR of decorrelated collinearity and only the important PC's are retained instead of all the data.

2.4 MULTIPLE LINEAR REGRESSION

Multiple Linear Regression techniques map a group of predictor variables x to a response variable y in the form of the equation of a line [Agnew '89, Hines '98]. The linear regression model is of the form:

$$y = Xw + \varepsilon$$

where: **y** is a matrix of conditions,

X is a matrix of values corresponding to **y**,

w is the weight matrix that linearly combines **x** to **y**, and

ε is a matrix of the prediction errors.

In other words **w** predicts **y** from **x** through the following:

$$y = w_1x_1 + w_2x_2 + w_3x_3 + \ldots + w_px_p + \varepsilon$$

This equation is solved by a least-squares method to minimize the sum-squared-error (SSE) to form the most optimal weight matrix. If the **X** matrix were invertable, it would be easy to solve for **w**:

$$\mathbf{w}=\mathbf{X}^{-1}*\mathbf{y}$$

For **x** to be invertable, it would have to be a square matrix with full rank that is non-singular [Agnew '89]. This is rarely the case for real data. When **x** is not invertable, a pseudoinverse technique can be used to solve for **w**.

This is the ordinary least-squares solution to solve for **w**:

$$\mathbf{W}=(\mathbf{X}^{T}*\mathbf{X})^{-1}*\mathbf{X}^{T}*\mathbf{y}$$

The pseudoinverse will minimize the error between the predicted **y** and the target **y** [Agnew '89]. This method involves inverting $(\mathbf{X}^{T}*\mathbf{X})$ which causes numerical instabilities when the columns of **X** are dependent or only marginally independent. This creates cases where $(\mathbf{X}^{T}*\mathbf{X})$ should not be inverted. If the columns of X are highly correlated or the number of samples is less than the number of variables, singularities will exist in that data that will prevent the pseudoinverse from calculating the optimal weight matrix. To get around this, SVD techniques can be used to better condition the matrix through a method known as Truncated SVD [Hansen '87].

Some of the instabilities are caused by collinearity between the observations in a data set. This collinearity is due to the fact that many of the observations have the same principal frequencies and therefore when one changes the others are likely to have a similar change at the same areas. The collinearity creates instabilities in the data because of the large difference between the largest and smallest singular values or the ill-conditioning of the matrix. By setting a tolerance for the smallest singular value to be used in the pseudoinverse, the values smaller than the tolerance can be removed thus improving the stability of the data through TSVD.

Since the linear regression model fits a straight line to the mapping through the origin, the data must be appended with a column of ones to allow for the y intercept in the linear model. The SSE is greatly reduced with this technique because the y-intercept is no longer anchored at the origin. Another method of allowing for the y-intercept is to mean-center the data and the misalignment conditions.

After the optimal weight matrix is determined, it can be used to test how well the MLR model predicts the data that it was trained on. The y predicted value is determined by multiplying

the frequency matrix by the weight matrix. Then the predicted misalignment conditions are compared to the actual misalignment conditions. This is also performed for test data by using the same weight matrix.

2.5 ARTIFICIAL NEURAL NETWORK

The use of an ANN was chosen because of its ability to learn patterns such as frequencies and classify them into categories such as alignment conditions. A neural network performs a mapping of input information to a corresponding output. A multi-layer feed-forward artificial neural network is divided into three layers, the input layer, the hidden layer, and the output layer. A graphical representation is shown in Figure 2.1.

A neural network with this type of architecture is known as a universal function approximator [Haykin '94, Kosko '92, Uhrig '97]. They can approximate any degree function

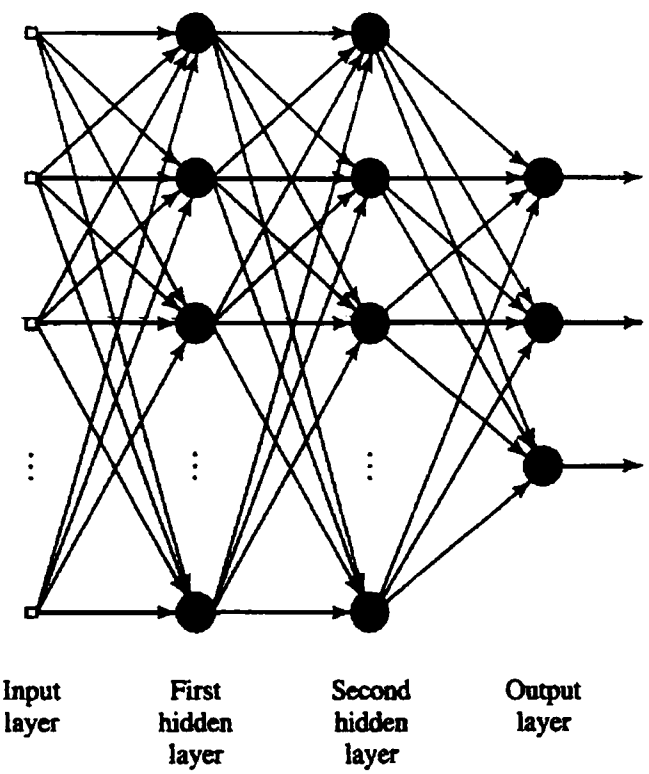


Figure 2.1. Schematic of a Feed-Forward Artificial Neural Network.

without requiring a mathematical description of how the output functionally depends on the input. A neural network performs this approximation within the weights, biases, and activation functions contained inside the architecture of the network itself. Theoretically, any function can be approximated by a one-hidden layer feed-forward neural network; this network incorporates a non-linear activation function in the nodes of its hidden layer, and a linear activation function in the nodes of its output layer. This type of architecture is capable of accommodating any degree function with non-linearity.

An input pattern is applied to the input layer and the network's output are the nodes of the output layer. The hidden layers are significant because they enable the network to learn complex relationships by extracting meaningful features from the input information. A network learns these complex relationships by a procedure known as training. For each iteration of training, there are two passes of information through a multi-layer neural network, a forward pass of the input signal, and a backward pass of error signal. Figure 2.1 is a representation of the basic feed-forward type artificial neural network used in this research.

The standard artificial neuron is a processing element whose output is calculated by multiplying its inputs by a weight vector, summing the results, and applying an activation function to the sum.

$$y = f\left[\sum_{k=1}^{n} x_k w_k + b_k\right]$$

Figure 2.2 depicts an artificial neuron with n inputs. In the forward pass, the input pattern is applied to the nodes of the input layer and then propagated forward. The signal then proceeds forward through the network. The synapses connecting the nodes have synaptic weights that multiply these forward-propagated signals. The nodes of each layer after the input layer incorporate an activation function. The forward-propagated signals to each node are summed and applied to this activation function to produce a modified function signal to pass to the next level. The node's activation function is a mathematical defined in the architecture to classify a layer. Two activation functions were used in the ANN's for this research. The hyperbolic tangential activation function was used in the hidden layers:

$$f(x) = \tanh(x) = \frac{e^{x} - e^{-x}}{e^{x} + e^{-x}}$$

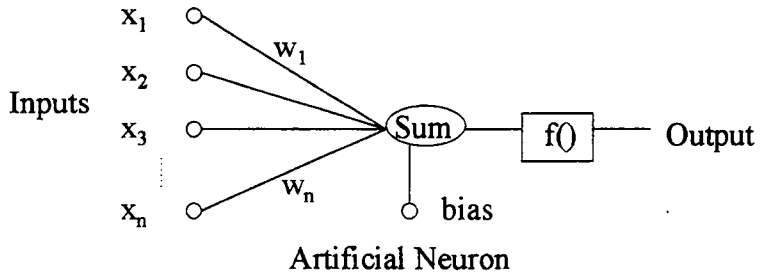


Figure 2.2. Schematic of Artificial Neuron

This activation function is favorable because it can model non-linear relationships that are present in the data with outputs between –1 and 1. The linear activation function was used for the output layer:

$$f(x) = x$$

In the backward pass phase of the network training, an error signal is passed back through the network so that the weights connecting the nodes in the network's layers can be modified to minimize the network's mean-squared error (MSE). The MSE is the mean of the squared errors between the network's prediction and the networks training values. Another type of error associated with ANNs is sum-squared-error (SSE). SSE is the sum of the squared errors. An individual output node's error is defined as [Haykin '94, Hines '97a]:

$$e_j^{\,2} = \left(d_j(n) - y_j(n)\right)^2$$

with $d_j(n)$ defined as the desired output of node j, and $y_j(n)$ is again defined as the nodes output. This error is then compared to the error goal and then back propagated through the network and the weights of the synapses are changed according to:

$$\Delta w_{ij} = \eta \cdot \delta_j(n) \cdot y_i(n)$$

where Δw_{ij} is the desired change to be made to the synaptic weight,

η is a user-defined learning-rate parameter,

$\delta_{ij}(n)$ is the local error gradient at node n,

and $y_i(n)$ is the input signal of node j.

The local gradient at node j is defined as:

$$\delta_j(n) = e_j(n)\varphi_j'\left(v_j(n)\right) \qquad \text{for output node } j$$

$$\delta_j(n) = \varphi_j'\left(v_j(n)\right)\sum_k \delta_k(n) w_{kj}(n) \qquad \text{for hidden node } j$$

where $e_j(n)$ is the error signal,

φ_j' is the first derivative of the node's activation function.

The summation over k term depends on two sets of terms; first the δ_k, is the prior knowledge of the error signals already calculated from the previous layer, and secondly the w_{kj} consists of the synaptic weights associated with the connecting synapses between nodes j and k [Haykin '94, Hines '97].

The results obtained from the output layer are desired to be the same as the output obtained from the physical system it is modeling. The synaptic weights connecting the various nodes are changed according to the back-propagation algorithm described above such that the next forward-propagation phase will yield a more correct output. This training procedure is iterated until it is stopped by a user-defined criterion. This stopping criterion can be the number of training epochs, the level of the sum-squared error, the level of mean-squared error, or the rate of change of the sum-squared error value.

Once one of the training goals is reached, the weights and biases are stored. The network can be tested to see how well it trained by multiplying the weights and biases by the input matrix to get a prediction of the misalignment conditions. If the stopping criterion was chosen adequately then the predicted misalignments will be nearly identical to the actual misalignment conditions and the network can perform the mapping. If the network learned the training data well, then it can be tested to see how well it performs on test data. The results of the generalization will depend on how well the training and testing sets were chosen as well as the inputs and the relationships evident in the data.

A cross validation method of training can be used to train the network in a supervised fashion. A data set that was not used for training is used to see how the network predicts while it is training. The stopping criterion is to train until the test set prediction stops getting better while trying to minimize the amount of error in the training set. This is a good method of reducing the amount of over fitting in a neural network. That is, it helps to prevent the network from learning the noise in the data.

2.6 PARTIAL LEAST SQUARES

Partial Least Squares (PLS) techniques allow a better generalization to a mapping when the data is highly correlated an limited in amount [Qin]. PLS is factor-based technique that generates factors for both the input and the output spaces to allow a one to one mapping in the

inner layer between the two factor spaces [Geladi '85]. PLS is a more robust technique for prediction than MLR or PCA [Geladi '85].

PLS is built on the same techniques that are used in PCA regression methods. The PLS model consists of an outer relationship between the input space and the input factor space and the output space and the output factor space separately, and an inner relationship between the two factor spaces [Geladi '85].

The input space outer relationship is explained by the following:

$$X = T \bullet P^T + E$$

where: X is the input matrix

T is the factor space input matrix

P is the matrix that iteratively builds the factor space.

E is the residual error between X and TP'.

The output space outer relationship is explained by the following:

$$Y = U \bullet Q^T + F$$

where: Y is the output matrix

U is the factor space output matrix

Q is the matrix that iteratively builds the factor space.

F is the residual error between Y and UQ'.

The inner relationship in a Linear Partial Least Squares model is a simple MLR. A non-linear PLS (NLPLS) can also be created by placing an ANN mapping between the two factor spaces. This ANN mapping allows the technique to map the inner relationship in a non-linear fashion.

The PLS method is an iterative technique where first principle components are used to approximate the input and output data. Then an inner mapping is performed relating the orthogonal spaces to determine the approximate output factor space. Then the approximate values are returned to their original spaces and are subtracted from the actual values to determine the errors of the approximations. The new input and output matrices are then set to the errors and the process is repeated until the maximum rank of the matrices is reached. When used for prediction, all of the PLS factors are usually not used [Geladi '85]. An optimal number of PLS factors are chosen in a qualitative fashion with a technique similar to cross validation.

This method reduces the inputs and the outputs to orthogonal spaces to remove the collinearity of the data. It uses the most correlated input data to the output for the prediction so it converges quickly giving rotated X and Y factors. There are as many factors available to use as

the rank of the matrix. Once the model has been developed, the optimal number of PLS factors must be determined to allow the model to perform the best prediction. The easiest way to determine the number of factors is by determining the errors for the training and testing data and then choosing a qualitative number based on them similar to the cross validation training method for ANNs. It is desirable to have the best prediction with the least number of factors while learning the training data to a minimum error.

The optimal LPLS model generally performs better on test data than simple MLR because overfitting in the model can be removed by removing factors. The NLPLS model usually performs better than the LPLS model if there is a nonlinear relationship between the inputs and outputs because it allows the model to learn the non-linearities that might be present in the data. The NLPLS model should perform better than any of the other models because it uses all of the input data and reduces it in a supervised manner to retain the most useful information and then train on this data with a method that allows any non-linearities to be mapped. This method uses information from all of the data in the ANN instead of picking features to use in the mapping.

2.7 Statistical Evaluation

The statistical evaluation simply compares the different methods of mapping frequency amplitudes to misalignment and determines the best performing procedure. Two comparisons are used to determine the best method of the five discussed in this thesis. These two comparisons are the average error between the predicted alignment and the actual alignment for the test data and the mean-squared-error (MSE) between the predicted alignment and the actual alignment for the test data. The average error is a good measure of the error in the prediction. The MSE is affected by the outliers and shows whether the overall error is good or whether the performance of the model is only good on certain events.

3.0 METHODOLOGY

This section first gives the overall procedure for developing the methods to detect and predict the misalignment conditions. It then gives a description of the experimental set-up of the Oak Ridge National Laboratory (ORNL), the types of couplings used, and how the data was collected. The data processing techniques are discussed such as signal processing, frequency resolution reduction, data set expansion, and the creation of training and testing data sets are also discussed. Lastly detailed examples of how each of the mapping techniques work is given followed by the statistical evaluation comparison method discussion.

3.1 PROCEDURE

The data was collected at the Oak Ridge National Laboratory (ORNL) Advanced Motor Testing Facility. Sensors were attached to a fifty horsepower Reliance AC three phase four-hundred-eighty-volt electric motor operating at three thousand five hundred and fifty revolutions per minute (RPM). This motor was attached through flexible couplings to a one hundred fifty horsepower Dynamatic roller bearing dynamometer. The sensors detected each of the three phase voltages and currents and sent them through a data acquisition board to be stored on a Teac digital tape recorder. Two of the raw signals for both the currents and voltages were then extracted from the tape at a sampling rate of six thousand hertz and stored in digital form on computer media.

Advanced signal processing techniques were then used to transform the raw voltage and current data into the power time waveform. Fast Fourier Transform (FFT) techniques were used to transform the time waveform into the frequency spectrum. Then the frequency domain data was divided into training and test sets. Finally, five procedures were used to map the frequency variables to their alignment conditions.

The first procedure was Multiple Linear Regression (MLR) to determine the misalignment conditions. The next prediction method used an Artificial Neural Network (ANN) trained on the most highly linearly correlated frequencies to each of the types of misalignment. The third prediction method trained an ANN on the input's principle components to determine the misalignment conditions. The fourth method used a linear Partial Least Squares (LPLS) regression to predict the misalignment conditions. The final method used a Non-Linear Partial Least Squares (NLPLS) technique to determine the misalignment conditions.

After all of these techniques were used to predict the misalignment conditions, the associated test errors were measured. A statistical comparison of the training and testing errors was then used to determine how each of the methods performed. Figure 3.1 shows the procedure used in this thesis.

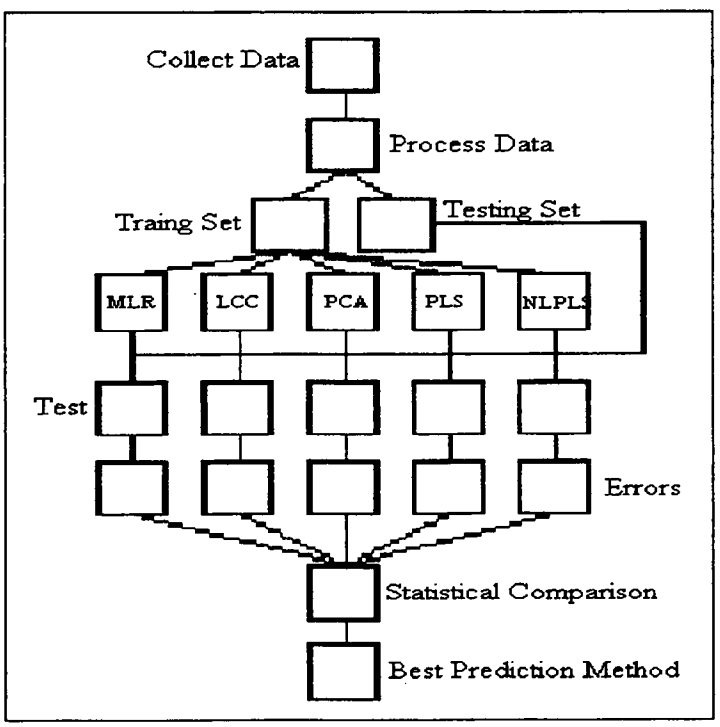


Figure 3.1 Procedure used to determine the best method for predicting motor shaft misalignment from power frequency spectrum.

3.2 EXPERIMENTAL SET-UP

The experimental set-up at the Oak Ridge National Laboratory (ORNL) Advanced Motor Testing Facility consisted of the motor dynamometer system with current and voltage sensors attached to it connected to a recorder. Data was recorded for three different types of couplings. Once the data was collected, it was digitized to computer media for analysis.

3.2.1 Mechanical Set-Up of ORNL Test Site

The data used for this research was obtained at the Oak Ridge National Lab (ORNL) Advanced Motor Testing Facility. Data was obtained using a three-phase fifty horsepower AC motor attached through three different flexible couplings to a 150 horsepower dynamometer at controlled parallel and angular offset conditions. Data for the input currents and voltages at these offset conditions was stored on digital tape using a Teac RD-135T DAT data recorder. Table 3.1 shows the specifications for the motor and the dynamometer.

The motor was attached to a 20" x 20" x 8" block of aluminum. There were two threaded rods fitting into the aluminum block that were used to adjust the motor's position in the horizontal plane. The aluminum motor support was clamped in place by four levers. The levers were supported on one end and held down through their centers by a bolt. Figure 3.2 shows the motor attached to the dynamometer. Figure 3.3 shows the plan view of the aluminum motor support plate.

Table 3.1 Motor and Dynamometer at ORNL.

Reliance Electric			
I.D. No.	22MN324503 G 001 SY		
Model No.	P3264503A	Volts	230/460
HP	50	Amps	118/59.3
RPM	3550	Phase	3
Bearing:	55BC03J 30X	Design B	Type P

Dynamatic	
Model No.	AD-8080
Serial	40001-213-6
Capacity	150 hp
Speed	2600-9000 rpm
Bearing	roller

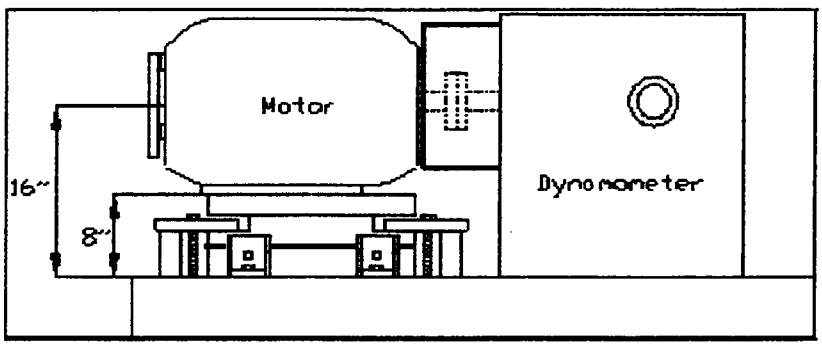


Figure 3.2 Motor and Dynamometer setup at ORNL.

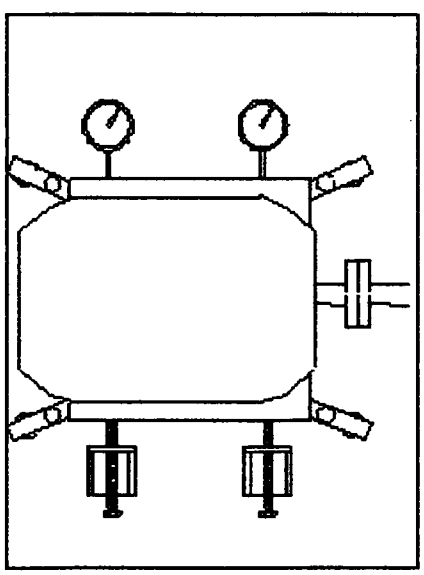


Figure 3.3 Plan view of aluminum motor support.

The alignment measurements were made using a Computational Systems Incorporated (CSI) UltraSpec® laser alignment system with the motor off line [CSI]. The thermal growth measurements were made using permanently installed CSI lasers and verified using Essinger bars. Current and voltage sensors were placed on each of the three phase inputs to the motor. The sensors were attached to an eight-channel TEAC digital tape recorder.

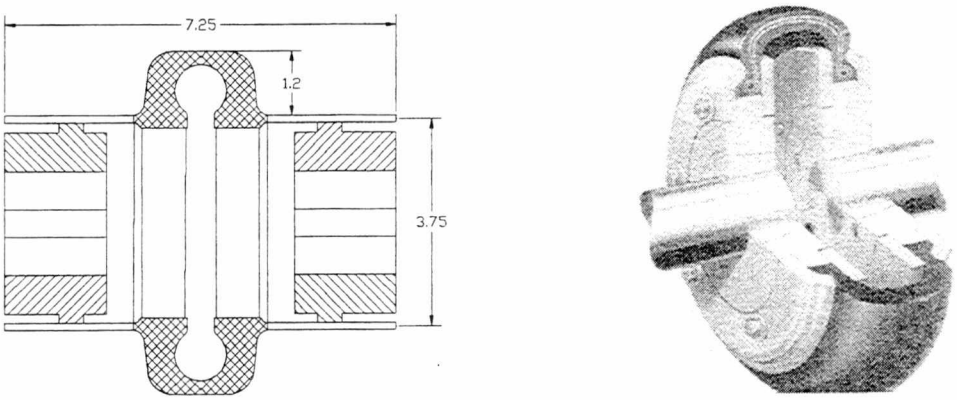
3.2.2 Flexible Couplings Used During Testing

Three different types of flexible couplings were tested, a Rexnord Elastomer type, a Zurn gear type, and a Dodge grid type. These couplings were chosen because Duke Power Company suggested them as representative of the most common coupling types used in today's industry [Hines '97a]. Table 3.2 shows the information for the couplings along with each manufacturer's specifications for maximum angular and parallel offset misalignments.

Figure 3.4 shows an elastomer type coupling. Figure 3.5 shows a grid type coupling. Figure 3.6 shows a gear type coupling. For each of the following figures, part (a) is the cross-sectional view with dimensions of the actual couplings used during the testing, while part (b) shows the isometric views of similar couplings to those tested.

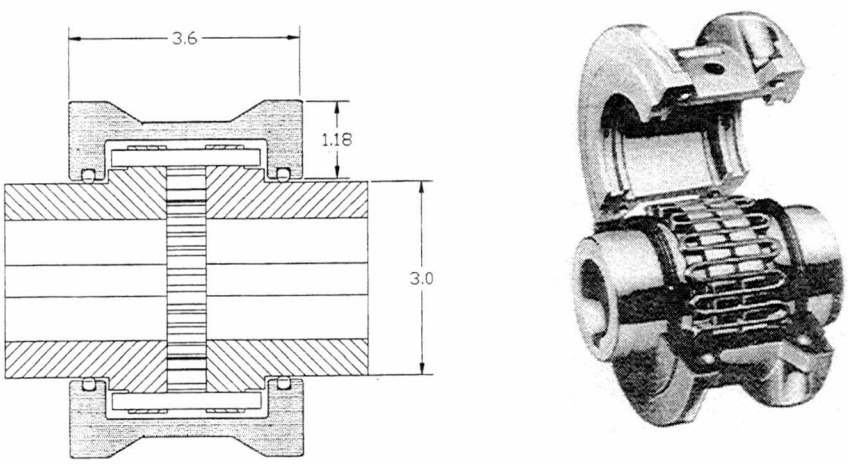
Table 3.2 Couplings used with the manufacturer's tolerances.

Type	Manufacturer	Model	Max. Offset (mil)	Max. Ang. (mil/inch)
Grid	Dodge	1060T	12	12
Elastomer (tire)	Rexnord	Omega ES10R el, 10SHRB hub	70	40
Gear	Zurn	3011/2GP	50	15



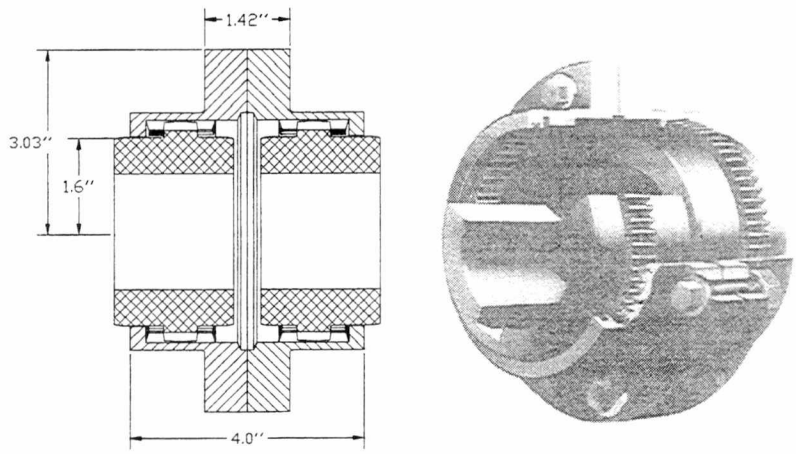
(a) (b)

Figure 3.4 Rexnord elastomer type coupling. [Hines '97a]



(a) (b)

Figure 3.5 Dodge Grid type coupling. [Hines '97a]



(a) (b)

Figure 3.6 Zurn Gear type coupling. [Hines '97a]

3.2.3 Data Collection Set-Up

Current and voltage sensors were placed on each of the three phases of the input to the electric motor for a total of six sensors. These sensors were connected to a TEAC Pulse Code Modulation digital data tape recorder. Two minutes of analog data was recorded for each of the couplings for each tested alignment condition. The digital tape recorder was then connected to a computer to convert the analog data to digital computer media.

An Apple Macintosh IIfx computer utilizing Labview 4.0.1 was used to digitize the data off of the tapes into computer files through a four channel Data Acquisition Board (DAQ). A four-channel analog to digital analyzer with an automatic trigger to IGOR Analytical software was used to digitize only the Phase A and Phase B voltages and currents. The signals were digitized off of the tape at a sample rate of 6000 Hz. The A/D board added a very small DC signal to the signals in the first $1/6^{th}$ of a hertz range.

3.3 DATA PREPARATION

The data was acquired from ORNL in digital form by digitizing two of t three phase currents and voltages off of the digital tape. The third of the three phase currents and voltages were calculated. The three three-phase currents and voltages were used to calculate the total power. This time domain power was then converted to the frequency domain. The resolution of the power frequency spectrum was then reduced to decrease the number of frequency bins. The five sets of data for each alignment condition were then expanded to thirty sets using a linear averaging technique to create more observations. Then the data was divided into training and testing sets.

3.3.1 Data Acquisition

Five sets of twelve seconds of data sampled at six thousand hertz were digitized to give five different seventy-two thousand data point time series for the Phase A and Phase B currents and voltages for each misalignment condition for each coupling. LabView scaled the data through the four-channel A/D converter with different scaling parameters for the current and voltage. The current data on the DAT was scaled using the relationship value/4 because the original signals were amplified by four when they were recorded on the digital tape while the voltage data was scaled using value*2.5 to make up for the amplification to the digital tape recorder. LabView automatically converted the data to IGOR statistical package format.

The data was then pulled into the IGOR software package and converted to ASCII text format. The ASCII text files were written in IBM compatible format on a CD-ROM. The CD-ROM contained the five sets data for the three couplings, the Rexnord, the Gear Type, and the Dodge Grid making 39 events. The tape events are shown in Table 3.3 The CD-ROM files were then read into MATLAB and saved in MATLAB Binary File format.

Table 3.3 Tape events corresponding to experimental alignment conditions.

Tape Event	Coupling	Parallel Offset (mils)	Angular Offset (mils/inch)
1	Rexnord	0	0
2	Rexnord	45	0
3	Rexnord	0	30
4	Rexnord	45	25
5	Rexnord	0	0
6	Rexnord	15	0
7	Rexnord	30	0
8	Rexnord	45	0
9	Rexnord	60	0
10	Rexnord	90	0
11	Rexnord	0	10
12	Rexnord	0	20
13	Rexnord	0	40
14	Rexnord	45	25
15	Rexnord	-45	25
16	Rexnord	0	0
17	Rexnord	10	0
18	Rexnord	20	0
19	Gear	0	10
20	Gear	0	0
21	Gear	0	6
22	Gear	0	12
23	Gear	0	15
24	Gear	20	0
25	Gear	20	0
26	Gear	35	0
27	Gear	50	0
28	Gear	40	10
29	Dodge Grid	0	0
30	Dodge Grid	4	0
31	Dodge Grid	8	0
32	Dodge Grid	12	0
33	Dodge Grid	0	4
34	Dodge Grid	4	4
35	Dodge Grid	8	4
36	Dodge Grid	-8	4
37	Dodge Grid	0	8
38	Dodge Grid	4	8
39	Dodge Grid	12	8

3.3.2 Signal Processing

The MATLAB Binary files for the Phase A and Phase B voltages and currents were read into MATLAB. The Phase C currents and voltages were calculated from them by the following:

Phase C = 0 – (Phase A + Phase B).

This is true because the Oak Ridge National Laboratory Advanced Motor Test Facility utilizes a floating ground electrical set-up to allow the electrical inputs to routed through a control room. A portion of the three-phase currents for a typical alignment condition is shown in Figure 3.7. The same portions for the typical three-phase voltages are shown in figure 3.8.

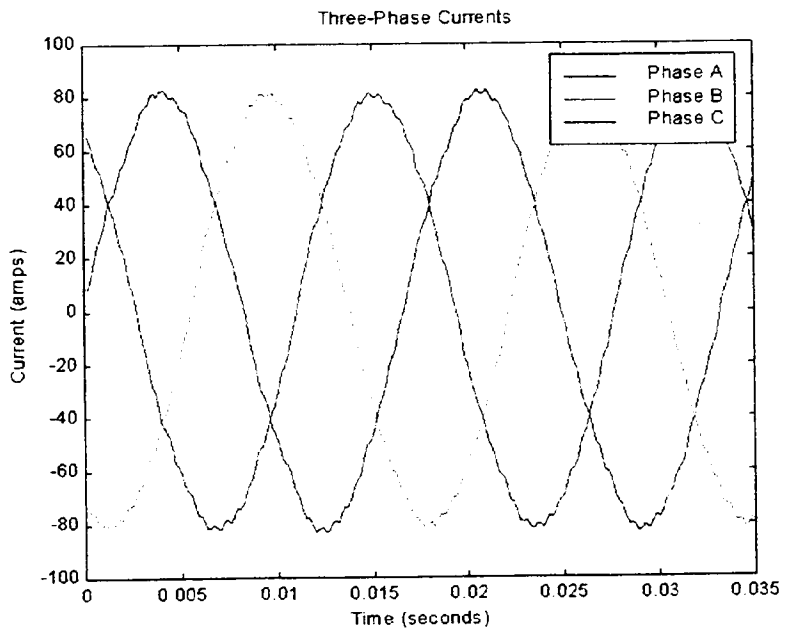


Figure 3.7 Typical three-phase currents.

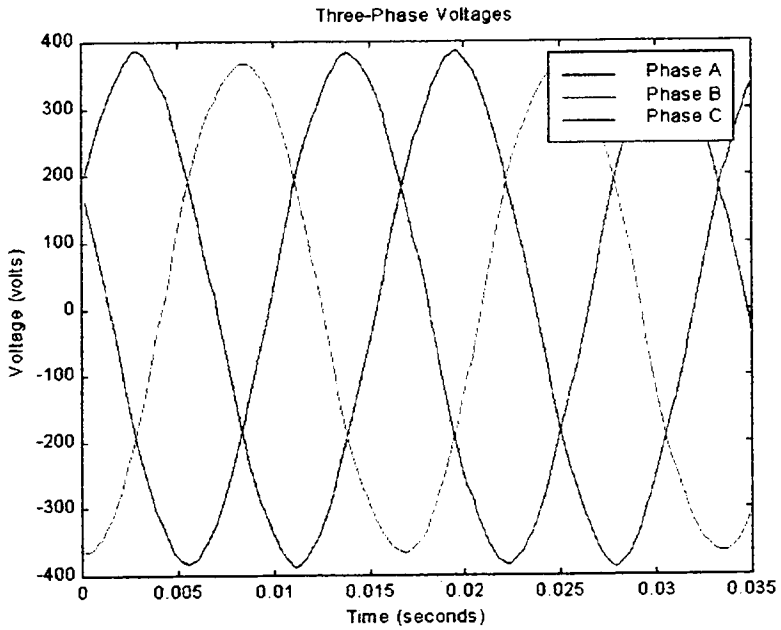


Figure 3.8 Typical three-phase voltages.

The three-phase powers were calculated using a variation of Ohm's law:

Power = voltage * current.

The total power for each event was then calculated by summing the three individual powers. This total power is the time domain waveform data for the motor and is shown in Figure 3.9. There are some differences in the power time domain for each alignment condition, such as different frequency components, or even some very small differences in magnitude. But, these differences are hard to detect visually in the time waveform, because the differences are very small. The amount of energy associated with each frequency component can not be determined in the time domain. The power frequency domain is more useful for determining these differences. There exists some spectral broadening due to the fact that the power curve might not start and end at the beginning and end of the periodic cycle. This was removed by scaling the time domain data with a Hanning window. The Hanning window fits the data to a gaussian curve to de-emphasize the values at the ends of the curve [Casada '98].

Next the Fast Fourier Transform (FFT) technique was used to transform the data to the frequency domain. The FFT operation gives data in both real and complex values, so to the magnitude of this data was taken to get the magnitude of the frequency in units of power. Since the original sampling rate was 6000 Hz, the amount of accurate data in the FFT was limited by the Nyquist Frequency to 3000 Hz. Therefore, the length of the FFT vector is half the length of

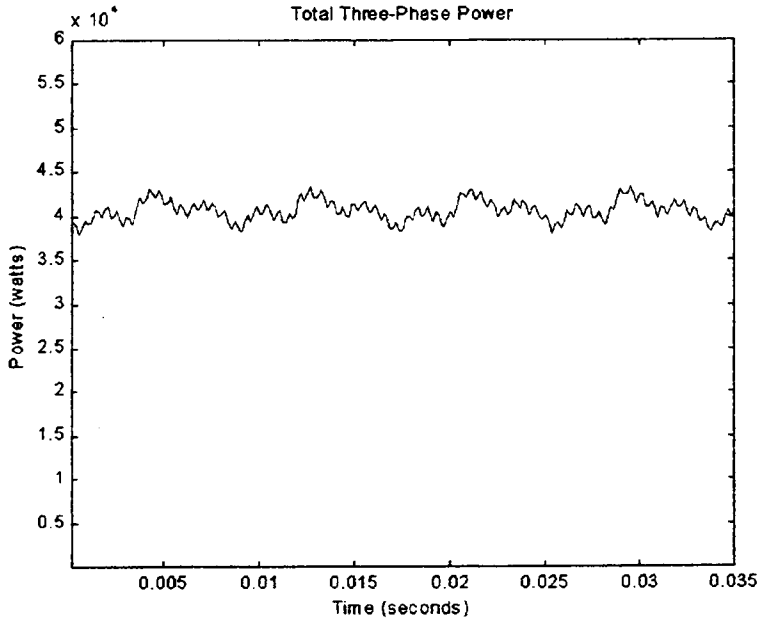


Figure 3.9. Typical Total Three-Phase Power.

the time-domain vector. The FFT data was scaled using a root mean squared (RMS) technique. This simply divided the magnitudes of the FFT with the product of the number of data points used and the standard RMS value of 0.707, the square root of two as shown in the following equation [Casada '98]:

$$R = |FFT| / (N * 0.707)$$

where: R is the RMS scaled FFT

FFT is the power frequency spectra

N is the number of frequency bins in the FFT.

A small amount of DC interference in the very low frequencies of the FFT was evident, so the first 0.12 Hz, or the first two frequency bins, was filtered to zero. This left 36000 frequency bins equally spaced between 1 and 3000 Hz with the magnitudes of the bins as RMS power. Figure 3.10 shows a typical FFT for an alignment condition.

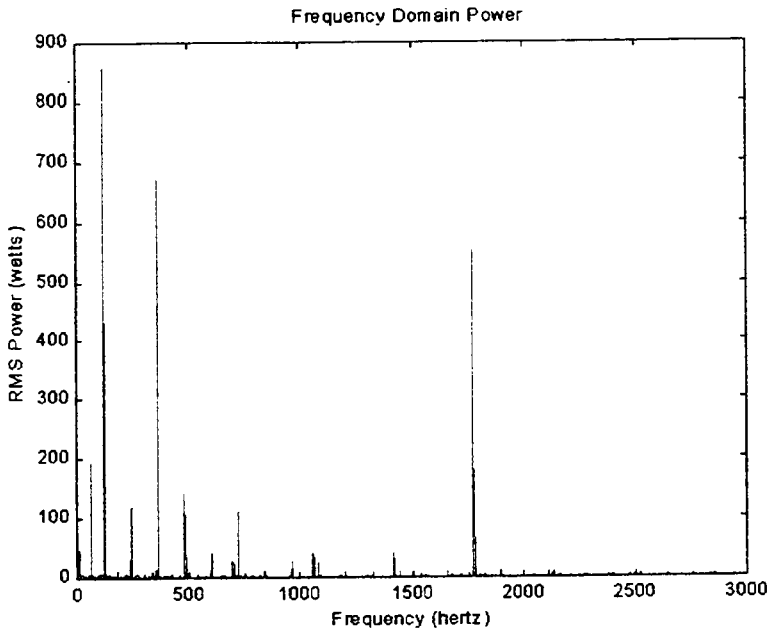


Figure 3.10 Typical FFT for an alignment condition.

Figure 3.11 shows ten FFT's plotted over each other to show that the frequency spectrum changes with the alignment conditions. There are some changes that can be seen. Notice that the some conditions have larger peaks in the lower frequencies while the other conditions have larger values in the higher frequencies.

3.3.3 Frequency Resolution Reduction

The frequency spectrum transformation produced frequencies from 0 to 3000 Hz over 36000 frequency bins. This meant that there were 12 bins corresponding to each frequency. The size of this vector caused computational difficulties when trying to map the inputs to the outputs. The major computational difficulties were that the computer memory requirements for some of the mapping techniques were greater than the resources available to perform the operations. Therefore the number of frequency bins had to be reduced to allow the prediction methods to perform more efficiently.

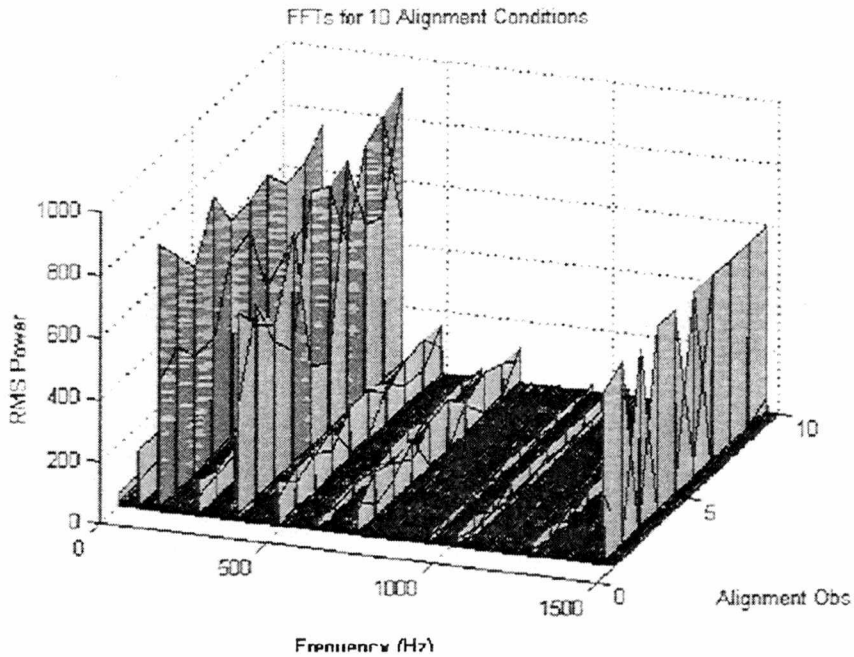


Figure 3.11 Differences in Frequency Spectrum with alignment condition.

The most common method of reducing the resolution of a frequency vector while retaining the importance of each bin in the original resolution is by taking the square root of the sum of the squares.

$$F_i = \sqrt{\sum_{N=i-6}^{i+6} F_N^2}$$

where F_i is the Frequency in 1 Hz increments

F_N is the Frequency in $1/12^{th}$ Hz increments

This method was used to reduce the resolution of the frequency vector from one twelfth of a hertz frequency bins to one hertz frequency bins. This reduced the length of the frequency vectors from 36000 bins to 3000 bins with each bin representing 1 Hz.

A vector with 3000 frequency bins still requires a lot of computations when performing prediction methods. A way to further reduce the size of the vectors is to remove the frequencies that have little or no power in them. A tolerance of 0.1 watts was used to further reduce the number of frequency bins.

3.3.4 Data Set Expansion

Five sets of time domain data were taken for each of the couplings. The frequency transforms were taken to create the 3000 frequency bin data sets. There were some small differences in the associated FFT's for the same alignment conditions, but for the most part these were minor. These data sets were combined to allow more observations for each alignment condition. Most of the techniques to map inputs to outputs perform more accurately with more observations than variables where the data corresponding to the alignment condition is the observation and the frequencies are the variables. This is especially true for the PCA techniques. Even with five sets of observations, there were considerably more variables than observations.

One way to expand the number of observations is to combine the data sets by averaging them. Taking all the possible combinations of two sets, three sets, four sets and all five sets expanded the data from five sets to thirty sets. This brought the number of observations closer to the number of variables. The resulting FFT's were slightly different than the original five sets of FFT's, but again the differences are very minor for the same alignment condition. This method does not increase the overall rank of the observation matrix because of the strong collinearity associated with averaging and therefore adds ill conditioning to the matrix. This collinearity creates problems that some of the mapping techniques handle better than others.

3.3.5 Creation of Training and Testing Sets

When using techniques to map inputs to outputs, the data is divided into two sets. These sets are the training and testing sets. Both of these data sets should cover the region of the input space as well as possible.

The training data is the data used to solve for a weight matrix in regression or to train an Artificial Neural Network. The test data is the data used to test the prediction model. The prediction model has never seen this data before, but it is very similar to the training data.

There are now 30 sets of observations, one entire set of observations was kept as testing data. Since 25 sets of observations were averages of the first five sets one of the first five was kept out. For uniformity, the fourth set of observations was used for testing. It is also desirable to test a model on data that has not been seen at all to see how well the model generalizes. To

accomplish this, one observation was kept out for all 30 sets of observations to also use in the test data set. This is shown in section 4.1.

3.4 MULTIPLE LINEAR REGRESSION

The baseline results for comparing the prediction models are the results from the multiple linear regression. This model simply uses the frequencies and the alignment conditions to calculate a weight matrix to multiply by subsequent frequency matrices to predict alignment conditions. This technique uses the pseudoinverse technique to invert the frequency matrix.

There is some collinearity between the observations due to the averaging techniques, so the pseudoinverse technique does not perform very well due to ill conditioning of the matrix and singularities present in it. MATLAB has a function called *pinv.m* that has a tolerance level below which all singular values are zeroed out. This function uses Truncated Singular Value Decomposition (TSVD) to determine the singular values of the matrix. Then it zeroes out all of the singularities below the tolerance to improve the condition of the matrix [Hansen '87]. The condition number of the matrix is the ratio of the largest eigenvalues to the smallest eigenvalues. A matrix with a condition number less than 100 is considered good and should not present computational instabilities. By removing the smallest singular values, the condition number is decreased significantly with this method of pseudoinverse.

The frequency matrix is all in the same units so there is no need to standardize it to unit variance, or to a normalized variance. It is not mean centered, however, so the frequency matrix was appended with a bias variable before the pseudoinverse algorithm was applied to allow for the linear mapping to not pass through the origin. Once the pseudoinverse was calculated it was multiplied by the alignment conditions to calculate the weight matrix necessary to map the data. Three weight matrices were calculated for each of the couplings. One for the parallel offset misalignment condition, one for the angular misalignment condition and one for both of the misalignment conditions For the MLR technique, the results from the combined misalignment conditions will be the same as the results from t he individual misalignment conditions. These weight matrices were saved to use on the test data.

The test data also had to have the bias column appended to it before the prediction was calculated. The test data was then used to predict the misalignment conditions with the three

models. The associated average errors and mean-squared-errors (MSE) were calculated to use in the statistical comparison.

3.5 Linear Correlation Coefficient Neural Network

The ANN training algorithm trains more efficiently when there are fewer inputs or variables to train. The first method for selecting the best frequencies to train on was to determine the linear correlation coefficients between the frequencies and the misalignment conditions. The most highly correlated frequencies with each misalignment condition were chosen as the inputs to the ANN. Figure 3.12 shows how the best correlated frequencies typically changed with the alignment condition. There is no significance to these frequencies other than they had the largest correlation coefficients. This shows that generally, the magnitude for the most linearly correlated frequencies increases with an increase in misalignment. There can also be an inverse relation between the frequency magnitude and the misalignment condition, so both the negative and positive correlation coefficients are evaluated.

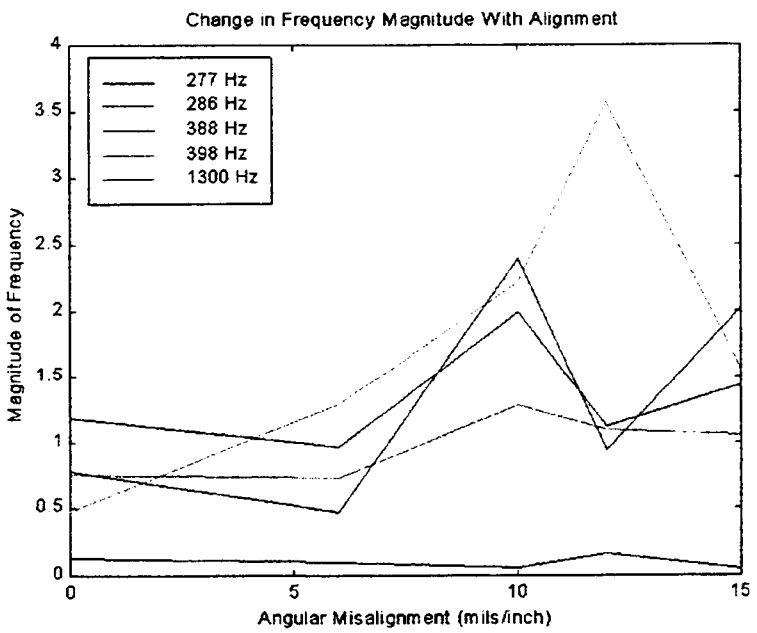


Figure 3.12 How Frequency Spectrum changes with Alignment.

The top thirty frequencies correlated to the parallel offset misalignment were chosen for the first ANN to just predict parallel offset misalignment. Next, the top thirty frequencies correlated to angular misalignment were used for an ANN to predict angular misalignment. These frequencies were then combined to train a third ANN to predict both the parallel offset and angular misalignment. The ANN parameters were stored so that the network could be tested with other data.

The appropriate frequencies were selected from the test data and the misalignment conditions were predicted for the three networks. The average errors and MSE's were calculated to use in the statistical comparison.

3.6 Principal Component Neural Network

The next method used to reduce the amount of inputs for the neural network was principal component analysis (PCA). For PCA to work properly, it was necessary to further to reduce the number of variables to less than the expanded number of observations [Jolliffe '86]. This was accomplished by increasing the minimum value of power threshold below which the data was discarded. This threshold varied with the coupling type. The data was mean centered to for all of the frequencies placing their mean at zero. Then SVD was used to calculate the principal component scores of the input. Next, linear correlation coefficient techniques were used to determine which of the principal components (PC's) are the most correlated with the alignment conditions.

The three PC's most highly correlated with the parallel offset misalignment were used to train an ANN to predict the parallel offset misalignment. Next, the three PC's most highly correlated to the angular misalignment were used to train an ANN to predict the angular misalignment. Finally, the PC's were analyzed to see which ones contained the most information or variability of the data. The six largest PC's were then used to train an ANN to predict both angular and parallel offset misalignment.

The ANN parameters and the input scaling parameters were saved to be used on further data sets to test the network. Each of the networks were tested on the test data to predict the alignment conditions. Then the associated average errors and MSE's were calculated to be used in the statistical comparison.

3.7 Partial Least Squares Linear Model

The linear Partial Least Squares (LPLS) model was applied to the entire frequency spectrum. Then an analysis was performed to determine how many of the PLS factors contained relevant data and should be retained. This method is shown in section 4.5. Then another PLS model was created just using the results form the PLS information analysis.

The training and testing for the LPLS model was performed using all of the PLS factors generated by this model. Then the associated errors were saved for statistical comparison. Next, the LPLS model was tested using a successive number of PLS factors to determine the optimal number to use for the prediction process. This number of PLS factors for the optimal model was chosen qualitatively with a judgement made from a plot of the associated errors for the training and testing data. Section 4.5 shows the implementation for this method.

Finally, the optimal LPLS model was tested and the errors were calculated to be used in the comparison. This process was repeated to create a model for the parallel offset misalignment condition, the angular misalignment condition, and both of the alignment conditions.

3.8 Partial Least Squares Non-Linear Model

The non-linear Partial Least Squares (NLPLS) method was applied the number of PLS factors determined to contain information using the results from the original PLS information analysis. The ANN Architecture was determined by trying different architectures and producing an error curve plot to compare with other architectures. Then a qualitative judgement was made using a technique similar to cross validation to choose the best architecture for the network to map the NLPLS factor spaces. This is shown in section 4.6. After the ANN layer architecture was chosen, the NLPLS model was created.

The training and testing for the NLPLS model was performed using all of the PLS factors generated by this model. Then the associated errors were saved for statistical comparison. Next, the NLPLS model was tested using a successive number of PLS factors to determine the optimal number to use for the prediction process. This number of PLS factors for the optimal model was chosen qualitatively with a judgement made from a plot of the associated errors for the training and testing data as in section 3.7. These are shown in section 4.8.

Finally, the optimal NLPLS model was tested and the errors were calculated to be used in the comparison. This process was repeated to create a model for the parallel offset misalignment condition, the angular misalignment condition, and both of the alignment conditions.

3.9 Statistical Evaluation

The average errors between the predicted misalignment conditions and the actual misalignment conditions were compared for each of the types of couplings and each of the prediction models. The MSE's were also compared to determine if the trends were the same for all of the couplings and comparison statistics.

Based on these comparisons, the best performing prediction model was then determined. The best performing models for each of the couplings were compared to see if the same model was the best for all couplings. Then the overall best performing model was determined.

4.0 RESULTS

This section presents the results of the different methods of mapping the frequency inputs to the misalignment conditions. It first presents the training and testing sets for the different couplings. The results for the data analysis are presented next. The results from the multiple linear regression models for each of the couplings are then presented. Then the results from the linear correlation coefficient neural network for each of the couplings are presented. Then the results of the principle component neural network are presented. The results from the partial least squares linear model are presented next followed by the results from the partial least squares neural network. Finally, the results of the statistical comparison of the models are given.

4.1 DATA ANALYSIS

There were different amounts of observations for each of the coupling types. The observations themselves were also different for each coupling. Therefore different size training and testing sets were created for each coupling. Since the FFT's were also different, the amount of frequency variables after the initial tolerance was also different for each coupling.

4.1.1 Training/Testing Sets for Elastomer Type Coupling

One set of observations for the Rexnord Elastomer type coupling contained eighteen observations with fourteen different alignment conditions. The five observation sets were expanded to 540 observations by 3000 frequency bins. The tolerance of .1 watts reduced the number of frequency bins to 1956. Table 4.1 shows the alignment conditions for each observation.

Table 4.1 Alignment conditions for Rexnord Elastomer type coupling.

Observation Numbers	Parallel Offset	Angular Misalignment
1-90	0	0
91-120	0	10
121-150	0	20
151-180	0	30
181-210	0	40
211-240	10	0
241-270	15	0
271-300	20	0
301-330	30	0
331-390	45	0
391-450	45	25
451-480	60	0
481-510	90	0
511-540	-45	25

The fourth observation set was kept out for testing, as was the misalignment condition 30 mils parallel offset misalignment with 0 mils/inch angular misalignment. This gave a training input matrix 493 observations by 1956 frequency variables and a testing set 47 observations by 1956 frequency variables.

4.1.2 Training/Testing Sets for Gear Type Coupling

One set of observations for the Zurn Gear type coupling contained ten observations with nine different alignment conditions. The five observation sets were expanded to 300 observations by 3000 frequency bins. The tolerance of .1 watts reduced the number of frequency bins to 1914. Table 4.2 shows the alignment conditions for each observation.

The fourth observation set was kept out for testing, as was the misalignment condition 35 mils parallel offset misalignment with 0 mils/inch angular misalignment. This gave a training input matrix 261 observations by 1914 frequency variables and a testing set 39 observations by 1914 frequency variables.

Table 4.2 Alignment conditions for Zurn Gear type coupling.

Observation Numbers	Parallel Offset	Angular Misalignment
1-30	0	0
31-60	0	6
61-90	0	10
91-120	0	12
121-150	0	15
151-210	20	0
211-240	35	0
241-270	40	10
271-300	50	0

4.1.3 Training/Testing Sets for the Grid Type Coupling

One set of observations for the Dodge Grid type coupling contained eleven observations with eleven different alignment conditions. The five observation sets were expanded to 330 observations by 3000 frequency bins. The tolerance of .1 watts reduced the number of frequency bins to 1357. Table 4.3 shows the alignment conditions for each observation.

The fourth observation set was kept out for testing, as was the misalignment condition 8 mils parallel offset misalignment with 4 mils/inch angular misalignment. This gave a training input matrix 290 observations by 1357 frequency variables and a testing set 40 observations by 1357 frequency variables.

4.2 Results from Multiple Linear Regression Model

Three weight matrices were created for each of the couplings. One for the parallel offset misalignment regression model, one for the angular misalignment regression model, and one that regressed both the parallel offset misalignment and the angular misalignment at the same time. The average error was calculated by taking the mean of the absolute values of the difference between the predicted alignment conditions and the actual alignment conditions. The graphs for the regression and the prediction are shown in Appendix A.

Table 4.3 Alignment conditions for Dodge Grid type coupling.

Observation Numbers	Parallel Offset	Angular Misalignment
1-30	0	0
31-60	0	4
61-90	0	8
91-120	4	0
121-150	4	4
151-180	4	8
181-210	8	0
211-240	8	4
241-270	12	0
271-300	12	8
301-330	-8	4

4.2.1 Results for Elastomer Type Coupling

The weights for the Rexnord Elastomer type coupling formed two vectors that were 1957 rows by 1 column for the parallel offset misalignment and the angular misalignment, and a matrix 1957 rows by two columns for the model that predicts both parallel offset and angular misalignments.

The parallel offset misalignment model regressed the model to an average error of 5.56×10^{-13} mils. The regressed MSE was 2.41×10^{-25}. The parallel offset misalignment model predicted the misalignment to an average error of 25.15 mils. The predicted MSE was 1.01×10^{3}.

The angular misalignment model regressed the model to an average error of 6.43×10^{-13} mils/inch. The regressed MSE was 4.87×10^{-25}. The angular misalignment model predicted the misalignment to an average error of 2.99 mils/inch. The predicted MSE was 18.75.

The model that regressed both the parallel offset misalignment and the angular misalignment regressed the parallel portion to an average error of 4.54×10^{-13} mils and the angular portion to an average error of 5.08×10^{-13} mils/inch. The regressed MSE was 3.52×10^{-25} for the parallel and 3.34×10^{-25} for the angular. The joint misalignment model predicted the parallel offset misalignment to an average error of 25.15 mils and the angular misalignment to an average error of 2.99 mils/inch. The predicted MSE for the parallel was 1.01×10^{3} and for the angular was 18.8.

The angular model was the best model for the elastomer type coupling. Figure 4.1 shows the prediction for the angular model on the test data.

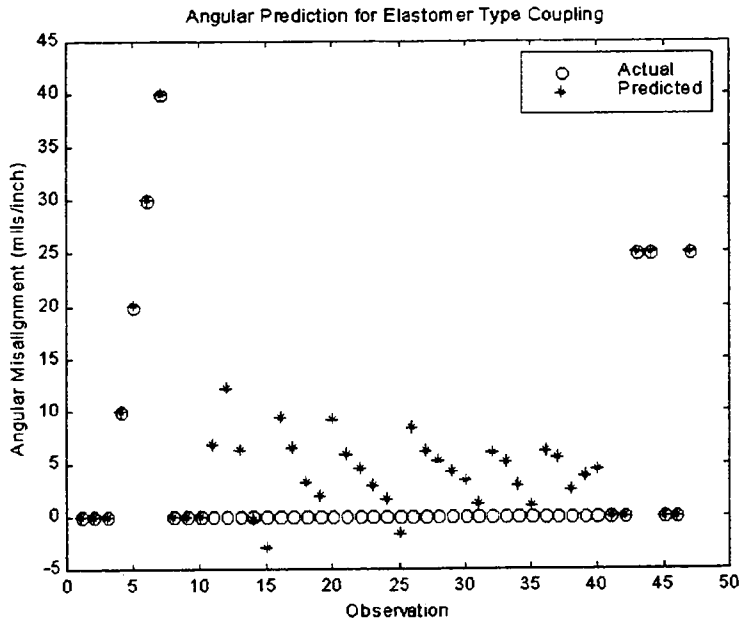


Figure 4.1. MLR Angular Prediction for Elastomer type coupling.

4.2.2 Results for Gear Type Coupling

The weights for the Zurn Gear type coupling formed two vectors that were 1915 rows by 1 column for the parallel offset misalignment and the angular misalignment, and a matrix 1915 rows by two columns for the model that predicts both parallel offset and angular misalignments.

The parallel offset misalignment model regressed the model to an average error of 1.22×10^{-13} mils. The regressed MSE was 2.30×10^{-26}. The parallel offset misalignment model predicted the misalignment to an average error of 7.34 mils. The predicted MSE was 70.91.

The angular misalignment model regressed the model to an average error of 8.01×10^{-14} mils/inch. The regressed MSE was 8.65×10^{-27}. The angular misalignment model predicted the misalignment to an average error of 3.97 mils/inch. The predicted MSE was 21.19.

The model that regressed both the parallel offset misalignment and the angular misalignment regressed the parallel portion to an average error of 1.40×10^{-14} mils and the angular portion to an average error of 8.74×10^{-14} mils/inch. The regressed MSE was 2.76×10^{-26} for the parallel and 1.11×10^{-26} for the angular. The joint misalignment model predicted the parallel offset misalignment to an average error of 7.34 mils and the angular misalignment to an

average error of 3.97 mils/inch. The predicted MSE for the parallel was 70.91 and for the angular was 21.19.

The angular model was the best model for the gear type coupling. Figure 4.2 shows the prediction for the angular model on the test data.

4.2.3 Results for Grid Type Coupling

The weights for the Dodge Grid type coupling formed two vectors that were 1358 rows by 1 column for the parallel offset misalignment and the angular misalignment, and a matrix 1358 rows by two columns for the model that predicts both parallel offset and angular misalignments.

The parallel offset misalignment model regressed the model to an average error of 2.27 x 10^{-13} mils. The regressed MSE was 6.67 x 10^{-26}. The parallel offset misalignment model predicted the misalignment to an average error of 3.04 mils. The predicted MSE was 13.14.

The angular misalignment model regressed the model to an average error of 7.42 x 10^{-14} mils/inch. The regressed MSE was 6.48 x 10^{-27}. The angular misalignment model predicted the misalignment to an average error of 0.93 mils/inch. The predicted MSE was 1.23.

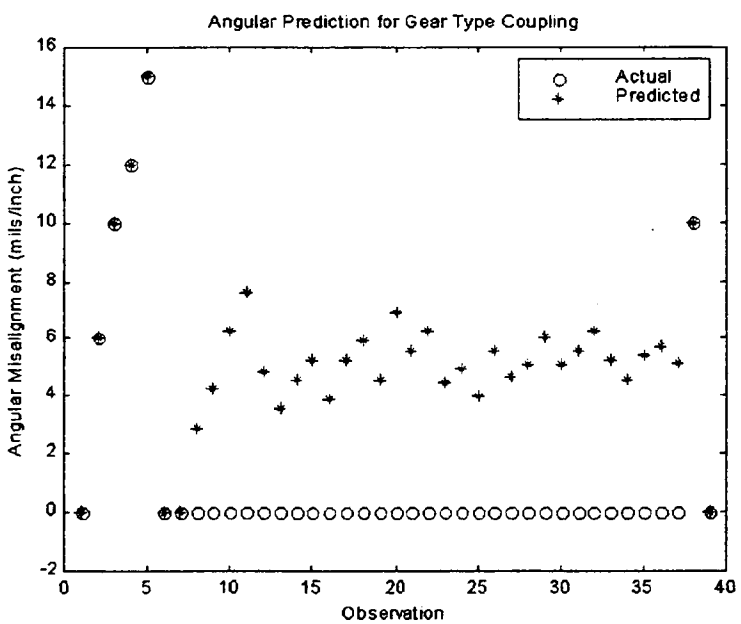


Figure 4.2. MLR Angular Prediction for Gear type coupling.

The model that regressed both the parallel offset misalignment and the angular misalignment regressed the parallel portion to an average error of 1.57×10^{-13} mils and the angular portion to an average error of 9.95×10^{-14} mils/inch. The regressed MSE was 3.43×10^{-26} for the parallel and 1.09×10^{-26} for the angular. The joint misalignment model predicted the parallel offset misalignment to an average error of 3.04 mils and the angular misalignment to an average error of 0.93 mils/inch. The predicted MSE for the parallel was 13.14 and for the angular was 1.23.

The angular model was the best model for the grid type coupling. Figure 4.3 shows the prediction for the angular model on the test data.

4.3 Results from Linear Correlation Neural Network

The most highly linearly correlated frequencies for the parallel and angular misalignment conditions were determined for each of the three couplings. Three ANN's were trained for each of the couplings. One for the parallel offset misalignment, one for the angular misalignment, and one for both the parallel offset misalignment and the angular misalignment at the same time. The Levenberq-Marquarht training algorithm was used to train an ANN with 6 hidden neurons in a

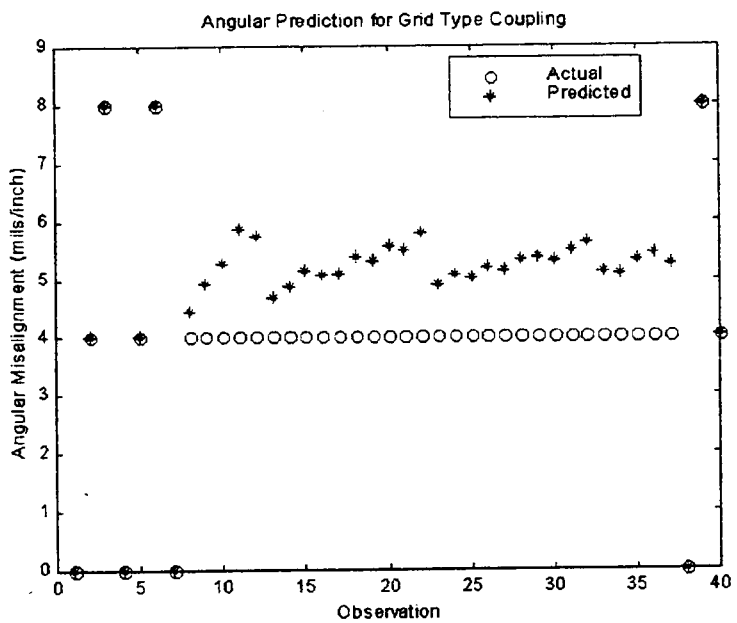


Figure 4.3. MLR Angular Prediction for Grid type coupling.

hyperbolic tangential hidden layer with a linear output layer to an error goal using cross validation training to try to reduce the MSE of the training data to zero but to stop training when the error in the validation training reached a minimum so as to not overfit the data. The average error was calculated by taking the mean of the absolute values of the difference between the predicted alignment conditions and the actual alignment conditions. Then the MSE's were also calculated. The graphs of the training and the prediction are given in Appendix A.

4.3.1 Results for Elastomer Type Coupling

The thirty most highly correlated frequencies to the parallel offset misalignment condition for the elastomer type coupling are shown in Table 4.4. These frequencies were used to train the parallel ANN.

The parallel offset misalignment network trained the model to an average error of 26.01 mils. The trained MSE was 1.5×10^3. The parallel offset misalignment network predicted the misalignment to an average error of 11.87 mils. The predicted MSE was 405.18.

The thirty most highly correlated frequencies to the angular misalignment condition are shown in Table 4.5.

The angular misalignment network trained to an average error of 3.04 mils/inch. The trained MSE was 28.9. The angular misalignment model predicted the misalignment to an average error of 3.04 mils/inch. The predicted MSE was 34.01.

The network that trained both the parallel offset misalignment and the angular misalignment learned the combination of the above frequencies for the parallel portion to an average error of 15.99 mils and the angular portion to an average error of 7.38 mils/inch. The trained MSE was 385.86 for the parallel and 100.53 for the angular. The joint misalignment network predicted the parallel offset misalignment to an average error of 17.09 mils and the angular misalignment to an average error of 5.91 mils/inch. The predicted MSE for the parallel was 350.02 and for the angular was 73.34.

The angular model was the best model for the elastomer type coupling. Figure 4.4 shows the prediction for the angular model on the test data.

Table 4.4 Parallel Frequencies for Elastomer type coupling.

	Frequency (Hz)
1	19
2	119
3	178
4	180
5	473
6	487
7	522
8	530
9	553
10	726
11	757
12	778
13	925
14	1012
15	1017
16	1216
17	1275
18	1314
19	1357
20	1397
21	1417
22	1484
23	1492
24	1521
25	1526
26	1570
27	1626
28	1643
29	1815
30	1927

Table 4.5 Angular Frequencies for Elastomer type coupling.

	Frequency (Hz)
1	41
2	67
3	70
4	100
5	103
6	113
7	117
8	118
9	177
10	199
11	221
12	223
13	226
14	691
15	696
16	807
17	983
18	992
19	993
20	1238
21	1242
22	1247
23	1320
24	1383
25	1435
26	1478
27	1550
28	1678
29	1710
30	1845

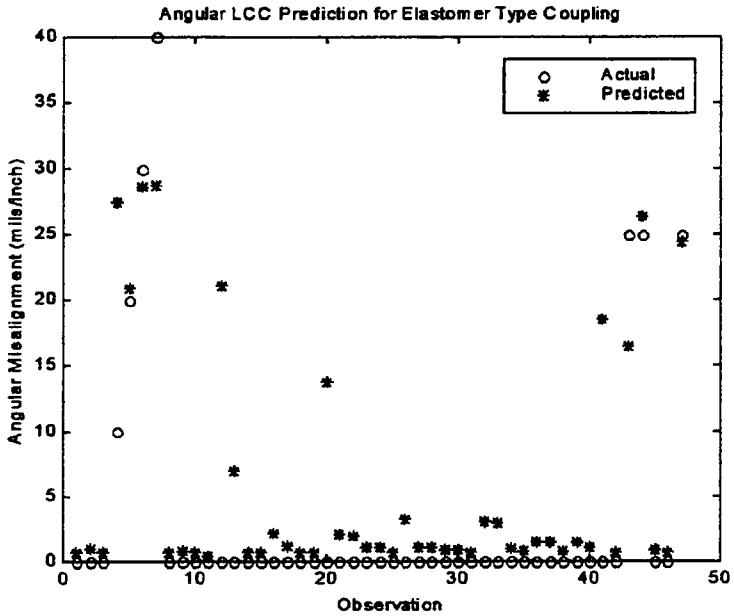


Figure 4.4. LCC ANN Angular Prediction for Elastomer type coupling.

4.3.2 Results for Gear Type Coupling

The thirty most highly correlated frequencies to the parallel offset misalignment condition for the Gear type coupling are shown in Table 4.6.

The parallel offset misalignment network trained the model to an average error of 6.29 mils. The trained MSE was 81.45. The parallel offset misalignment network predicted the misalignment to an average error of 4.22 mils. The predicted MSE was 28.99.

The thirty most highly correlated frequencies to the angular misalignment condition are shown in Table 4.7.

The angular misalignment network trained to an average error of 0.17 mils/inch. The trained MSE was 6.35×10^{-2}. The angular misalignment model predicted the misalignment to an average error of 0.13 mils/inch. The predicted MSE was 6.35×10^{-2}.

Table 4.6 Parallel Frequencies for Gear type coupling.

	Frequency (Hz)
1	61
2	732
3	734
4	736
5	740
6	744
7	856
8	860
9	874
10	878
11	910
12	1125
13	1183
14	1261
15	1323
16	1324
17	1325
18	1326
19	1327
20	1328
21	1334
22	1380
23	1391
24	1554
25	1753
26	1754
27	1766
28	1800
29	1801
30	1802

Table 4.7 Angular Frequencies for Gear type coupling.

	Frequency (Hz)
1	277
2	278
3	279
4	280
5	282
6	283
7	285
8	286
9	351
10	372
11	373
12	377
13	378
14	387
15	388
16	389
17	392
18	393
19	395
20	396
21	397
22	398
23	404
24	405
25	407
26	529
27	826
28	1234
29	1300
30	1713

The network that trained both the parallel offset misalignment and the angular misalignment learned the combination of the above frequencies for the parallel portion to an average error of 6.03 mils and the angular portion to an average error of 1.38 mils/inch. The trained MSE was 53.74 for the parallel and 3.75 for the angular. The joint misalignment network predicted the parallel offset misalignment to an average error of 3.52 mils and the angular misalignment to an average error of 1.57 mils/inch. The predicted MSE for the parallel was 24.11 and for the angular was 7.27.

The angular model was the best model for the gear type coupling. Figure 4.5 shows the prediction for the angular model on the test data.

4.3.3 Results for Grid Type Coupling

The thirty most highly correlated frequencies to the parallel offset misalignment condition for the Grid type coupling are shown in Table 4.8.

The parallel offset misalignment network trained the model to an average error of 1.37 mils. The trained MSE was 2.61. The parallel offset misalignment network predicted the misalignment to an average error of 2.03 mils. The predicted MSE was 6.07.

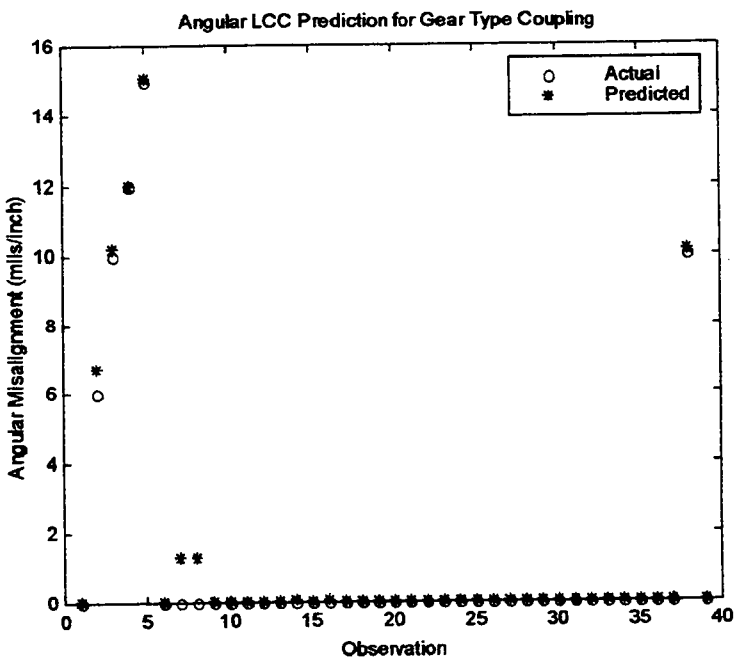


Figure 4.5. LCC ANN Angular Prediction for Gear type coupling.

Table 4.8 Parallel Frequencies for Grid type coupling.

	Frequency (Hz)
1	98
2	102
3	103
4	104
5	105
6	106
7	108
8	114
9	115
10	129
11	132
12	133
13	134
14	138
15	159
16	182
17	184
18	197
19	203
20	208
21	220
22	222
23	223
24	226
25	323
26	606
27	901
28	1066
29	1931
30	2446

The thirty most highly correlated frequencies to the angular misalignment condition are shown in Table 4.9.

The angular misalignment network trained to an average error of 0.49 mils/inch. The trained MSE was 0.57. The angular misalignment model predicted the misalignment to an average error of 0.31 mils/inch. The predicted MSE was 0.23.

The network that trained both the parallel offset misalignment and the angular misalignment learned the combination of the above frequencies for the parallel portion to an average error of 1.39 mils and the angular portion to an average error of 0.99 mils/inch. The trained MSE was 3.94 for the parallel and 1.55 for the angular. The joint misalignment network predicted the parallel offset misalignment to an average error of 2.82 mils and the angular misalignment to an average error of 1.45 mils/inch. The predicted MSE for the parallel was 11.05 and for the angular was 2.51.

The angular model was the best model for the grid type coupling. Figure 4.6 shows the prediction for the angular model on the test data.

4.4 Results from Principal Component Neural Network

The amount of variables in the input matrices was reduced by using a larger tolerance above which to keep. Then a PCA was performed on the mean centered input matrices and the amount of information was plotted to show the overall usefulness of each PC. Then most highly linearly correlated principal components for the parallel and angular misalignment conditions were determined for each of the three couplings. Three ANN's were trained for each of the couplings. One for the parallel offset misalignment, one for the angular misalignment, and one for both the parallel offset misalignment and the angular misalignment at the same time using the largest PC's. The Levenberq-Marquarht training algorithm was used to train an ANN with 6 hidden neurons in a hyperbolic tangential hidden layer with a linear output layer to an error goal using cross validation training to try to reduce the MSE of the training data to zero but to stop training when the error in the validation training reached a minimum so as to not overfit the data. The average error was calculated by taking the mean of the absolute values of the difference between the predicted alignment conditions and the actual alignment conditions. Then the MSE's and the SSE's were also calculated. These results are graphed in Appendix A.

Table 4.9 Angular Frequencies for Grid type coupling.

	Frequency (Hz)
1	600
2	664
3	744
4	745
5	840
6	865
7	969
8	985
9	1080
10	1122
11	1124
12	1140
13	1203
14	1225
15	1242
16	1320
17	1360
18	1440
19	1478
20	1585
21	1668
22	1680
23	1705
24	1713
25	1800
26	1912
27	1949
28	2264
29	2467
30	2760

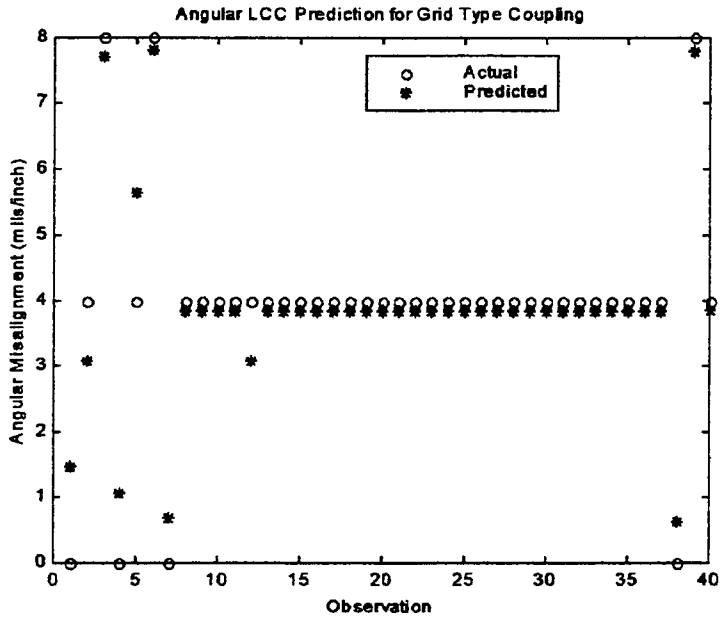


Figure 4.6. LCC ANN Angular Prediction for Grid type coupling.

4.4.1 Results for Elastomer Type Coupling

A tolerance of 0.95 watts was used to reduce the number of variables for the elastomer type coupling to less than the number of observations. The plot of the amount of information contained in each of the Principle Components for the elastomer type coupling is shown in Figure 4.7.

The three most highly linearly correlated PC's to the parallel offset misalignment condition are the 2^{cd}, 3rd, and 5th ones. The parallel offset misalignment network trained on them to an average error of 18.99 mils. The trained MSE was 575.21. The parallel offset misalignment network predicted the misalignment to an average error of 21.1 mils. The predicted MSE was 539.01.

The three most highly linearly correlated PC's to the angular misalignment condition are the 1st, 4th, and 6th ones. The angular misalignment network trained on them to an average error of 6.31 mils/inch. The trained MSE was 68.45. The angular misalignment model predicted the misalignment to an average error of 3.72 mils/inch. The predicted MSE was 31.22.

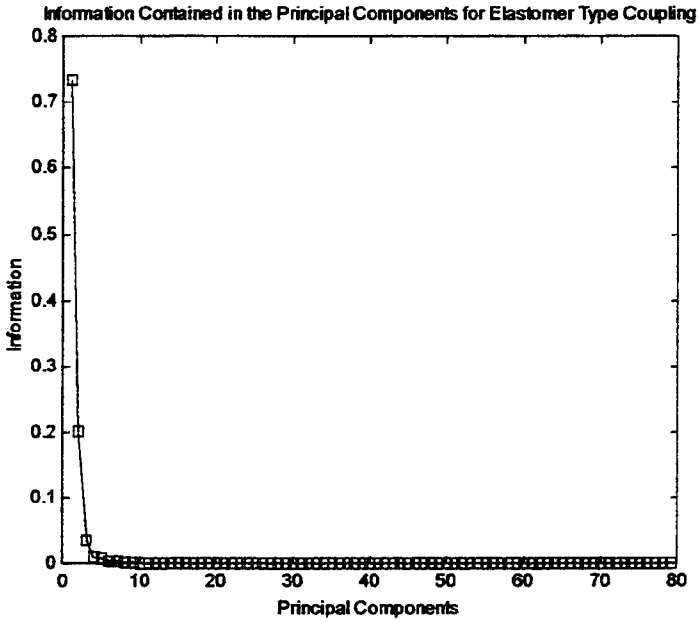


Figure 4.7 Information contained in each PC for Elastomer type coupling.

The network that trained both the parallel offset misalignment and the angular misalignment learned the six largest PC's for the parallel portion to an average error of 23.99 mils and the angular portion to an average error of 12.42 mils/inch. The trained MSE was 792.78 for the parallel and 233.97 for the angular. The joint misalignment network predicted the parallel offset misalignment to an average error of 16.44 mils and the angular misalignment to an average error of 6.04 mils/inch. The predicted MSE for the parallel was 400.14 and for the angular was 90.05.

The angular model was the best model for the grid type coupling. Figure 4.8 shows the prediction for the angular model on the test data.

4.4.2 Results for Gear Type Coupling

A tolerance of 2.00 watts was used for the Gear type coupling to reduce the number of variables to less than the number of observations. The plot of the amount of information contained in each of the Principle Components for the gear type coupling is shown in Figure 4.9.

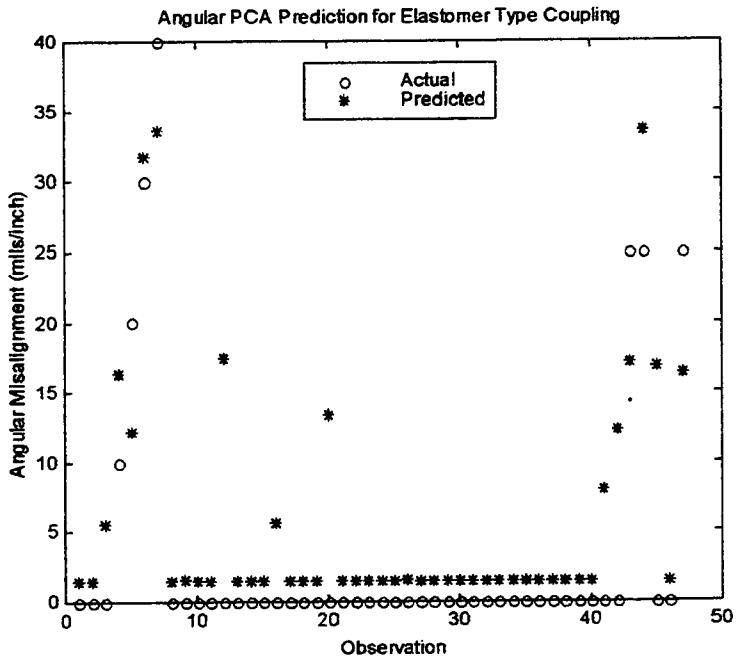


Figure 4.8. PCA ANN Angular Prediction for Elastomer type coupling.

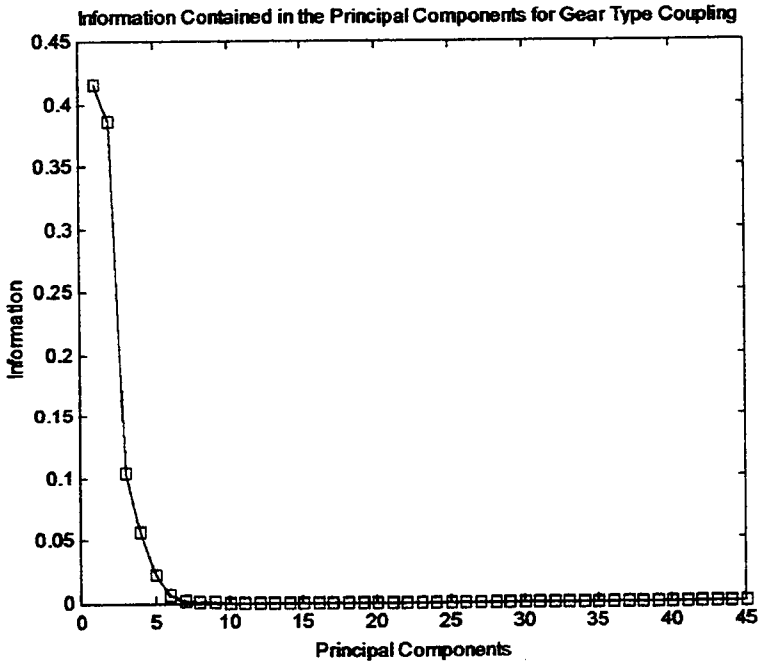


Figure 4.9 Information contained in each PC for Gear type coupling.

The three most highly linearly correlated PC's to the parallel offset misalignment condition for the gear type coupling are the 1st, 3rd, and 4th ones. The parallel offset misalignment network trained on them to an average error of 5.68 mils. The trained MSE was 69.72. The parallel offset misalignment network predicted the misalignment to an average error of 2.71 mils. The predicted MSE was 16.8.

The three most highly correlated PC's to the angular misalignment condition are the 2cd, 5th, and 6th ones. The angular misalignment network trained on them to an average error of 2.5 mils/inch. The trained MSE was 13.96. The angular misalignment model predicted the misalignment to an average error of 0.84mils/inch. The predicted MSE was 3.41.

The network that trained both the parallel offset misalignment and the angular misalignment learned the six largest PC's for the parallel portion to an average error of 9.77 mils and the angular portion to an average error of 4.87 mils/inch. The trained MSE was 123.2 for the parallel and 31.25 for the angular. The joint misalignment network predicted the parallel offset misalignment to an average error of 13.52 mils and the angular misalignment to an average error of 3.73 mils/inch. The predicted MSE for the parallel was 244.97 and for the angular was 18.83.

The angular model was the best model for the grid type coupling. Figure 4.10 shows the prediction for the angular model on the test data.

4.4.3 Results for Grid Type Coupling

A tolerance of 0.85 watts was used to reduce the number of variables for the Grid type coupling to less than the number of observations. The plot of the amount of information contained in each of the Principle Components for the grid type coupling is shown in Figure 4.11.

The three most highly correlated PC's to the parallel offset misalignment condition are the 2cd, 3rd, and 5th ones. The parallel offset misalignment network trained on them to an average error of 3.03 mils. The trained MSE was 16.65. The parallel offset misalignment network predicted the misalignment to an average error of 3.09 mils. The predicted MSE was 11.15.

The three most highly correlated PC's to the angular misalignment condition are the 1st, 4th, and 6th ones. The angular misalignment network trained on them to an average error of 2.18 mils/inch. The trained MSE was 5.81. The angular misalignment model predicted the misalignment to an average error of 1.65 mils/inch. The predicted MSE was 3.35.

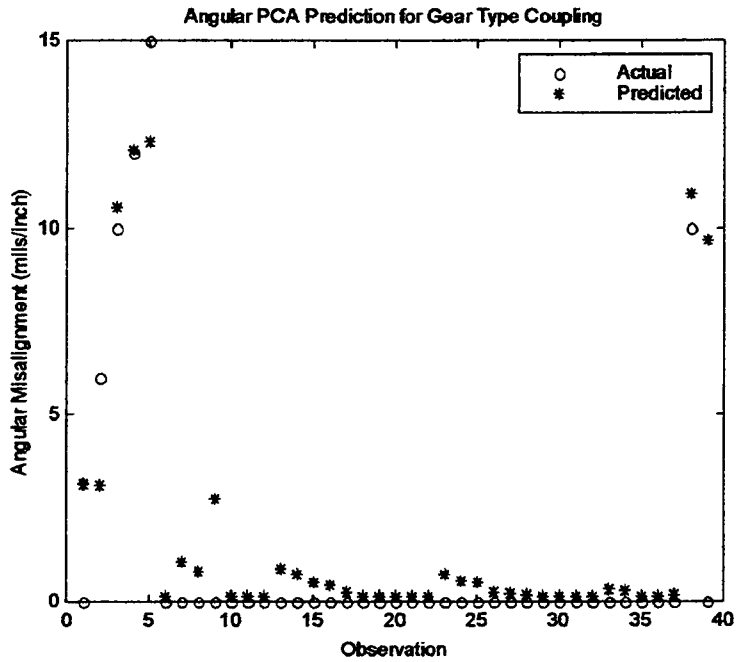


Figure 4.10. PCA ANN Angular Prediction for Gear type coupling

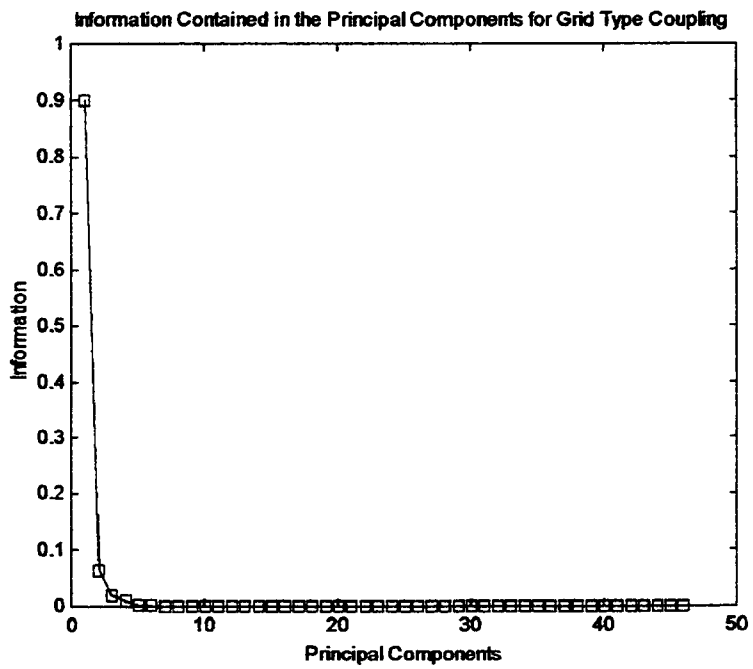


Figure 4.11 Information contained in each PC for the Grid type coupling.

The network that trained both the parallel offset misalignment and the angular misalignment learned the six largest PC's for the parallel portion to an average error of 3.47 mils and the angular portion to an average error of 1.69 mils/inch. The trained MSE was 17.43 for the parallel and 4.3 for the angular. The joint misalignment network predicted the parallel offset misalignment to an average error of 4.18 mils and the angular misalignment to an average error of 0.79 mils/inch. The predicted MSE for the parallel was 18.9 and for the angular was 1.85

The angular prediction for the joint model was best for the grid type coupling. Figure 4.12 shows the prediction for the joint model on the test data.

4.5 Results from Partial Least Squares Linear Model

The number of PLS factors that contained information was determined for each of the three couplings using the magnitudes of the reduced eigenvalues. Three Linear PLS models were created for each of the couplings. One for the parallel offset misalignment, one for the angular misalignment, and one for both the parallel offset misalignment and the angular misalignment at

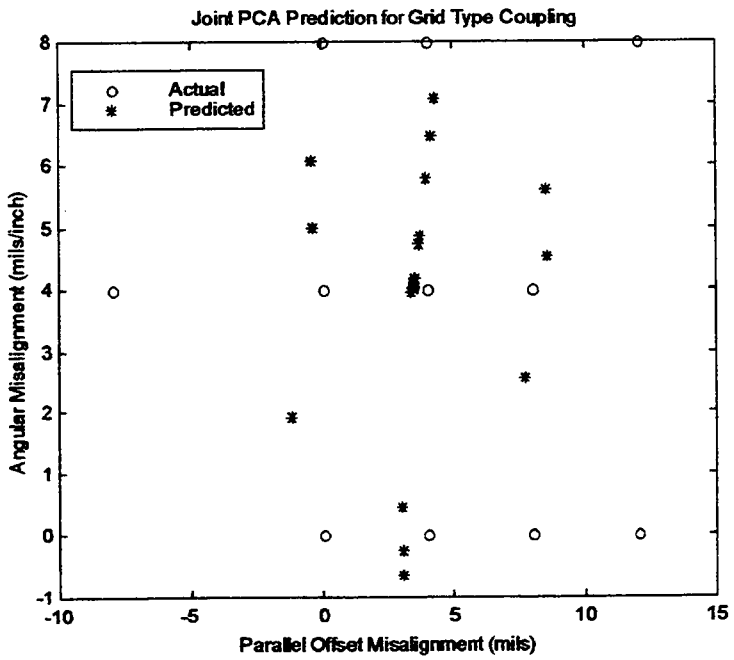


Figure 4.12. PCA ANN Joint Prediction for Grid type coupling

the same time using the useful PLS factors. Then, the models were tested to see how many of the PLS factors resulted in the smallest average error for the test data. Then three more LPLS models were created with the optimal number of PLS factors. The average error was calculated by taking the mean of the absolute values of the difference between the predicted alignment conditions and the actual alignment conditions. These results are graphed in Appendix A.

4.5.1 Results for Elastomer Type Coupling

The magnitudes of the reduced eigenvalues were plotted on a semi-log scale to show how many of the PLS factors contained the majority of the information relating the frequency spectrum to the misalignment conditions. Figure 4.13 shows this relationship. This analysis showed that there were 79 useful PLS factors in the elastomer type coupling set.

The parallel offset misalignment PLS model using all 79 PLS factors regressed the model to an average error of 3.74×10^{-13} mils. The regressed MSE was 1.65×10^{-25}. The parallel offset misalignment network predicted the misalignment to an average error of 25.15 mils. The predicted MSE was 1.01×10^{3}.

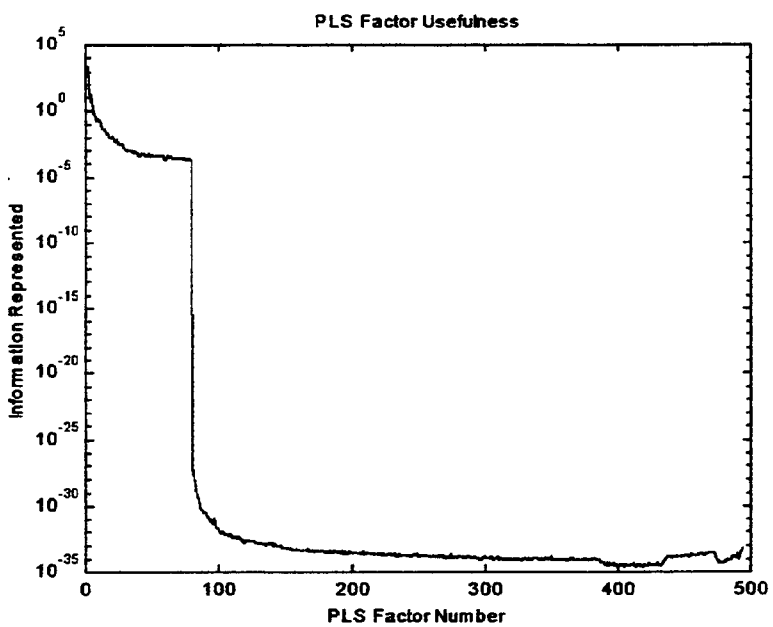


Figure 4.13 Information contained in PLS factors for Elastomer type coupling.

The PLS model was tested by iteratively adding another PLS factor to the model to determine the optimal number of factors to reduce the average error. Figure 4.14 shows the relationship between the number of PLS factors and the average prediction error for training data and the test data for the parallel PLS model. This analysis showed that 21 PLS factors was the optimal number for the parallel model of the elastomer type coupling set.

The parallel offset misalignment PLS model using 21 PLS factors regressed the model to an average error of 1.23 mils. The regressed MSE was 2.84. The parallel offset misalignment model predicted the misalignment to an average error of 23.18 mils. The predicted MSE was 805.94.

The angular misalignment PLS model using all 79 PLS factors regressed the model to an average error of 9.46×10^{-14} mils/inch. The regressed MSE was 1.54×10^{-26}. The angular misalignment model predicted the misalignment to an average error of 2.99 mils/inch. The predicted MSE was 18.75.

The PLS model was tested by iteratively adding another PLS factor to the model to determine the optimal number of factors to reduce the average error. Figure 4.15 shows the

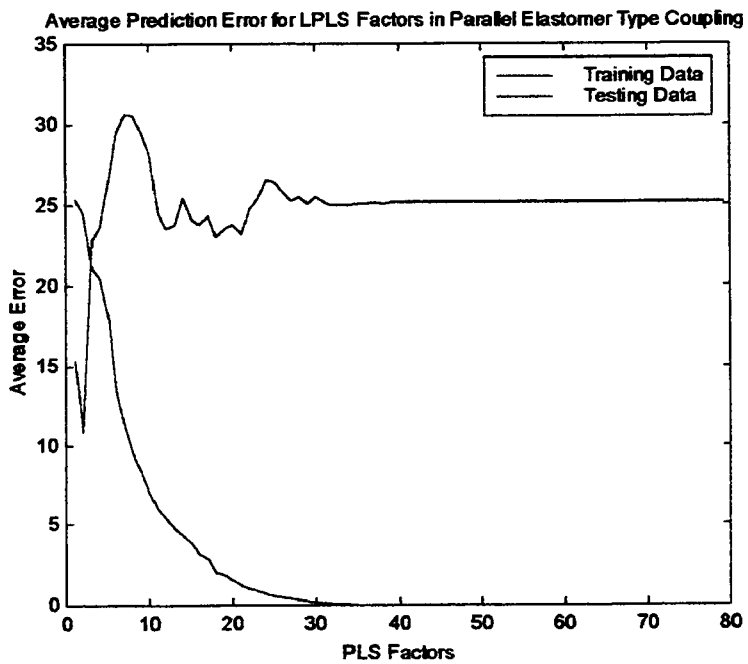


Figure 4.14. Parallel errors for PLS factors for elastomer type coupling.

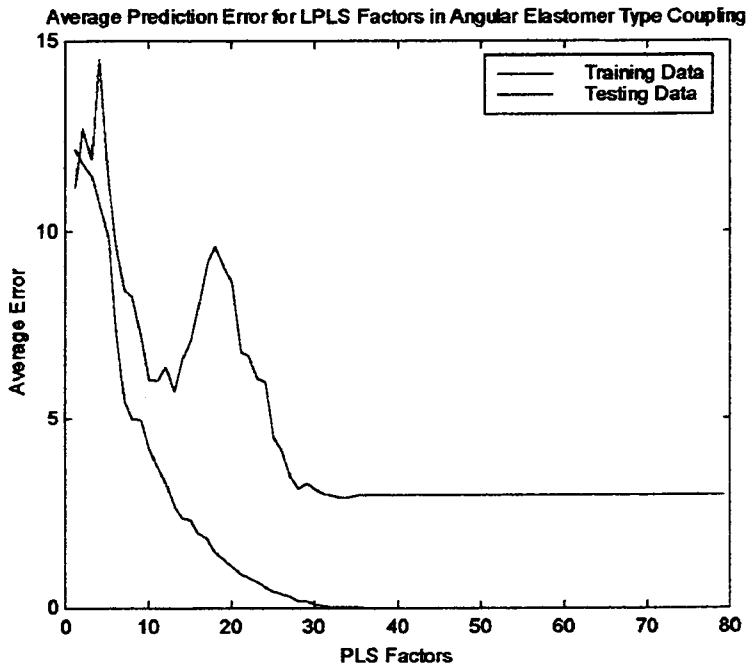


Figure 4.15. Angular errors for PLS factors for elastomer type coupling.

relationship between the number of PLS factors and the average prediction error for the training data and the test data for the angular PLS model. This analysis showed that 34 PLS factors was the optimal number for the angular model of the elastomer type coupling set.

The angular misalignment PLS model using 34 PLS factors regressed the model to an average error of 0.03 mils/inch. The regressed MSE was 2.0×10^{-3}. The angular misalignment model predicted the misalignment to an average error of 2.92 mils/inch. The predicted MSE was 17.66.

The joint misalignment PLS model using all 79 PLS factors regressed the model to an average error 1.14×10^{-13} mils for the parallel offset condition and an average error of 4.61×10^{-14} mils/inch for the angular condition. The regressed MSE was 2.31×10^{-26} and 3.05×10^{-27} for the parallel and angular conditions respectively. The joint misalignment PLS model using all 79 PLS factors predicted the alignment to an average error 25.15 mils for the parallel offset condition and an average error of 2.99 mils/inch for the angular condition. The predicted MSE was 1.01×10^{3} and 18.8 for the parallel and angular conditions respectively.

The PLS model was tested by iteratively adding another PLS factor to the model to determine the optimal number of factors to reduce the average error. Figure 4.16 shows the

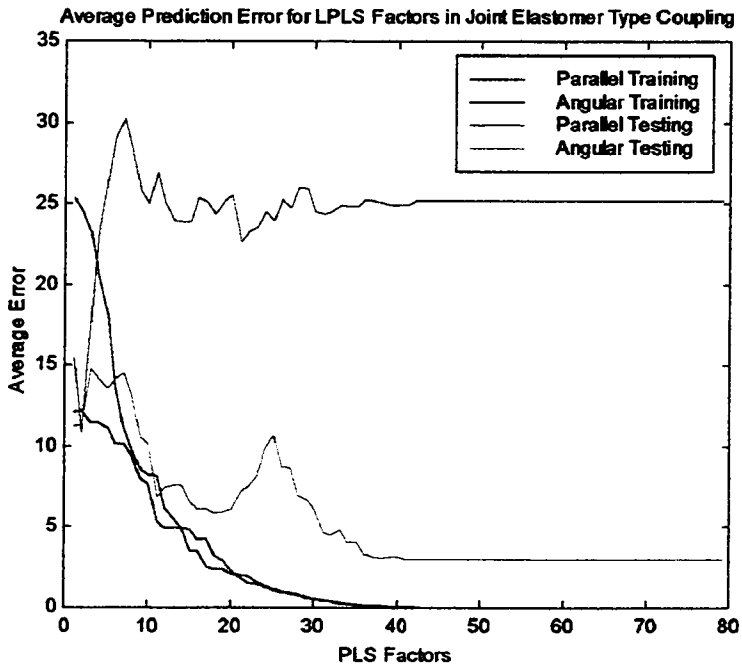


Figure 4.16. Joint errors for PLS factors for elastomer type coupling.

relationship between the number of PLS factors and the average prediction error for the training and the test data for the joint PLS model. This analysis showed that 41 PLS factors was the optimal number for the joint model of the elastomer type coupling set.

The joint misalignment PLS model using 41 PLS factors regressed the model to an average error 0.06 mils for the parallel offset condition and an average error 0.05 mils/inch for the angular condition. The regressed MSE was 8.9×10^{-3} and 4.1×10^{-3} for the parallel and angular conditions respectively. The joint misalignment PLS model using 41 PLS factors predicted the alignment to an average error 24.93 mils for the parallel offset condition and an average error of 2.99 mils/inch for the angular condition. The predicted MSE was 994.97 and 18.26 for the parallel and angular conditions respectively.

The angular optimal LPLS model was best for the elastomer type coupling. Figure 4.17 shows the prediction for the angular model on the test data.

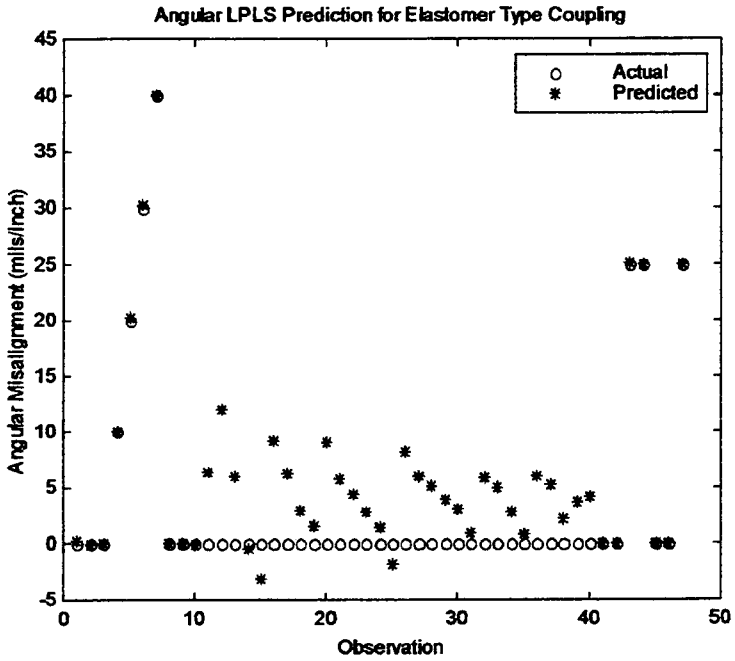


Figure 4.17. LPLS Angular Prediction for Elastomer type coupling

4.5.2 Results for Gear Type Coupling

The magnitudes of the reduced eigenvalues were plotted on a semi-log scale to show how many of the PLS factors contained the majority of the information relating the frequency spectrum to the misalignment conditions. Figure 4.18 shows this relationship. This analysis showed that there were 45 useful PLS factors in the elastomer type coupling set.

The parallel offset misalignment PLS model using all 45 PLS factors regressed the model to an average error of 4.43×10^{-14} mils. The regressed MSE was 3.04×10^{-27}. The parallel offset misalignment network predicted the misalignment to an average error of 7.34 mils. The predicted MSE was 70.91.

The PLS model was tested by iteratively adding another PLS factor to the model to determine the optimal number of factors to reduce the average error. Figure 4.19 shows the relationship between the number of PLS factors and the average prediction error for training data and the test data for the parallel PLS model.

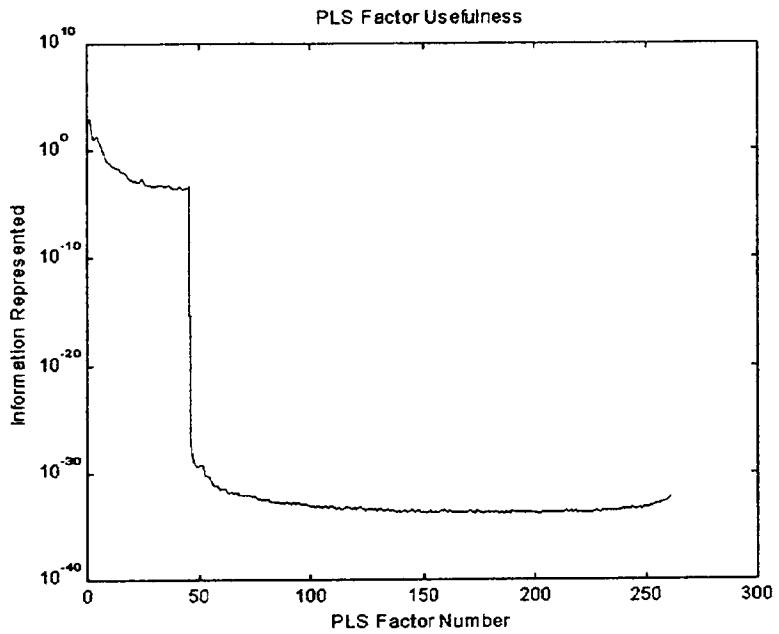


Figure 4.18 Information contained in PLS factors for Gear type coupling.

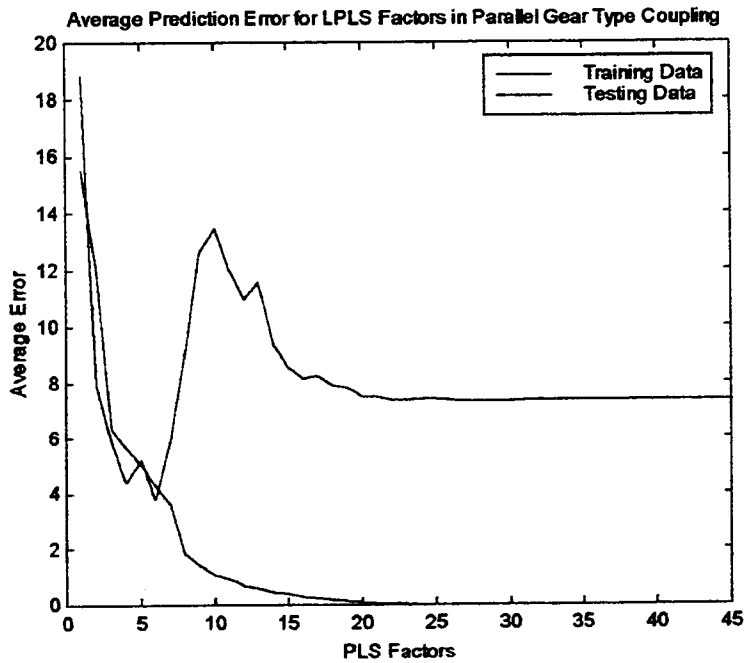


Figure 4.19. Parallel errors for PLS factors for Gear type coupling.

This analysis showed that 20 PLS factors was the optimal number for the parallel model of the elastomer type coupling set.

The parallel offset misalignment PLS model using 20 PLS factors regressed the model to an average error of 8.24×10^{-2} mils. The regressed MSE was 1.28×10^{-2}. The parallel offset misalignment model predicted the misalignment to an average error of 7.89 mils. The predicted MSE was 78.54.

The angular misalignment PLS model using all 45 PLS factors regressed the model to an average error of 2.55×10^{-14} mils/inch. The regressed MSE was 1.11×10^{-27}. The angular misalignment model predicted the misalignment to an average error of 3.97 mils/inch. The predicted MSE was 21.19.

The PLS model was tested by iteratively adding another PLS factor to the model to determine the optimal number of factors to reduce the average error. Figure 4.20 shows the relationship between the number of PLS factors and the average prediction error for the training data and the test data for the angular PLS model. This analysis showed that 9 PLS factors was the optimal number for the angular model of the gear type coupling set.

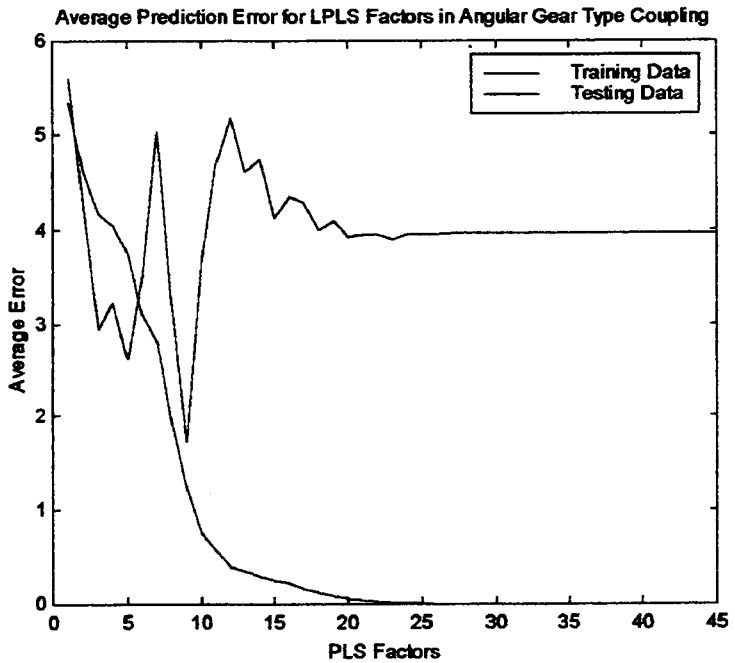


Figure 4.20. Angular errors for PLS factors for Gear type coupling.

The angular misalignment PLS model using 9 PLS factors regressed the model to an average error of 1.23 mils/inch. The regressed MSE was 2.73. The angular misalignment model predicted the misalignment to an average error of 1.72 mils/inch. The predicted MSE was 5.86.

The joint misalignment PLS model using all 45 PLS factors regressed the model to an average error 3.85×10^{-14} mils for the parallel offset condition and an average error of 8.22×10^{-15} mils/inch for the angular condition. The regressed MSE was 2.24×10^{-27} and 1.11×10^{-28} for the parallel and angular conditions respectively. The joint misalignment PLS model using all 45 PLS factors predicted the alignment to an average error 7.34 mils for the parallel offset condition and an average error of 3.97 mils/inch for the angular condition. The predicted MSE was 70.91 and 21.19 for the parallel and angular conditions respectively.

The PLS model was tested by iteratively adding another PLS factor to the model to determine the optimal number of factors to reduce the average error. Figure 4.21 shows the relationship between the number of PLS factors and the average prediction error for the training and the test data for the joint PLS model. This analysis showed that 18 PLS factors was the optimal number for the joint model of the gear type coupling set.

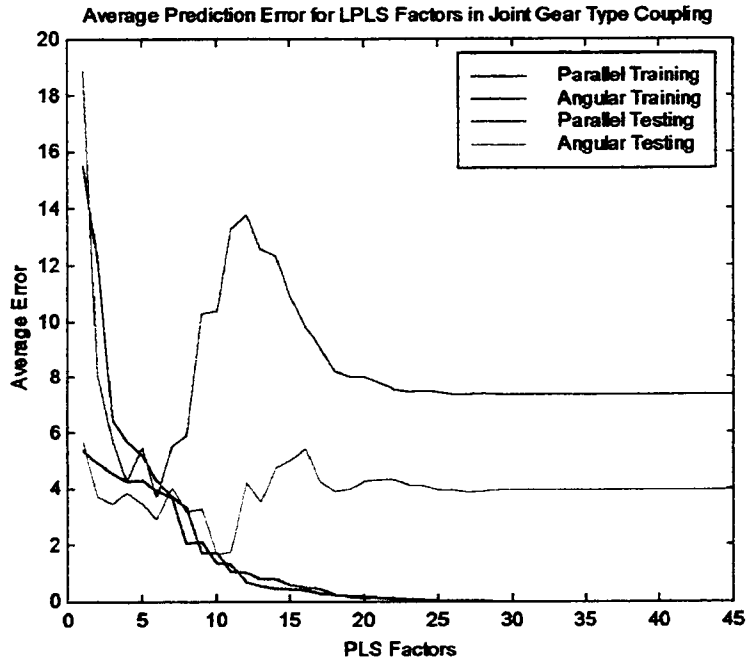


Figure 4.21. Joint errors for PLS factors for Gear type coupling.

The joint misalignment PLS model using 18 PLS factors regressed the model to an average error 0.26 mils for the parallel offset condition and an average error 0.25 mils/inch for the angular condition. The regressed MSE was 0.15 and 0.11 for the parallel and angular conditions respectively. The joint misalignment PLS model using 18 PLS factors predicted the alignment to an average error 7.34 mils for the parallel offset condition and an average error of 3.97 mils/inch for the angular condition. The predicted MSE was 70.91 and 21.19 for the parallel and angular conditions respectively

The angular optimal LPLS model was best for the gear type coupling. Figure 4.22 shows the prediction for the angular model on the test data.

4.5.3 Results for Grid Type Coupling

The magnitudes of the reduced eigenvalues were plotted on a semi-log scale to show how many of the PLS factors contained the majority of the information relating the frequency spectrum to the misalignment conditions. Figure 4.23 shows this relationship. This analysis showed that there were 46 useful PLS factors in the grid type coupling set.

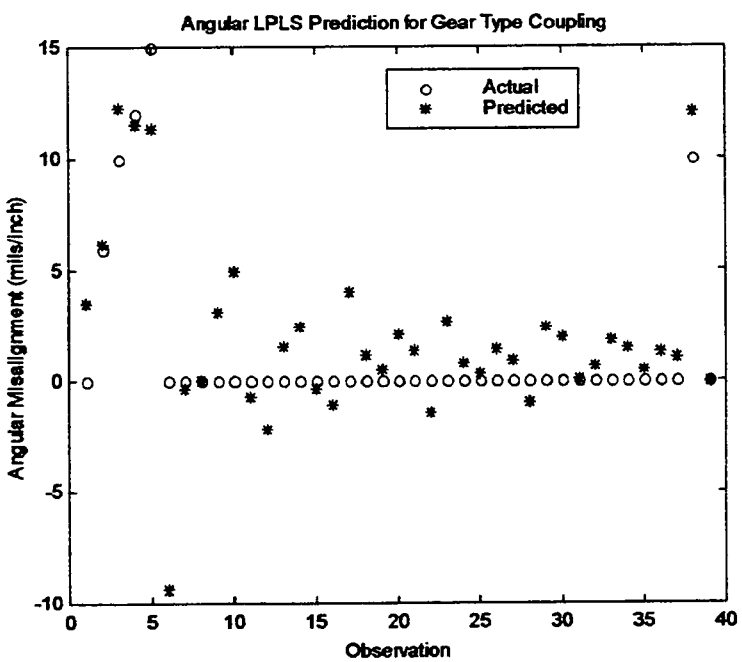


Figure 4.22. LPLS Angular Prediction for Gear type coupling

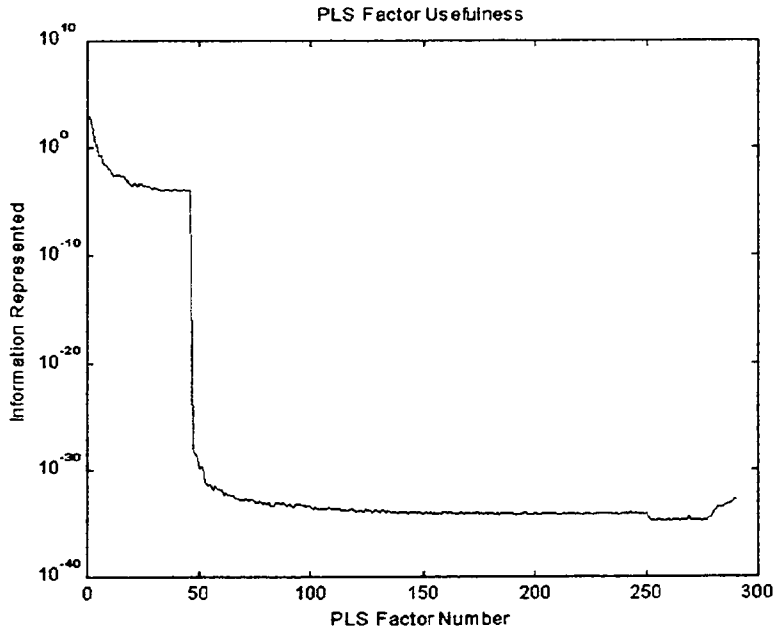


Figure 4.23 Information contained in PLS factors for Grid type coupling.

The parallel offset misalignment PLS model using all 46 PLS factors regressed the model to an average error of 1.71×10^{-14} mils. The regressed MSE was 4.35×10^{-28}. The parallel offset misalignment network predicted the misalignment to an average error of 3.04 mils. The predicted MSE was 13.14.

The PLS model was tested by iteratively adding another PLS factor to the model to determine the optimal number of factors to reduce the average error. Figure 4.24 shows the relationship between the number of PLS factors and the average prediction error for training data and the test data for the parallel PLS model. This analysis showed that 17 PLS factors was the optimal number for the parallel model of the grid type coupling set.

The parallel offset misalignment PLS model using 17 PLS factors regressed the model to an average error of 0.11 mils. The regressed MSE was 2.16×10^{-2}. The parallel offset misalignment model predicted the misalignment to an average error of 2.87 mils. The predicted MSE was 11.32.

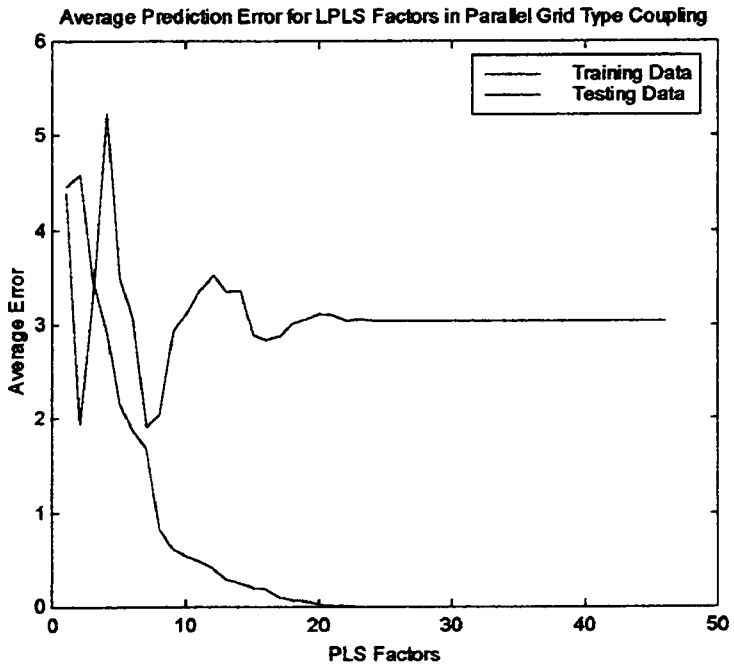


Figure 4.24. Parallel errors for PLS factors for Grid type coupling.

The angular misalignment PLS model using all 46 PLS factors regressed the model to an average error of 8.97×10^{-15} mils/inch. The regressed MSE was 4.35×10^{-28}. The angular misalignment model predicted the misalignment to an average error of 0.93 mils/inch. The predicted MSE was 1.23.

The PLS model was tested by iteratively adding another PLS factor to the model to determine the optimal number of factors to reduce the average error. Figure 4.25 shows the relationship between the number of PLS factors and the average prediction error for the training data and the test data for the angular PLS model.

This analysis showed that 16 PLS factors was the optimal number for the angular model of the grid type coupling set.

The angular misalignment PLS model using 16 PLS factors regressed the model to an average error of .06 mils/inch. The regressed MSE was 8.3×10^{-3}. The angular misalignment model predicted the misalignment to an average error of 0.86 mils/inch. The predicted MSE was 0.94.

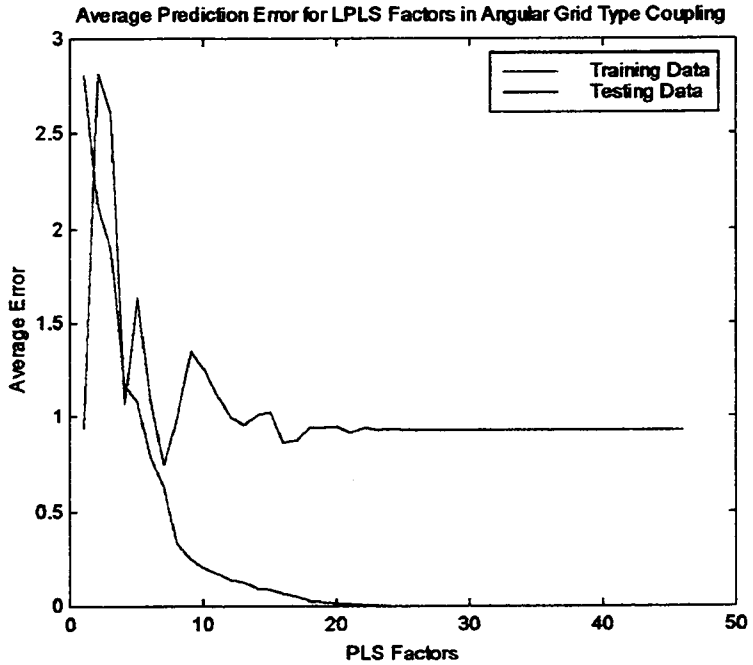


Figure 4.25. Angular errors for PLS factors for Grid type coupling.

The joint misalignment PLS model using all 46 PLS factors regressed the model to an average error 2.77×10^{-14} mils for the parallel offset condition and an average error of 5.78×10^{-15} mils/inch for the angular condition. The regressed MSE was 1.09×10^{-27} and 5.0×10^{-29} for the parallel and angular conditions respectively. The joint misalignment PLS model using all 46 PLS factors predicted the alignment to an average error 3.04 mils for the parallel offset condition and an average error of 0.93 mils/inch for the angular condition. The predicted MSE was 13.14 and 1.23 for the parallel and angular conditions respectively.

The PLS model was tested by iteratively adding another PLS factor to the model to determine the optimal number of factors to reduce the average error. Figure 4.26 shows the relationship between the number of PLS factors and the average prediction error for the training and the test data for the joint PLS model. This analysis showed that 16 PLS factors was the optimal number for the joint model of the grid type coupling set.

The joint misalignment PLS model using 16 PLS factors regressed the model to an average error 0.21 mils for the parallel offset condition and an average error 0.18 mils/inch for the angular condition. The regressed MSE was 8.16×10^{-2} and 6.23×10^{-2} for the parallel and angular conditions respectively. The joint misalignment PLS model using 16 PLS factors predicted the

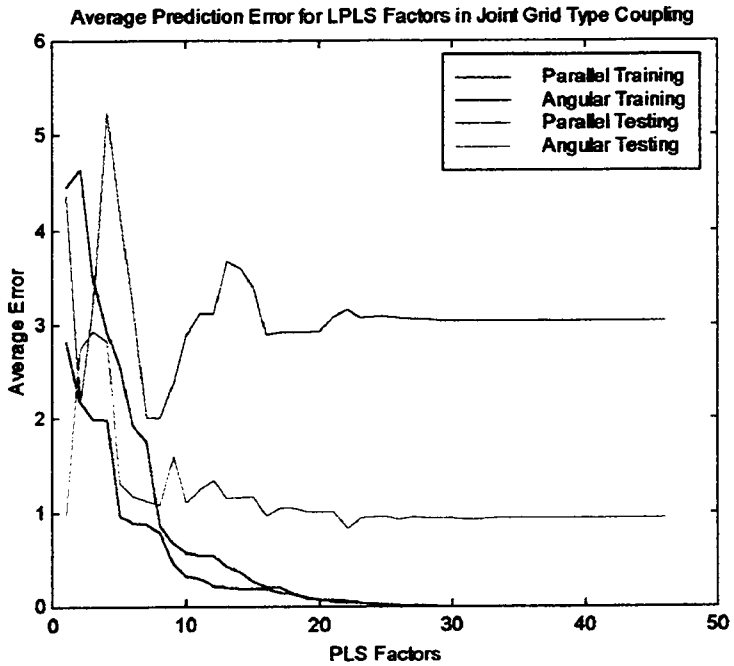


Figure 4.26. Joint errors for PLS factors for Grid type coupling.

alignment to an average error 2.9 mils for the parallel offset condition and an average error of 0.97 mils/inch for the angular condition. The predicted MSE was 10.87 and 1.07 for the parallel and angular conditions respectively.

The angular optimal LPLS model was best for the grid type coupling. Figure 4.27 shows the prediction for the angular model on the test data.

4.6 Results from Partial Least Squares Non-Linear Model

The Non-Linear Partial Least Squares (NLPLS) models were created with the same number of PLS factors that were found to contain information as in the LPLS model. These PLS factors were run through multiple ANN architectures to determine the best network for the inner relationship in the NLPLS model. Figure 4.28 shows the error curves for several of the network architectures. It was found that 15 hidden hyperbolic tangential neurons were necessary to map accurately map the non-linearities.

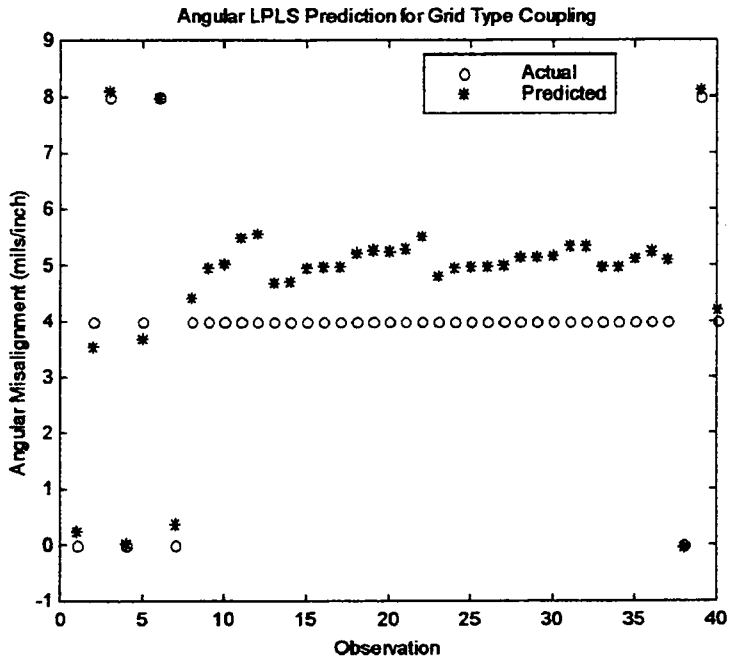
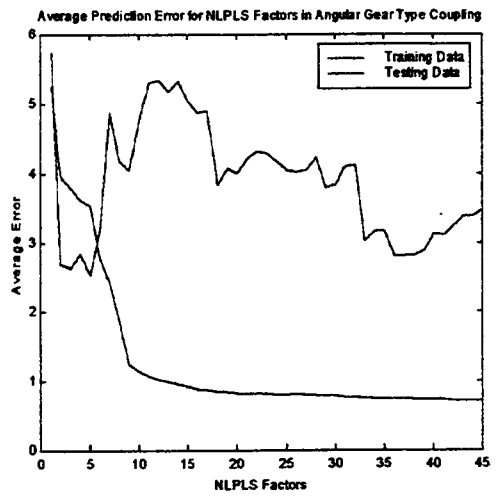


Figure 4.27. LPLS Angular Prediction for Grid type coupling

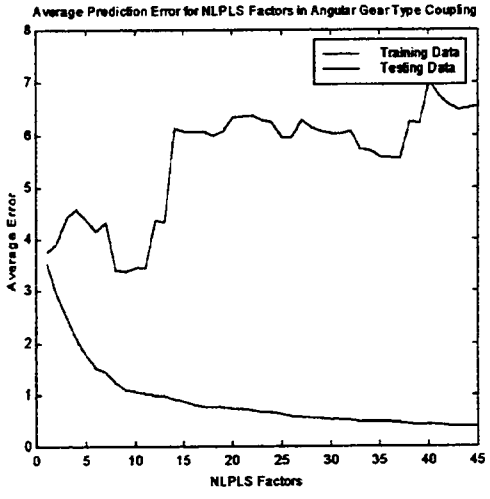
Three NLPLS models were created for each of the couplings. One for the parallel offset misalignment, one for the angular misalignment, and one for both the parallel offset misalignment and the angular misalignment at the same time using the useful NLPLS factors. Then, the models were tested to see how many of the NLPLS factors resulted in the smallest average error for the test data. Then three more NLPLS models were created with the optimal number of NLPLS factors. The average error was calculated by taking the mean of the absolute values of the difference between the predicted alignment conditions and the actual alignment conditions.

4.6.1 Results for Elastomer Type Coupling

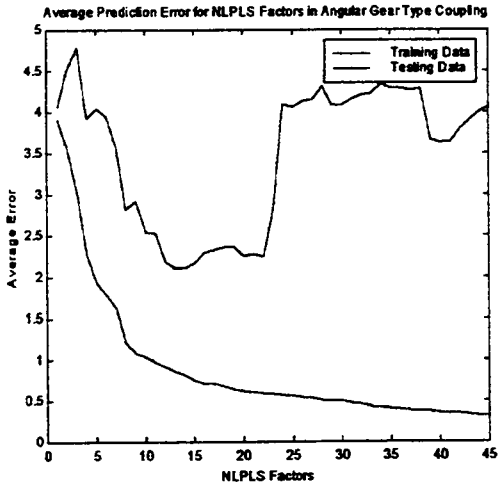
The parallel offset misalignment NLPLS model using all 79 PLS factors regressed the model to an average error of 2,15 mils. The regressed MSE was 8.99. The parallel offset misalignment network predicted the misalignment to an average error of 18.69 mils. The predicted MSE was 639.54.



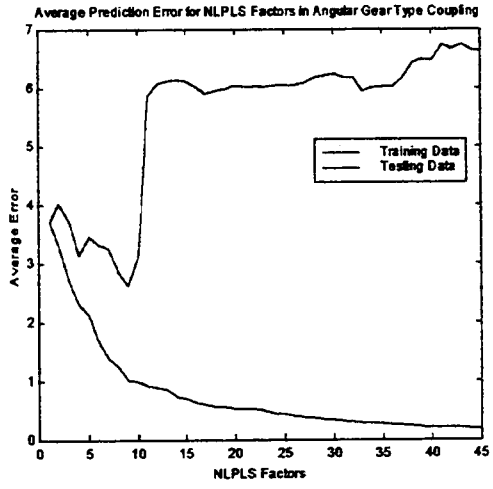
a) 3 Hidden Neurons



b) 10 Hidden Neurons



c) 15 Hidden Neurons



d) 20 Hidden Neurons

Figure 4.28. Prediction Errors for different NLPLS Network Architectures.

The NLPLS model was tested by iteratively adding another NLPLS factor to the model to determine the optimal number of factors to reduce the average error. Figure 4.29 shows the relationship between the number of NLPLS factors and the average prediction error for the training data and the test data for the parallel NLPLS model. This analysis showed that 35 NLPLS factors was the optimal number for the parallel model of the elastomer type coupling set.

The parallel offset misalignment NLPLS model using 35 NLPLS factors regressed the model to an average error of 3.99 mils. The regressed MSE was 27.47. The parallel offset misalignment model predicted the misalignment to an average error of 16.8 mils. The predicted MSE was 494.92.

The angular misalignment NLPLS model using all 79 NLPLS factors regressed the model to an average error of 0.67 mils/inch. The regressed MSE was 0.84. The angular misalignment model predicted the misalignment to an average error of 13.1 mils/inch. The predicted MSE was 284.81.

The NLPLS model was tested by iteratively adding another NLPLS factor to the model to determine the optimal number of factors to reduce the average error. Figure 4.30 shows the relationship between the number of NLPLS factors and the average prediction error for the training data and the test data for the angular NLPLS model. This analysis showed that 27

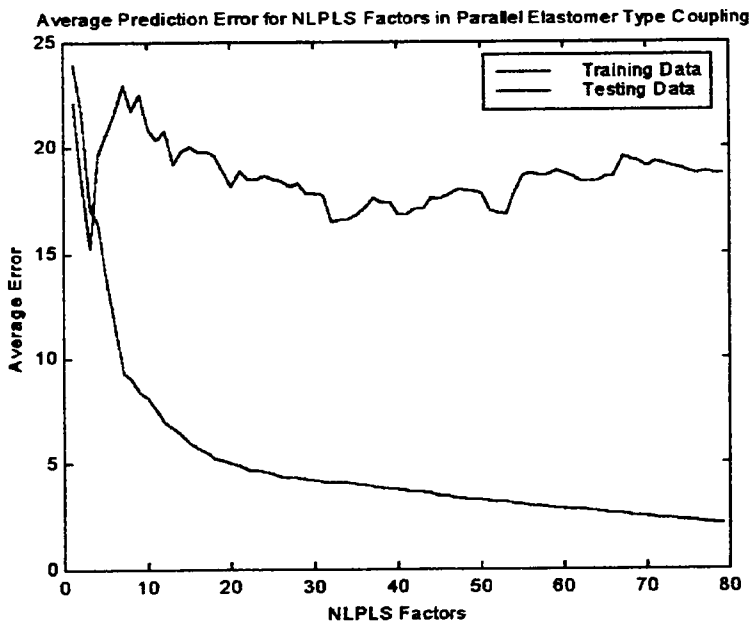


Figure 4.29. Parallel errors for NLPLS factors for Elastomer type coupling.

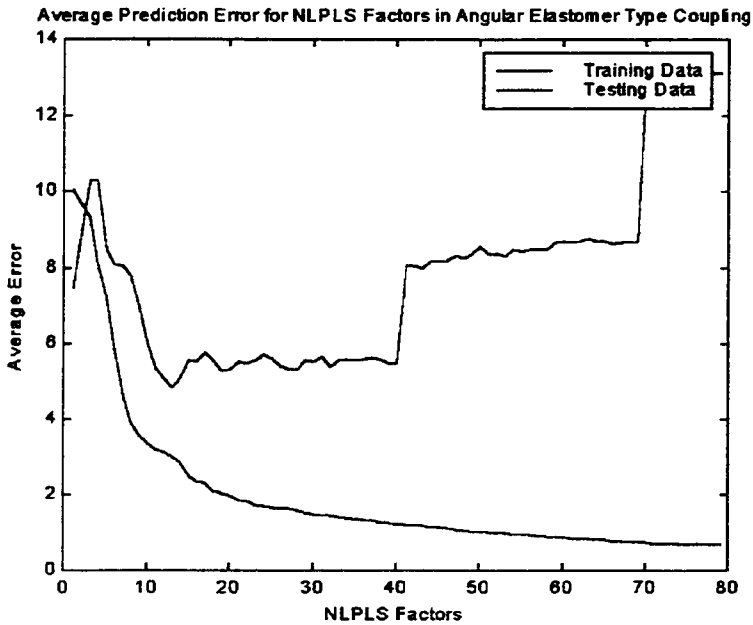


Figure 4.30. Angular errors for NLPLS factors for Elastomer type coupling.

NLPLS factors was the optimal number for the angular model of the elastomer type coupling set.

The angular offset misalignment NLPLS model using 27 NLPLS factors regressed the model to an average error of 1.62 mils/inch. The regressed MSE 4.35. The angular misalignment model predicted the misalignment to an average error of 5.33 mils/inch. The predicted MSE was 4.35.

The joint misalignment NLPLS model using all 79 NLPLS factors regressed the model to an average error of 2.49 mils for the parallel offset condition and an average error of 2.16 mils/inch for the angular condition. The regressed MSE was 10.83 and 7.72 for the parallel and angular conditions respectively. The joint misalignment NLPLS model using all 79 NLPLS factors predicted the alignment to an average error 22.59 mils for the parallel offset condition and an average error of 11.85 mils/inch for the angular condition. The predicted MSE was 710.55 and 207.13 for the parallel and angular conditions respectively

The NLPLS model was tested by iteratively adding another NLPLS factor to the model to determine the optimal number of factors to reduce the average error. Figure 4.31 shows the relationship between the number of NLPLS factors and the average prediction error for the training and the test data for the joint NLPLS model. This analysis showed that 25 NLPLS factors was the optimal number for the joint model of the elastomer type coupling set.

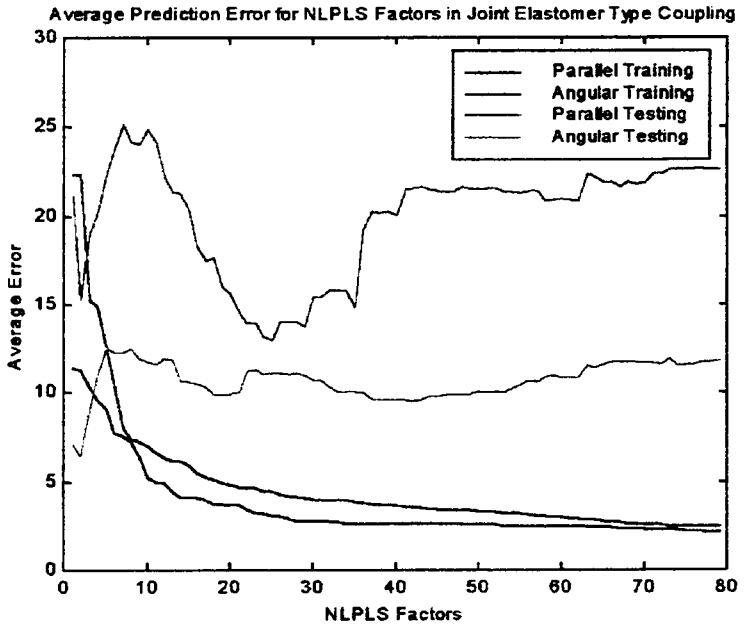


Figure 4.31. Joint errors for NLPLS factors for Elastomer type coupling.

The joint misalignment NLPLS model using 25 NLPLS factors regressed the model to an average error 4.48 mils for the parallel offset condition and an average error 3.05 mils/inch for the angular condition. The regressed MSE was 35.95 and 15.97 for the parallel and angular conditions respectively. The joint misalignment NLPLS model using 25 NLPLS factors predicted the alignment to an average error 13.05 mils for the parallel offset condition and an average error of 11.11 mils/inch for the angular condition. The predicted MSE was 257.33 and 247.61 for the parallel and angular conditions respectively.

The angular optimal NLPLS model was best for the elastomer type coupling. Figure 4.32 shows the prediction for the angular model on the test data.

4.6.2 Results for Gear Type Coupling

The parallel offset misalignment NLPLS model using all 45 NLPLS factors regressed the model to an average error of 0.86 mils. The regressed MSE was 1.3. The parallel offset misalignment network predicted the misalignment to an average error of 20.66 mils. The predicted MSE was 534.41

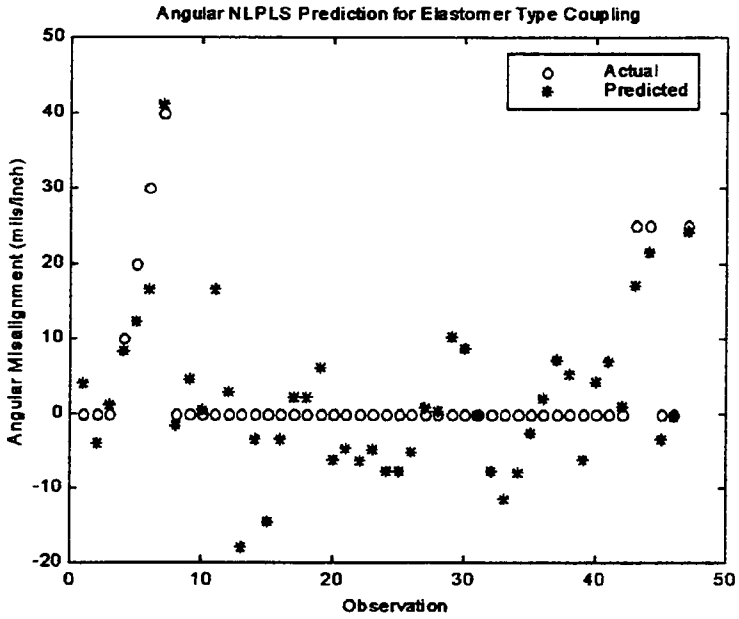


Figure 4.32. NLPLS Angular Prediction for Elastomer type coupling

The NLPLS model was tested by iteratively adding another NLPLS factor to the model to determine the optimal number of factors to reduce the average error. Figure 4.33 shows the relationship between the number of NLPLS factors and the average prediction error for training data and the test data for the parallel NLPLS model. This analysis showed that 12 NLPLS factors was the optimal number for the parallel model of the gear type coupling set.

The parallel offset misalignment NLPLS model using 12 NLPLS factors regressed the model to an average error of 2.27 mils. The regressed MSE was 10.08. The parallel offset misalignment model predicted the misalignment to an average error of 8.48 mils. The predicted MSE was 104.73.

The angular misalignment NLPLS model using all 45 NLPLS factors regressed the model to an average error of 0.3 mils/inch. The regressed MSE was 0.17. The angular misalignment model predicted the misalignment to an average error of 3.61 mils/inch. The predicted MSE was 22.03.

The NLPLS model was tested by iteratively adding another NLPLS factor to the model to determine the optimal number of factors to reduce the average error. Figure 4.34 shows the relationship between the number of NLPLS factors and the average prediction error for the training data and the test data for the angular NLPLS model.

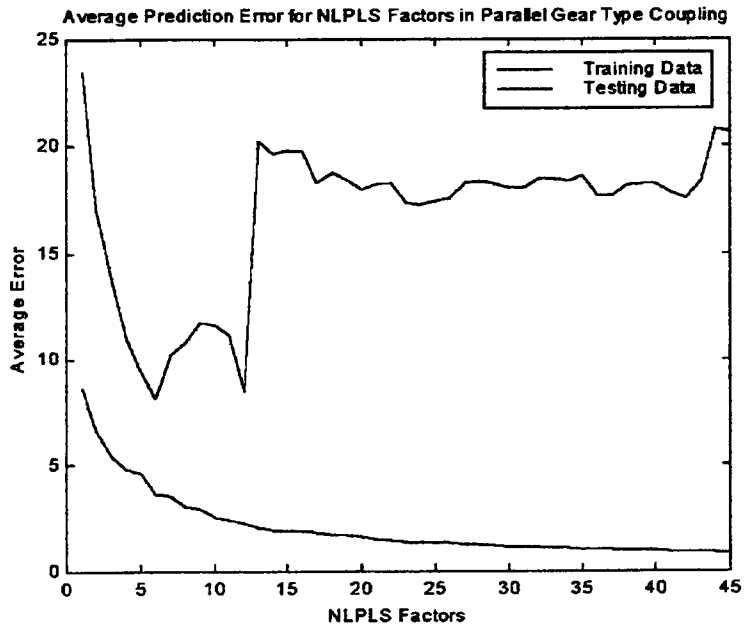


Figure 4.33. Parallel errors for NLPLS factors for Gear type coupling.

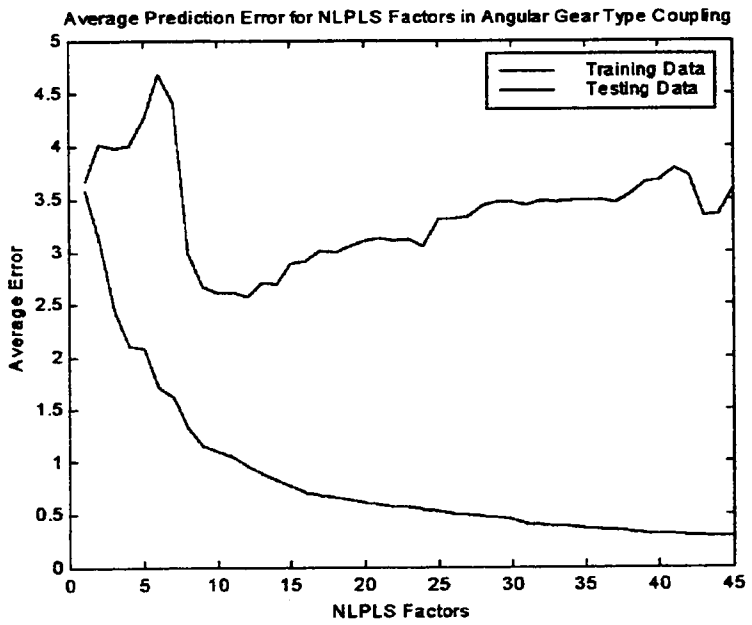


Figure 4.34. Angular errors for NLPLS factors for Gear type coupling.

This analysis showed that 12 NLPLS factors was the optimal number for the angular model of the gear type coupling set.

The angular misalignment NLPLS model using 12 NLPLS factors regressed the model to an average error of 0.96 mils/inch. The regressed MSE was 1.66. The angular misalignment model predicted the misalignment to an average error of 2.58 mils/inch. The predicted MSE was 10.84.

The joint misalignment NLPLS model using all 45 NLPLS factors regressed the model to an average error 1.1 mils for the parallel offset condition and an average error of 1.02 mils/inch for the angular condition. The regressed MSE was 2.06 and 1.69 for the parallel and angular conditions respectively. The joint misalignment NLPLS model using all 45 NLPLS factors predicted the alignment to an average error 12.47 mils for the parallel offset condition and an average error of 6.66 mils/inch for the angular condition. The predicted MSE was 232.5 and 83.76 for the parallel and angular conditions respectively.

The NLPLS model was tested by iteratively adding another NLPLS factor to the model to determine the optimal number of factors to reduce the average error. Figure 4.35 shows the relationship between the number of NLPLS factors and the average prediction error for the training and the test data for the joint NLPLS model.

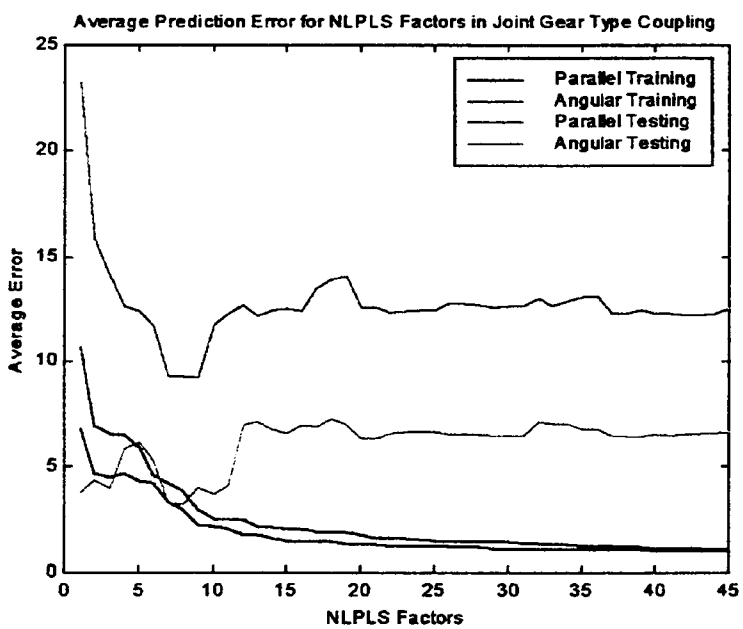


Figure 4.35. Joint errors for NLPLS factors for Gear type coupling.

This analysis showed that 12 NLPLS factors was the optimal number for the joint model of the gear type coupling set.

The joint misalignment NLPLS model using 12 NLPLS factors regressed the model to an average error 2.49 mils for the parallel offset condition and an average error 1.77 mils/inch for the angular condition. The regressed MSE was 10.62 and 5.17 for the parallel and angular conditions respectively. The joint misalignment NLPLS model using 12 NLPLS factors predicted the alignment to an average error 12.69 mils for the parallel offset condition and an average error of 6.92 mils/inch for the angular condition. The predicted MSE was 214.46 and 82.42 for the parallel and angular conditions respectively.

The angular optimal NLPLS model was best for the gear type coupling. Figure 4.36 shows the prediction for the angular model on the test data.

4.6.3 Results for Grid Type Coupling

The parallel offset misalignment NLPLS model using all 46 NLPLS factors regressed the model to an average error of 0.24 mils. The regressed MSE was 0.11. The parallel offset

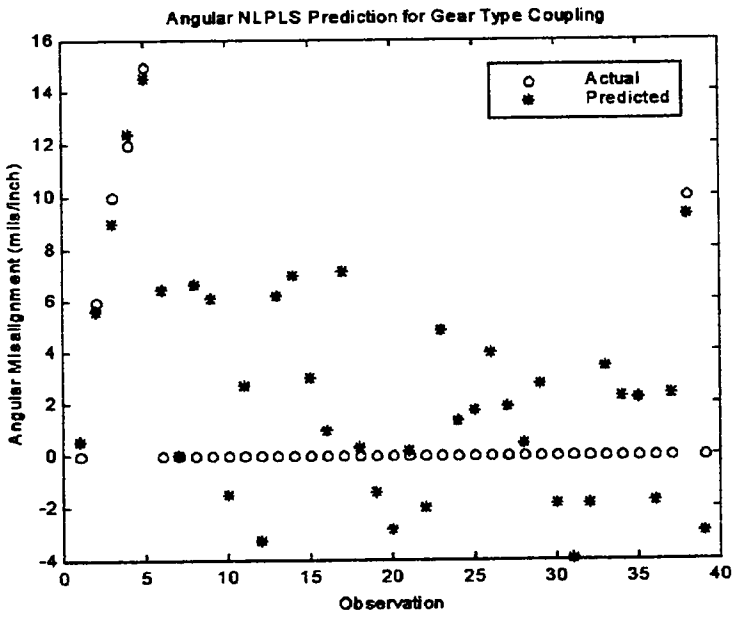


Figure 4.36. NLPLS Angular Prediction for Gear type coupling

misalignment network predicted the misalignment to an average error of 3.95 mils. The predicted MSE was 22.94.

The NLPLS model was tested by iteratively adding another NLPLS factor to the model to determine the optimal number of factors to reduce the average error. Figure 4.37 shows the relationship between the number of NLPLS factors and the average prediction error for training data and the test data for the parallel NLPLS model. This analysis showed that 17 NLPLS factors was the optimal number for the parallel model of the grid type coupling set.

The parallel offset misalignment NLPLS model using 17 NLPLS factors regressed the model to an average error of 0.6 mils. The regressed MSE was 0.61. The parallel offset misalignment model predicted the misalignment to an average error of 3.04 mils. The predicted MSE was 13.62.

The angular misalignment NLPLS model using all 46 NLPLS factors regressed the model to an average error of 0.17 mils/inch. The regressed MSE was 5.77×10^{-2}. The angular misalignment model predicted the misalignment to an average error of 1.97 mils/inch. The predicted MSE was 6.15.

The NLPLS model was tested by iteratively adding another NLPLS factor to the model to determine the optimal number of factors to reduce the average error. Figure 4.38 shows the

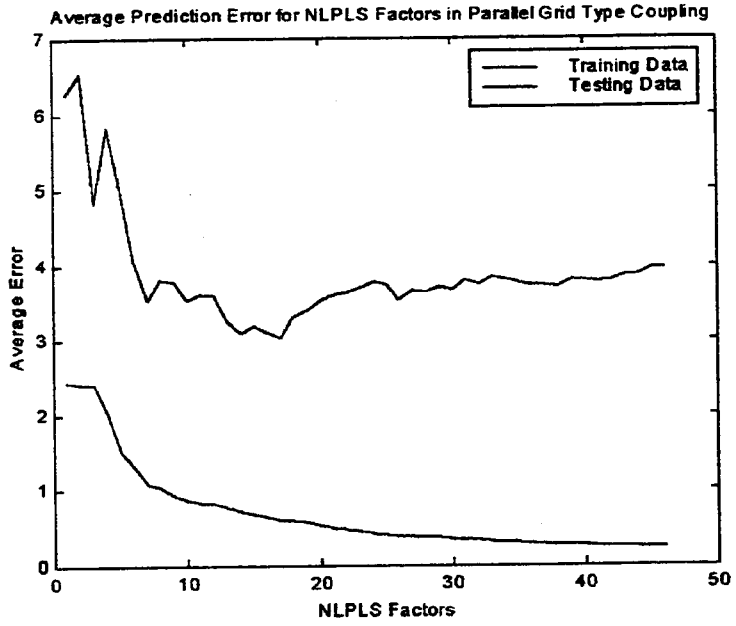


Figure 4.37. Parallel errors for NLPLS factors for Grid type coupling.

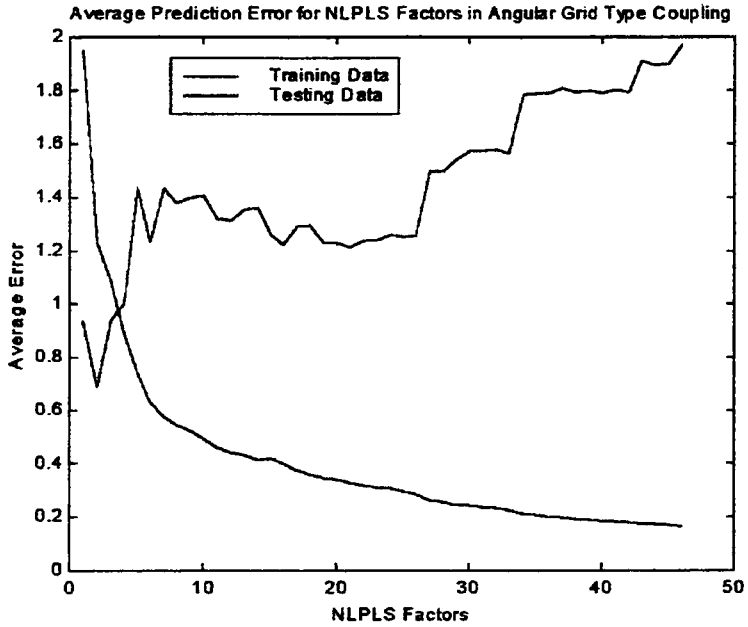


Figure 4.38. Angular errors for NLPLS factors for Grid type coupling.

relationship between the number of NLPLS factors and the average prediction error for the training data and the test data for the angular NLPLS model. This analysis showed that 21 NLPLS factors was the optimal number for the angular model of the grid type coupling set.

The angular misalignment NLPLS model using 21 NLPLS factors regressed the model to an average error of 0.33 mils/inch. The regressed MSE was 0.2. The angular misalignment model predicted the misalignment to an average error of 1.21 mils/inch. The predicted MSE was 2.61.

The joint misalignment NLPLS model using all 46 NLPLS factors regressed the model to an average error 0.36 mils for the parallel offset condition and an average error of 0.32 mils/inch for the angular condition. The regressed MSE was 0.26 and 0.18 for the parallel and angular conditions respectively. The joint misalignment NLPLS model using all 46 NLPLS factors predicted the alignment to an average error 2.06 mils for the parallel offset condition and an average error of 2.03 mils/inch for the angular condition. The predicted MSE was 6.71 and 6.64 for the parallel and angular conditions respectively.

The NLPLS model was tested by iteratively adding another NLPLS factor to the model to determine the optimal number of factors to reduce the average error. Figure 4.39 shows the relationship between the number of NLPLS factors and the average prediction error for the training and the test data for the joint NLPLS model. This analysis showed that 22 NLPLS factors

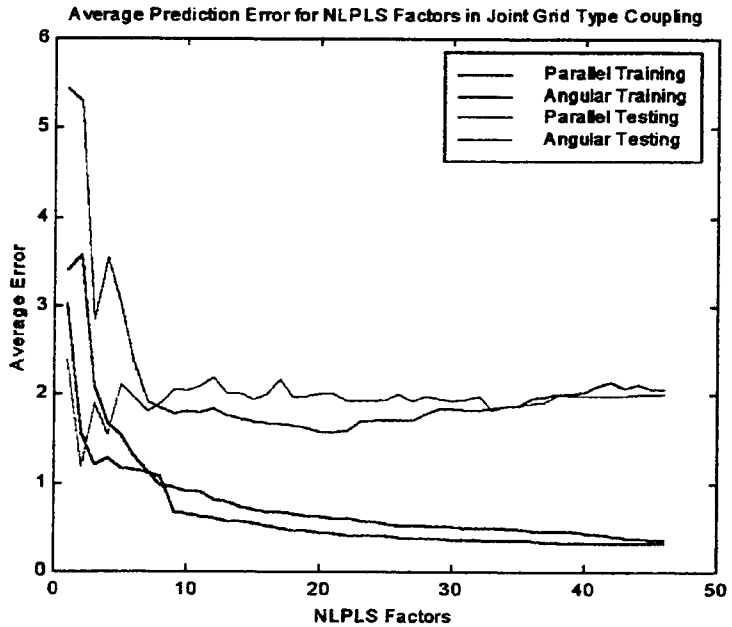


Figure 4.39. Joint errors for NLPLS factors for Grid type coupling.

was the optimal number for the joint model of the grid type coupling set.

The joint misalignment NLPLS model using 22 NLPLS factors regressed the model to an average error 0.61 mils for the parallel offset condition and an average error 0.42 mils/inch for the angular condition. The regressed MSE was 0.6 and 0.28 for the parallel and angular conditions respectively. The joint misalignment NLPLS model using 22 NLPLS factors predicted the alignment to an average error 1.59 mils for the parallel offset condition and an average error of 1.93 mils/inch for the angular condition. The predicted MSE was 3.97 and 5.5 for the parallel and angular conditions respectively.

The angular optimal NLPLS model was best for the grid type coupling. Figure 4.40 shows the prediction for the angular model on the test data.

4.7 Statistical Evaluation Remarks

The five types of alignment prediction methods all performed differently for the three types of couplings. Some of the differences in the mapping procedures are due to the way that the method performs the mapping. The MLR simply fits a straight line between the inputs and outputs, so its prediction results will be highly dependent on changes in the motor system and

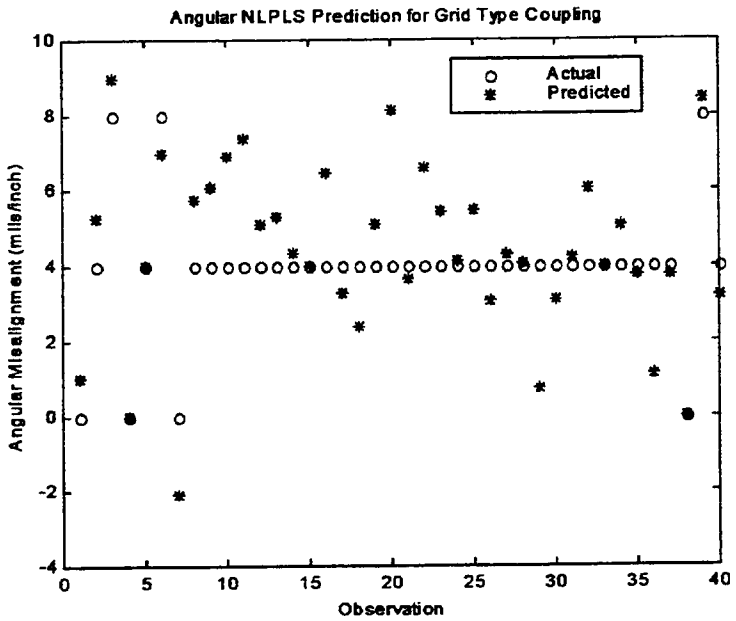


Figure 4.40. NLPLS Angular Prediction for Grid type coupling

the amount of linearity between the inputs and outputs. The LCC Neural Network method is also highly dependent on the linearities in the motor system, but it is more robust than the MLR method because the ANN allows the non-linearities to be fitted. The PCA method is not as dependent on the motor system because it removes the collinearity in the data. It may not produce the best principal components for the mapping because the PC's are chosen based on the variability of the input data alone. The LPLS method is more robust than the MLR method because it maps based on the PC's that are determined in a supervised manner between the variability of the input and its relationship to the outputs. The NLPLS method is the most robust of the techniques because it allows the non-linearities of the mapping to be learned while training on PC's that were determined in the supervised manner.

The summary for the training and testing of the elastomer type coupling is given in Table 4.10. The summary for the training and testing of the gear type coupling is given in Table 4.11. The summary for the training and testing of the grid type coupling is given in Table 4.12.

To perform a comparison of the mapping techniques it is easier by comparing the types of misalignment for each coupling. Table 4.13 shows the parallel offset misalignment prediction errors for the elastomer type coupling.

Table 4.10 Training and Testing Errors for Elastomer Type Coupling.

ELASTOMER TYPE COUPLING TRAINING AND TESTING ERRORS					
		Mean Error		Mean Squared Error	
		Training	Testing	Training	Testing
Multiple	parallel offset	5.56E-13	25.15	2.41E-25	1.01E+03
Linear	angular	6.43E-13	2.99	4.87E-25	18.75
Regression	joint parallel offset	4.54E-13	25.15	3.52E-25	1.01E+03
	joint angular	5.08E-13	2.99	3.34E-25	18.8
Linear	parallel offset	26.01	11.87	1.05E+03	405.18
Correlation	angular	3.04	3.04	2.89E+01	3.40E+01
Coefficient	joint parallel offset	15.99	17.09	385.86	350.02
ANN	joint angular	7.38	5.91	100.53	73.34
Principle	parallel offset	18.99	21.1	575.21	539.01
Component	angular	6.31	3.72	68.45	31.22
Analysis	joint parallel offset	23.99	16.44	792.78	400.14
ANN	joint angular	12.42	6.04	233.97	90.05
Linear	parallel offset	3.74E-13	25.15	1.65E-25	1.01E+03
Partial	angular	9.46E-14	2.99	1.54E-26	18.75
Least	joint parallel offset	1.14E-13	25.15	2.31E-26	1.01E+03
Squares	joint angular	4.61E-14	2.99	3.05E-27	18.8
	parallel offset	1.23E+00	23.18	2.84E+00	805.94
Reduced	angular	0.03	2.92	2.00E-03	17.66
LPLS	joint parallel offset	0.06	24.93	8.90E-03	994.97
	joint angular	0.05	2.99	4.10E-03	18.26
Non-Linear	parallel offset	2.15	18.69	8.99	639.54
Partial	angular	0.67	13.1	0.84	284.81
Least	joint parallel offset	2.49	22.59	10.83	710.55
Squares	joint angular	2.16	11.85	7.72	207.13
	parallel offset	3.99	16.8	27.47	494.92
Reduced	angular	1.62	5.33	4.35	46.31
NLPLS	joint parallel offset	4.48	13.05	35.95	257.33
	joint angular	3.05	11.11	15.97	247.61

Table 4.11 Training and Testing Errors for Gear Type Coupling.

GEAR TYPE COUPLING TRAINING AND TESTING ERRORS					
		Mean Error		Mean Squared Error	
		Training	Testing	Training	Testing
Multiple	parallel offset	1.22E-13	7.34	2.30E-26	70.91
Linear	angular	8.01E-14	3.97	8.65E-27	21.19
Regression	joint parallel offset	1.40E-14	7.34	2.76E-26	70.91
	joint angular	8.74E-14	3.97	1.11E-26	21.19
Linear	parallel offset	6.29	4.22	81.45	28.99
Correlation	angular	0.17	0.13	6.35E-02	1.03E-01
Coefficient	joint parallel offset	6.03	3.52	53.74	24.11
	joint angular	1.38	1.57	3.75	7.27
Principle	parallel offset	5.68	2.71	69.72	16.8
Component	angular	2.5	0.84	13.96	3.41
Analysis	joint parallel offset	9.77	13.52	123.2	244.97
	joint angular	4.87	3.73	31.25	18.83
Linear	parallel offset	4.43E-14	7.34	3.04E-27	70.91
Partial	angular	2.55E-14	3.97	1.11E-27	21.19
Least	joint parallel offset	3.85E-14	7.34	2.24E-27	70.91
Squares	joint angular	8.22E-15	3.97	1.11E-28	21.19
	parallel offset	8.24E-02	7.89	1.28E-02	78.54
Reduced	angular	1.23	1.72	2.73	5.86
LPLS	joint parallel offset	0.26	7.34	0.15	70.91
	joint angular	0.25	3.97	0.11	21.19
Non-Linear	parallel offset	0.86	20.66	1.3	534.41
Partial	angular	0.3	3.61	0.17	22.03
Least	joint parallel offset	1.1	12.47	2.06	232.5
Squares	joint angular	1.02	6.66	1.69	83.76
	parallel offset	2.27	8.48	10.08	104.73
Reduced	angular	0.96	2.58	1.66	10.84
NLPLS	joint parallel offset	2.49	12.69	10.62	214.46
	joint angular	1.77	6.92	5.17	82.42

Table 4.12 Training and Testing Errors for Grid Type Coupling.

GRID TYPE COUPLING TRAINING AND TESTING ERRORS					
		Mean Error		Mean Squared Error	
		Training	Testing	Training	Testing
Multiple	parallel offset	2.27E-13	3.04	6.67E-26	13.14
Linear	angular	7.42E-14	0.93	6.48E-27	1.23
Regression	joint parallel offset	1.57E-13	3.04	3.43E-26	13.14
	joint angular	9.95E-14	0.93	1.09E-26	1.23
Linear	parallel offset	1.37	2.03	2.61	6.07
Correlation	angular	0.49	0.31	5.70E-01	2.30E-01
Coefficient	joint parallel offset	1.39	2.82	3.94	11.05
	joint angular	0.99	1.45	1.55	2.51
Principle	parallel offset	3.03	3.09	16.65	11.15
Component	angular	2.18	1.65	5.81	3.35
Analysis	joint parallel offset	3.47	4.18	17.43	18.9
	joint angular	1.69	0.79	4.3	1.85
Linear	parallel offset	1.71E-14	3.04	4.35E-28	13.14
Partial	angular	8.97E-15	0.93	1.28E-28	1.23
Least	joint parallel offset	2.77E-14	3.04	1.09E-27	13.14
Squares	joint angular	5.78E-15	0.93	5.00E-29	1.23
	parallel offset	1.10E-01	2.87	2.16E-02	11.32
Reduced	angular	6.37E-02	0.86	8.30E-03	0.94
LPLS	joint parallel offset	0.21	2.9	8.16E-02	10.87
	joint angular	0.18	0.97	6.23E-02	1.07
Non-Linear	parallel offset	0.24	3.95	0.11	22.94
Partial	angular	0.17	1.97	5.77E-02	6.15
Least	joint parallel offset	0.36	2.06	0.26	6.71
Squares	joint angular	0.32	2.03	0.18	6.64
	parallel offset	0.6	3.04	0.61	13.62
Reduced	angular	0.33	1.21	0.2	2.61
NLPLS	joint parallel offset	0.61	1.59	0.6	3.97
	joint angular	0.42	1.93	0.28	5.5

Table 4.13 Parallel Offset Misalignment Prediction Errors for the Elastomer Type Coupling.

	Mean Error (mils)	Percent of Tolerance Limits
MLR	25.15	17.96
Joint MLR	25.15	17.96
LCC	**11.87**	**8.48**
Joint LCC	17.09	12.21
PCA	21.1	15.07
Joint PCA	16.44	11.74
LPLS	25.15	17.96
Joint LPLS	25.15	17.96
Optimal LPLS	23.18	16.56
Joint Optimal LPLS	24.93	17.81
NLPLS	18.69	13.35
Joint NLPLS	22.59	16.14
Optimal NLPLS	16.8	12.00
Joint Optimal NLPLS	**13.05**	**9.32**

The best performer in terms of error alone is the LCC model. The Joint Optimal NLPLS method was quite a lot better than the simple MLR method and not much worse than the LCC method and would probably be a better predictor than the LCC method. These were the only two models that could even predict the parallel offset alignment condition to within 10 percent of the manufacturer's operating tolerances.

Table 4.14 shows the angular misalignment prediction errors for the elastomer type coupling. The best performer in terms of error alone is the Optimal LPLS model. The Optimal NLPLS method did not perform as well as the MLR. This is probably due to the flexibility of the elastomer material not transferring the forces to the power spectrum very efficiently. There were a few other models that were able to predict better than 10 percent of the tolerance.

Table 4.15 shows the parallel offset misalignment prediction errors for the gear type coupling. The best performer in terms of error alone is the PCA model. It out performed the rest of the predictors enough to probably be the most robust predictor. There were several other methods that were able to predict to a small percentage of manufacturer's tolerances.

Table 4.16 shows the angular misalignment prediction errors for the gear type coupling. The best performer in terms of error alone is the LCC model. The PCA model performed rather well too and would probably be the most robust of these two models. These two were much better than the other methods.

Table 4.14 Angular Misalignment Prediction Errors for the Elastomer Type Coupling.

	Mean Error (mils/inch)	Percent of Tolerance limits
MLR	2.99	7.46
Joint MLR	2.99	7.46
LCC	3.04	7.60
Joint LCC	5.91	14.78
PCA	3.72	9.30
Joint PCA	6.04	15.10
LPLS	2.99	7.46
Joint LPLS	2.99	7.46
Optimal LPLS	**2.92**	**7.30**
Joint Optimal LPLS	2.99	7.46
NLPLS	13.1	32.75
Joint NLPLS	11.85	29.63
Optimal NLPLS	5.33	13.33
Joint Optimal NLPLS	11.11	27.78

Table 4.15 Parallel Offset Misalignment Prediction Errors for the Gear Type Coupling.

	Mean Error (mils)	Percent of Tolerance Limits
MLR	7.34	7.34
Joint MLR	7.34	7.34
LCC	4.22	4.22
Joint LCC	**3.52**	**3.52**
PCA	**2.71**	**2.71**
Joint PCA	13.52	13.52
LPLS	7.34	7.34
Joint LPLS	7.34	7.34
Optimal LPLS	7.89	7.89
Joint Optimal LPLS	7.34	7.34
NLPLS	20.66	20.66
Joint NLPLS	12.47	12.47
Optimal NLPLS	8.48	8.48
Joint Optimal NLPLS	12.9	12.9

Table 4.16 Angular Misalignment Prediction Errors for the Gear Type Coupling.

	Mean Error (mils/inch)	Percent of Tolerance Limits
MLR	3.97	26.47
Joint MLR	3.97	26.47
LCC	**0.13**	**0.87**
Joint LCC	1.57	10.47
PCA	**0.84**	**5.60**
Joint PCA	3.73	24.86
LPLS	3.97	26.47
Joint LPLS	3.97	26.47
Optimal LPLS	1.72	11.47
Joint Optimal LPLS	3.97	26.47
NLPLS	3.61	24.07
Joint NLPLS	6.66	44.40
Optimal NLPLS	2.58	17.20
Joint Optimal NLPLS	6.92	46.13

Table 4.17 shows the parallel offset misalignment prediction errors for the grid type coupling. The best performer in terms of error alone in the Joint Optimal NLPLS model. This model would be a good robust predictor. The LCC model was again one of the better methods for predicting the alignment.

Table 4.18 shows the angular misalignment prediction errors for the elastomer type coupling. The best performer in terms of error alone is the LCC model. The Optimal LPLS method performed better than the MLR but is probably not as robust a model as the LCC ANN. The Joint PCA model performed rather well also.

From these results, it is possible to create a system to monitor the power inputs to a motor system and predict the alignment and or detect motor shaft misalignment. The LCC Neural Network seemed to predict the misalignment conditions better than the other methods for these examples. This is probably due to the fact that the choices for inputs were more higly selective than those for the other models.

Table 4.17 Parallel Offset Misalignment Prediction Errors for the Grid Type Coupling.

	Mean Error (mils)	Percent of Tolerance Limits
MLR	3.04	12.67
Joint MLR	3.04	12.67
LCC	**2.03**	**8.46**
Joint LCC	2.82	11.75
PCA	3.09	12.88
Joint PCA	4.18	17.42
LPLS	3.04	12.67
Joint LPLS	3.04	12.67
Optimal LPLS	2.87	11.96
Joint Optimal LPLS	2.90	12.08
NLPLS	3.95	16.46
Joint NLPLS	**2.06**	**8.58**
Optimal NLPLS	3.04	12.67
Joint Optimal NLPLS	**1.59**	**6.63**

Table 4.18 Angular Misalignment Prediction Errors for the Grid Type Coupling.

	Mean Error (mils/inch)	Percent of Tolerance Limits
MLR	0.93	7.75
Joint MLR	0.93	7.75
LCC	**0.31**	**2.58**
Joint LCC	1.45	12.08
PCA	1.65	13.75
Joint PCA	**0.79**	**6.58**
LPLS	0.93	7.75
Joint LPLS	0.93	7.75
Optimal LPLS	0.86	7.16
Joint Optimal LPLS	0.97	8.08
NLPLS	1.97	16.42
Joint NLPLS	2.03	16.92
Optimal NLPLS	1.21	10.08
Joint Optimal NLPLS	1.93	16.08

5.0 CONCLUSIONS

This section gives some conclusions for the misalignment prediction methods discussed in this thesis. Then it gives some recommendations for future work to improve the performance of the models and the overall prediction.

5.1 CONCLUSIONS FOR MISALIGNMENT PREDICTION

The examples for the elastomer type flexible coupling, the gear type flexible coupling, and the grid type flexible coupling shown in this thesis show that the alignment conditions of a motor system can be predicted for all of the couplings and alignment types to better than 10 percent of the operating limits for the individual coupling from the input power frequency spectrum of an electric motor. The five types of alignment prediction methods all performed differently for the three types of couplings. Some of the differences in the mapping procedures are due to the way that the method performs the mapping. The MLR method simply fits a straight line between the inputs and outputs, so its prediction results will be highly dependent on changes in the motor system and the amount of linearity between the inputs and outputs. The LCC Neural Network method is also highly dependent on the linearities in the motor system, but it is more robust than the MLR method because the ANN allows the non-linearities to be fitted. The PCA method is not as dependent on the motor system because it removes the collinearity in the data. It may not produce the best principal components for the mapping because the PC's are chosen based on the variability of the input data alone. The LPLS method is more robust than the MLR method because it maps based on the PC's that are determined in a supervised manner between the variability of the input and its relationship to the outputs. The NLPLS method is the most

robust of the techniques because it allows the non-linearities of the mapping to be learned while training on PC's that were determined in the supervised manner.

Another reason that the mappings performed differently was the couplings' designs themselves. The Rexnord Elastomer type coupling was very flexible. When it as subjected to parallel offset, the load was not significantly changed. Therefore, there was not an increased load on the motor to transmit through the power. When this type coupling was subjected to an angular misalignment, the elastomer material created a binding in the coupling that caused fluctuations in the power spectrum. The Zurn Gear type coupling was more rigid than the elastomer type. Parallel offsets did change the geometry of the coupling enough to effect the power spectrum in a detectable amount. The angular misalignment effected the power spectrum more than the parallel because it changed the geometry of the coupling in a more detectable amount. The Dodge Grid type coupling was similar to the gear type coupling, Parallel offset effected the power spectrum in a detectable fashion, while the angular misalignment effected it in a more noticeable one.

The methods that performed the best for each of the couplings and the alignment conditions were as follows. The method that produced the smallest mean error for the elastomer type coupling to predict the parallel offset misalignment was the LCC Neural Network mapping with an average prediction error of 11.87 mils or 8.48 percent of the tolerance compared to 25.15 mils or 17.96 percent for a MLR. The second best method was the NLPLS method resulting in an average prediction error of 13.05 mils or 9.32 percent. The best method for predicting the angular misalignment in the elastomer type coupling was the LPLS method with an average prediction error of 2.92 mils/inch or 7.30 percent of the tolerance compared to the MLR error of 2.99 mils/inch or 7.46 percent.

The method that produced the smallest mean error for the gear type coupling to predict the parallel offset misalignment was the PCA Neural Network mapping with an average prediction error of 2.71 mils or 2.71 percent of the tolerance compared to 7.34 mils or 7.34 percent for a MLR. The best method for predicting the angular misalignment in the gear type coupling was the LCC Neural Network method with an average prediction error of 0.13 mils/inch or 0.87 percent of the tolerance compared to the MLR error of 3.97 mils/inch or 26.47 percent.

The method that produced the smallest mean error for the grid type coupling to predict the parallel offset misalignment was the NLPLS mapping with an average prediction error of 1.59 mils or 6.63 percent of the tolerance compared to 3.04 mils or 12.67 percent for a MLR. The best method for predicting the angular misalignment in the grid type coupling was the LCC Neural

Network method with an average prediction error of 0.31 mils/inch or 2.58 percent of the tolerance compared to the MLR error of 0.93 mils/inch or 7.75 percent.

The LCC Neural Network seemed to predict the misalignment conditions better than the other methods for these examples. The NLPS models can probably be improved by different architectures in the mapping layer and choosing different numbers of NLPLS factors. The NLPLS method should be able to predict as well as any of the other methods and in a more robust fashion. The NLPLS methods should be able to form a system that is able to predict the alignment conditions that is not as sensitive to fluctuations in motor speed or motor system variables such as rigidity.

An online system can be implemented by placing sensors on two of the three phase voltages and currents to determine the total input power to a system. The system would then have to be trained on the operating parameters for each system that it is placed on to be able to more accurately predict the alignment conditions. A combination of these methods could be used as the predictor function, but the most robust method would use the NLPLS techniques.

This research produced a more sensitive method of detecting rotating machinery misalignment than previous methods. The vibration analysis methods are very sensitive to motor system variables such as rigidity of the coupling, rigidity of the structure, and ability of the structure to transmit vibration from the source to the detectors. While this method is still sensitive to the coupling types, the other concerns are not as important. A change in the coupling geometry that effects the power spectrum is immediately detected rather than having to be transmitted through the various structures in the motor.

5.2 Recommendations for Future Work

There are several areas that the methods of alignment prediction can be improved. The first method of improvement would be a trial and error type method to determine the optimal NLPLS model. The factors would be what type of ANN to use for the internal mapping, and how many of the NLPLS factors to keep for the prediction network. There are several factors that can improve the ANN mapping such as the number of hidden neurons, the type of training algorithm, and the error goals used as stopping criterion. It would be ideal to use a cross validation technique to train the mapping so that the data would not be overfit or underfit. Another good technique would try different numbers of hidden neurons for each PLS factor to create the optimal mapping.

A more quantitative method for determining how many of the NLPLS factors to keep would be another way of improving the prediction abilities.

Another method of increasing the performance of the system would be to take a more complete spectrum of the possible operating parameters to give a larger number of observations to train the system on. This would allow the system to not have to generalize over as broad of a range of step sizes in the training data.

Other areas of future work would include using the NLPLS methods on the vibration spectra and the magnetic flux spectrum. The earlier studies showed that the vibration spectrum contained information that could be used to predict the alignment conditions. The use of NLPLS techniques could remove some of the dependencies that the PCA methods possessed on the rigidity of the structure and the coupling type, etc. The magnetic flux could also contain the same information. If it does, a magnetic flux sensor would be much easier to use than multiple sensors for voltage and current. The NLPLS methods should be easy to apply in a straightforward method to both the vibration information and the magnetic flux methods.

~~LIST OF~~ REFERENCES

LIST OF REFERENCES

1. Agnew, J.L., Knapp, R.C., Linear Algebra with Applications, Brooks-Cole Publishing Co., 1989.

2. Bishop, C.M., Neural Networks for Pattern Recognition, Claredon Press, Oxford, 1995.

3. Casada, D.A., Personal Communication, ORNL, Fall 1997 to Summer 1998.

4. Casada, D.A., Personal Internet Homepage, HTTP://user.icx.net/~doncasada, 1998

5. Chapra, S.C., Numerical Methods for Engineers, 2^{cd} Edition, McGraw-Hill Inc., New York, 1988.

6. Computational Systems Inc. (CSI), 835 Innovation Drive, Knoxville, Tennessee 37932-2470, (423) 675-2110.

7. Daintith, E., Glatt, P., Reduce Costs With Laser Shaft Alignment, Hydrocarbon Processing, August 1996.

8. Demuth, H., Beale, M., Neural Network Toolbox: For Use with MATLAB, The Mathworks Inc., 1998.

9. Diamantaris, K.I.,Kung, S.Y., Principal Component Neural Networks, John Wiley & Sons Inc., New York, 1996.

10. Emmert, J., Stidman, E., Maintenance Task Assessment and Selection, Reliability Vol. 2 No. 6, April 1996.

11. Geladi,P., Kowalski, B.R.,Partial Least Squares: A Tutorial, Analytica Chimica Acta 185, 1986.

12. Hansen, P.C., The Truncated SVD as a Method for Regularization, BIT 27, 1987.

13. Haykin, S., Neural Networks, Macmillian College Publishing Company, New York, 1994.

14. Heideman, M.T., Johnson, D.H., Burrus, C.S., Gauss and the History of the Fast Fourier Transform, IEEE ASSP 1, 1984

15. Hines, J.W., Fault Detection and Isolation, NE 597, Summer Semester 1998.
16. Hines, J.W., A. Edmonson, Motor Shaft Misalignment Analysis and Detection Phase 1, PPM, 1997a.
17. Hines, J. W., MATLAB Supplement to Fuzzy and Neural Approaches in Engineering, John Wiley & Sons Inc., 1997b.
18. Hines, J.W., Personal Communication, UTK, Fall 1997 to Summer 1998.

19. Jolliffe, I.T., Principal Component Analysis, Springer-Verlag New York Inc, 1986.

20. Kosko, B., Neural Networks and Fuzzy Systems, Prentice Hall, Englewood Cliffs, NJ, 1992.

21. Kuropatwinski, James, A Methodology for Predicting Motor Misalignment Using Artificial Neural Networks, University of Tennessee, August 1997.

22. Ludeca Inc. Maintenance Study, Evaluating Energy Consumption on Misaligned Machines, 1994.

23. Ludeca Inc.,1527 N.W. 89th Court, Miami, Florida 33172, (305) 591-8935.

24. MATLAB, Chemometrics Toolbox User's Guide, Mathworks Inc, 1993.

25. Nower D., Alignment Tolerances – Why Use Them?, 1996 Vibration Institution Meeting Proceedings, 1996.

26. Nower, D., Misalignment: Challenging the Rules, Reliability Magazine, May/June 1994.

27. Pardue, F., Piety, K.R., Elements of Reliability Based Maintenance: Future Vision for Industrial Management, CSI 1996 User Conference Proceedings, Computational Systems Inc., Nashville, Tennessee, 1996.

28. Piotrowski, J., Shaft Alignment Handbook 2cd Edition, Marcel Dekker Inc., New York, New York, 1995.

29. Qin, S.J., McAvoy, T.J., Non-Linear PLS Modeling Using Neural Networks, Computers Chem. Engng. Vol. 16 No. 4, 1992.

30. Simpson, R.E., Introductory Electronics, Allyn & Bacon, Boston Mass., 1987.

31. Smith, S.F., Machine Monitoring Via Motor-Current Demodulation Techniques, ORNL, 1991

32. Uhrig, R.E., Tsoukalas, L.H., Fuzzy and Neural Approaches in Engineering, John Wiley & Sons, 1997.

33. Upadhyaya, B., Introduction to Maintenance and Reliability Engineering, NE 484, Spring 1998.

34. Weiss, W., Laser Alignment Saves Amps, Dollars, Plant Services, April 1991.

35. Wowk, V., Machinery Vibration, McGraw-Hill Inc., New York, 1991.

36. Xu, M., Zatezalo, J.M., Marangoni, R.D., Reducing Power Loss Through Shaft Alignment, P/PM Technology, October 1993.

Thesis 97.K87

APPENDICES

APPENDIX A

GRAPHS OF THE RESULTS

GRAPHS OF RESULTS FROM MULTIPLE LINEAR REGRESSION MODEL

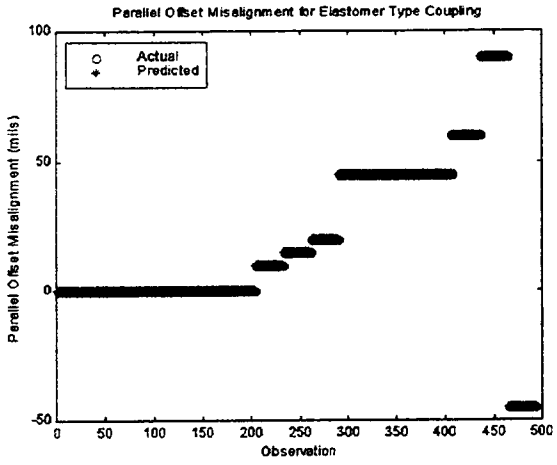


Figure A.1 Regression for the parallel offset misalignment model.

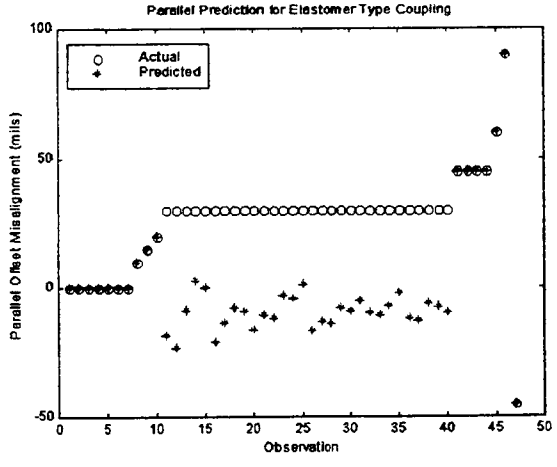


Figure A.2 Prediction for the parallel offset misalignment model.

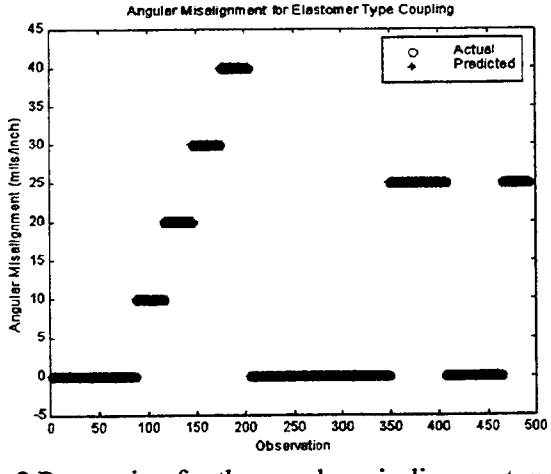


Figure A.3 Regression for the angular misalignment model.

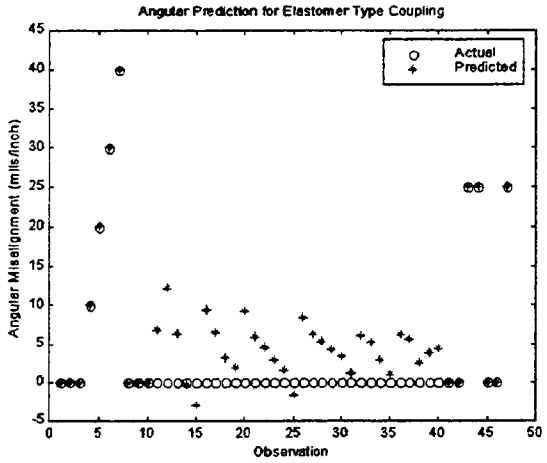


Figure A.4 Prediction for the angular misalignment model.

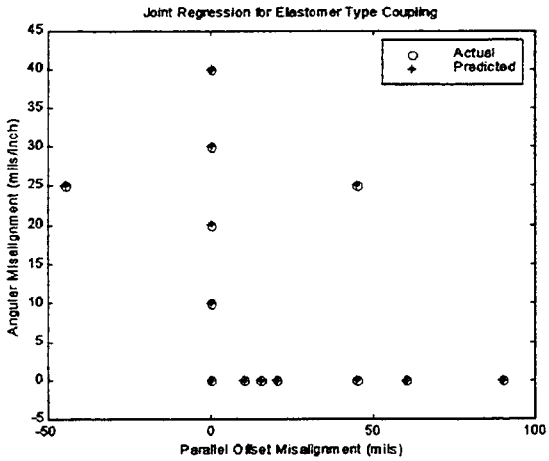


Figure A.5 Regression for the joint misalignment model.

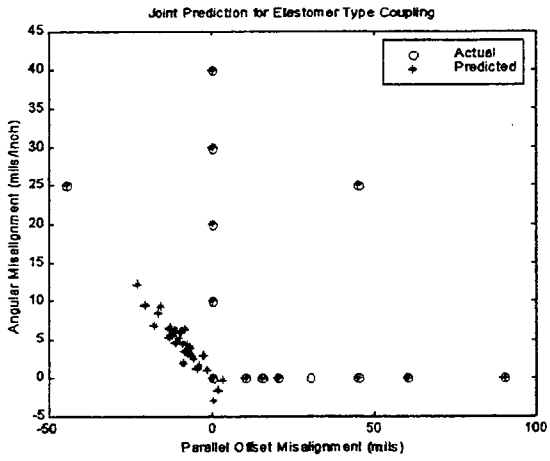


Figure A.6 Prediction for the joint misalignment model.

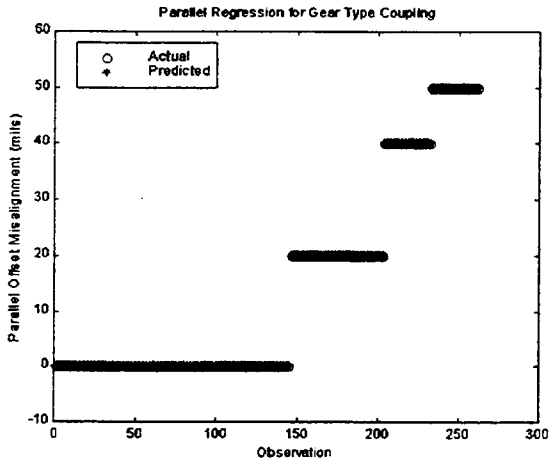


Figure A.7 Regression for the parallel offset misalignment model.

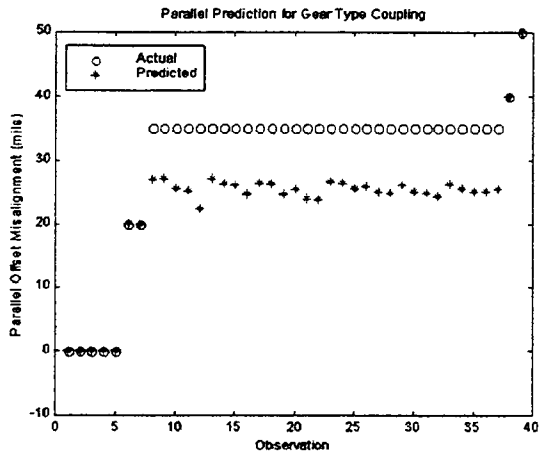


Figure A.8 Prediction for the parallel offset misalignment model.

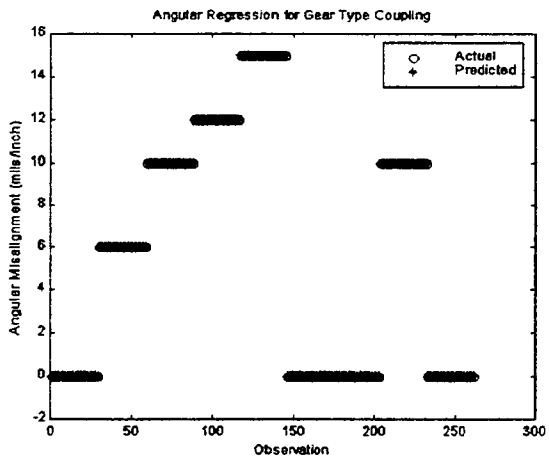


Figure A.9 Regression for the angular misalignment model.

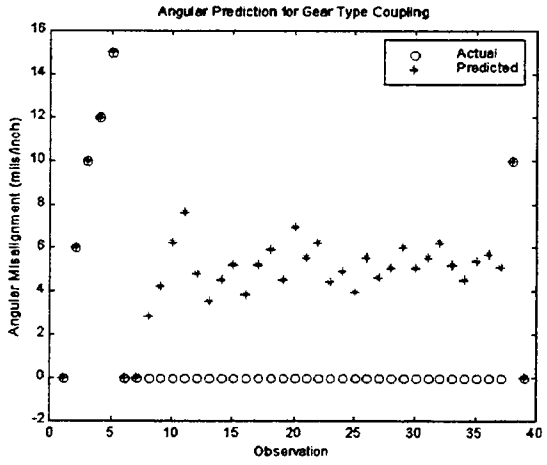


Figure A.10 Prediction for the angular misalignment model.

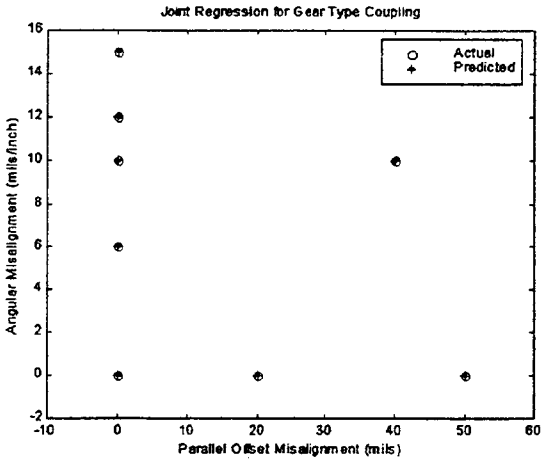


Figure A.11 Regression for the joint misalignment model.

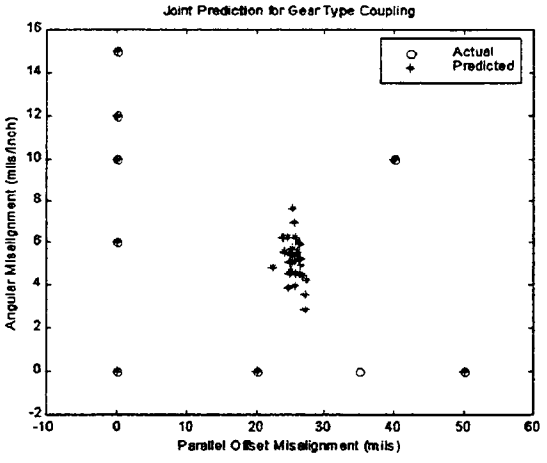


Figure A.12 Prediction for the joint misalignment model.

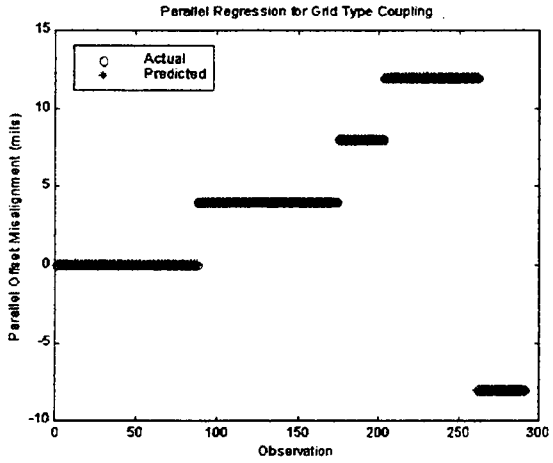


Figure A.13 Regression for the parallel offset misalignment model.

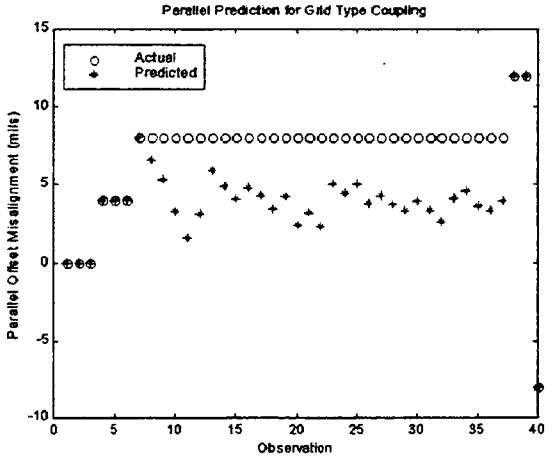


Figure A.14 Prediction for the parallel offset misalignment model.

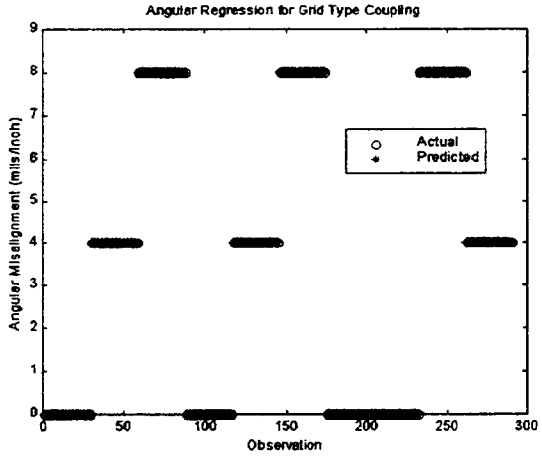


Figure A.15 Regression for the angular misalignment model.

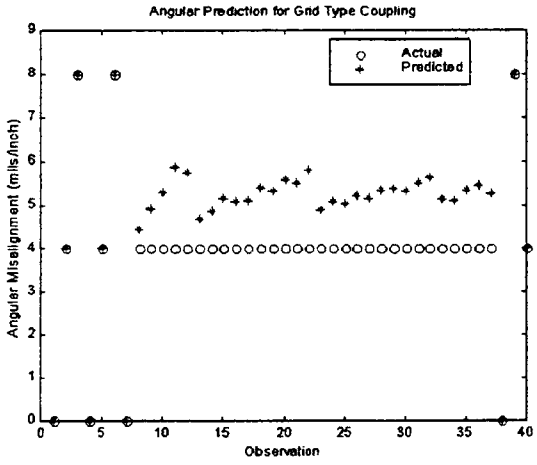


Figure A.16 Prediction for the angular misalignment model.

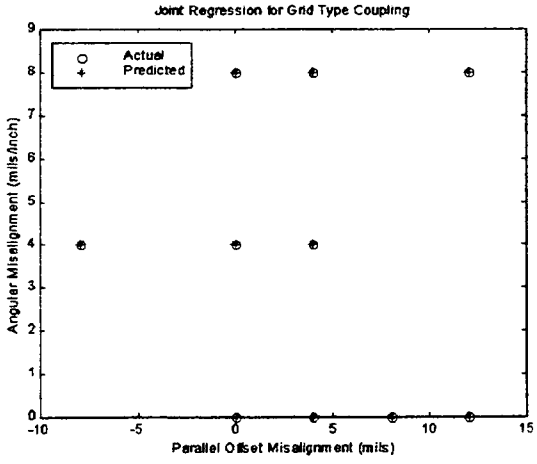


Figure A.17 Regression for the joint misalignment model.

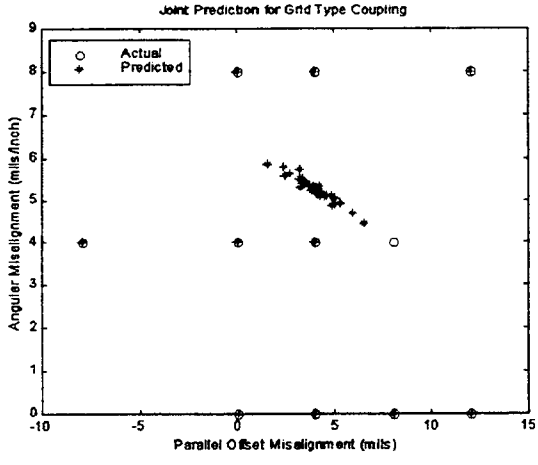


Figure A.18 Prediction for the joint misalignment model.

GRAPHS OF RESULTS FROM LINEAR CORRELATION NEURAL NETWORK

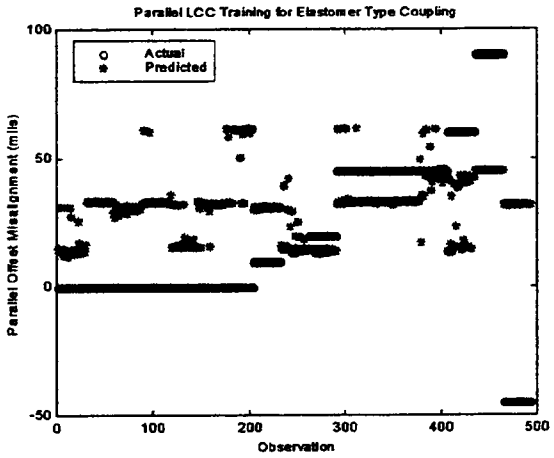


Figure A.19 Training for the parallel offset misalignment network.

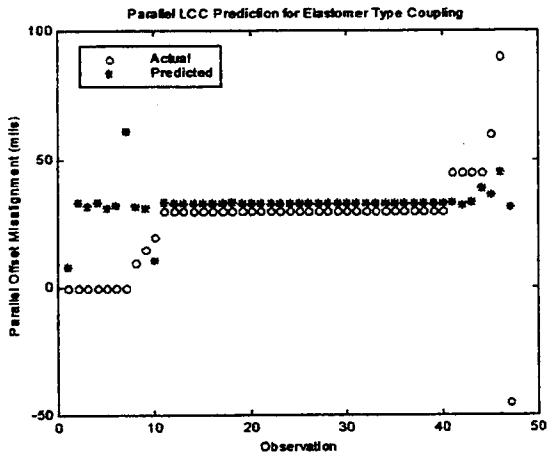


Figure A.20 Prediction for the parallel offset misalignment network.

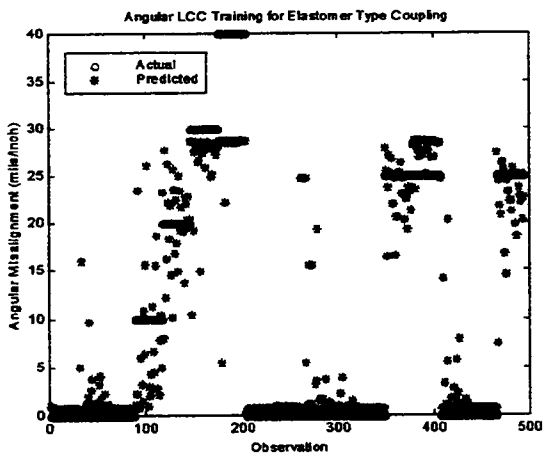


Figure A.21 Training for the angular misalignment ANN.

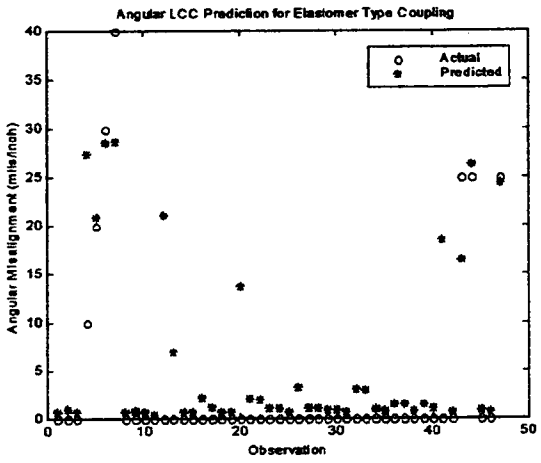


Figure A.22 Prediction for the angular misalignment ANN.

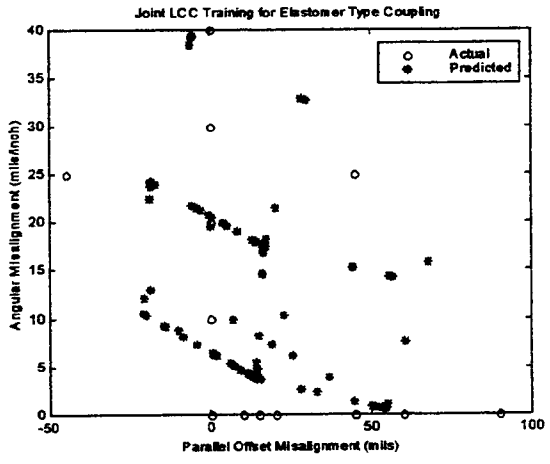


Figure A.23 Training for the joint misalignment ANN.

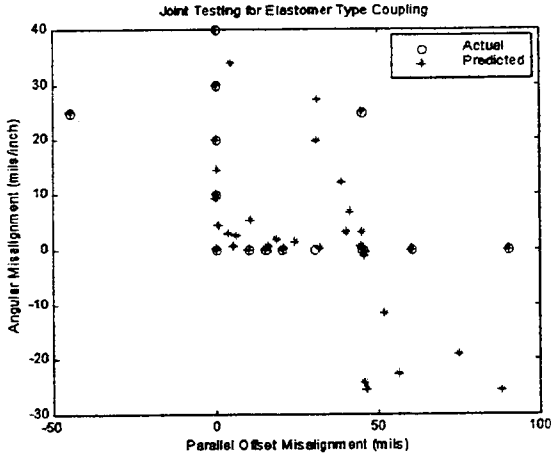


Figure A.24 Prediction for the joint misalignment ANN.

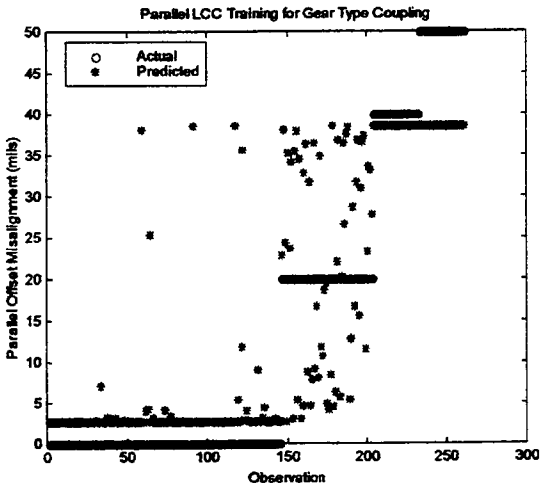


Figure A.25 Training for the parallel offset misalignment network.

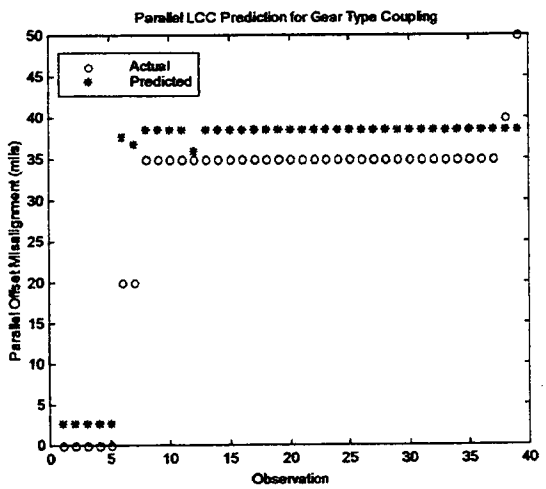


Figure A.26 Prediction for the parallel offset misalignment network.

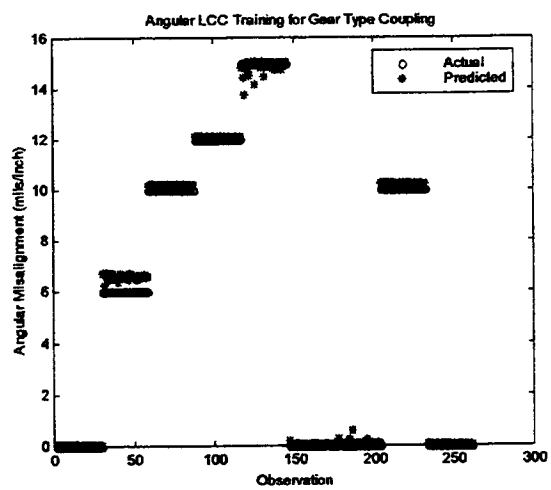


Figure A.27 Training for the angular misalignment ANN.

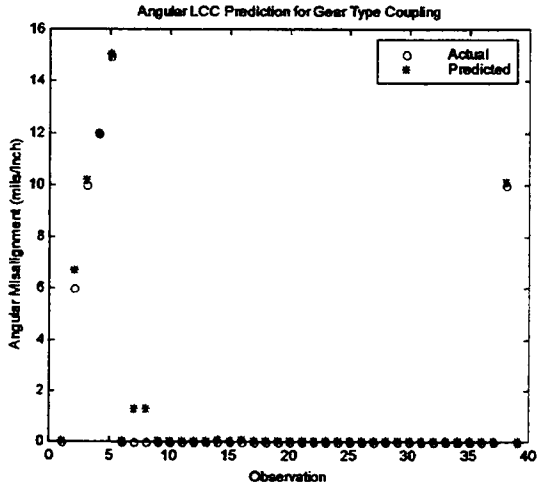


Figure A.28 Prediction for the angular misalignment ANN.

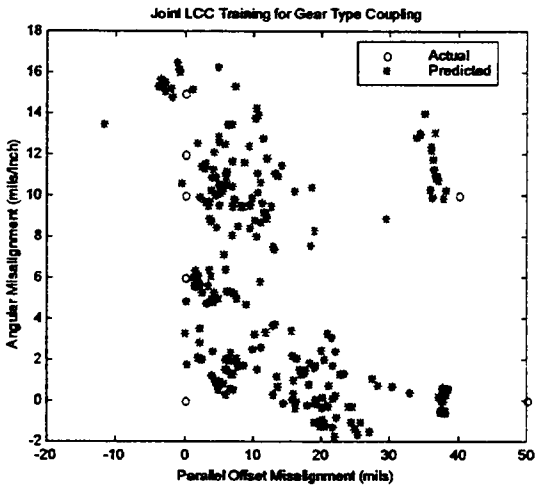


Figure A.29 Training for the joint misalignment ANN.

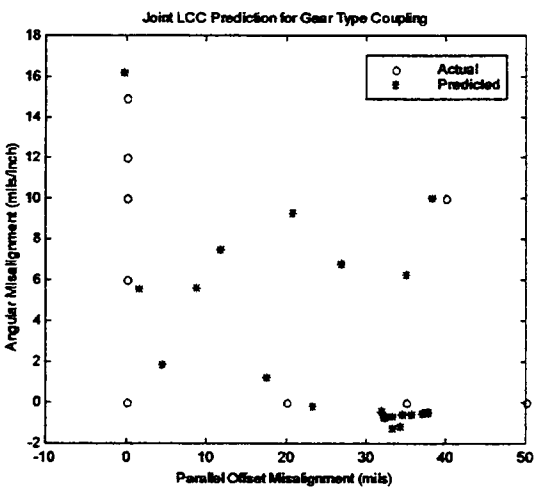


Figure A.30 Prediction for the joint misalignment ANN.

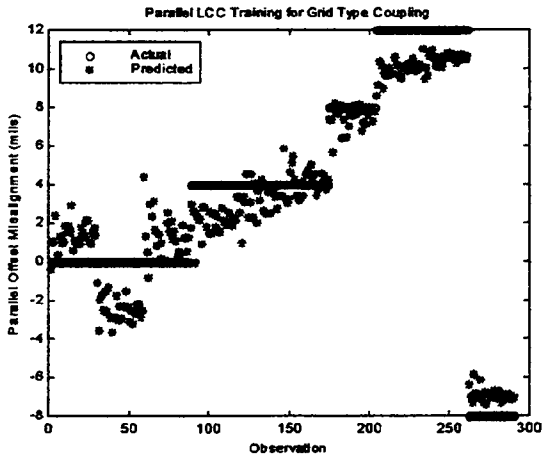


Figure A.31 Training for the parallel offset misalignment network.

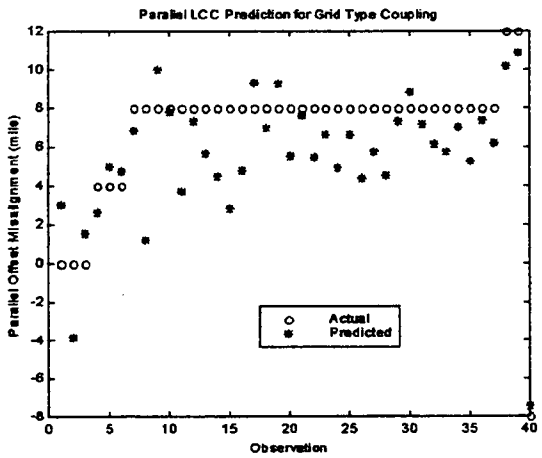


Figure A.32 Prediction for the parallel offset misalignment network.

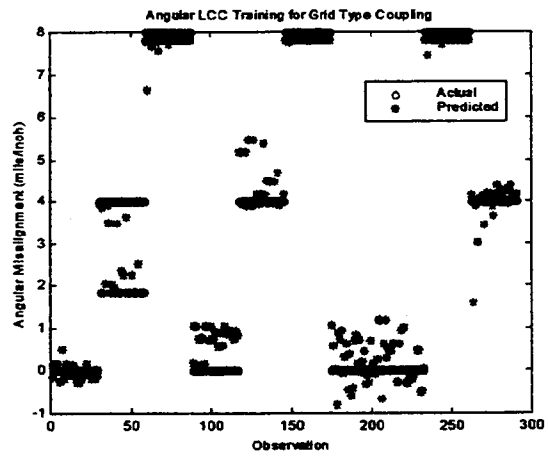


Figure A.33 Training for the angular misalignment ANN.

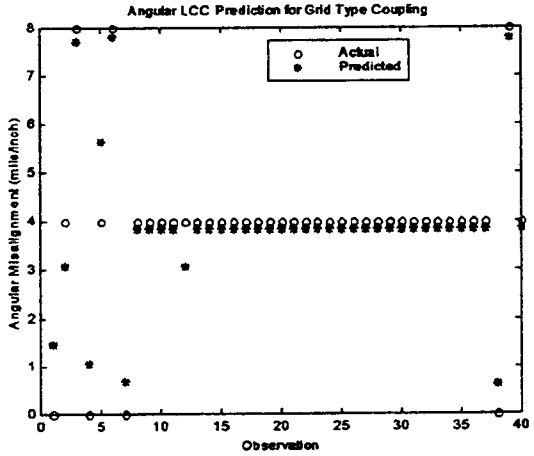


Figure A.34 Prediction for the angular misalignment ANN.

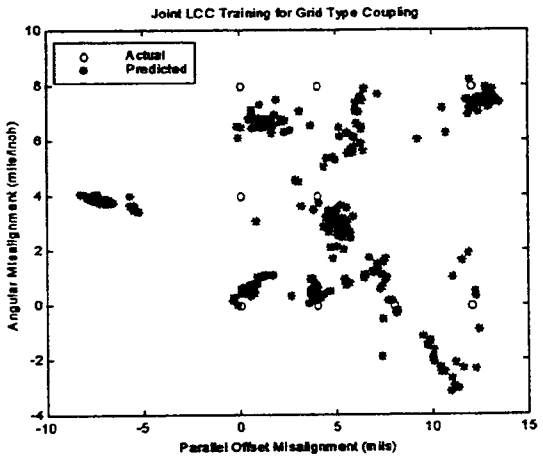


Figure A.35 Training for the joint misalignment ANN.

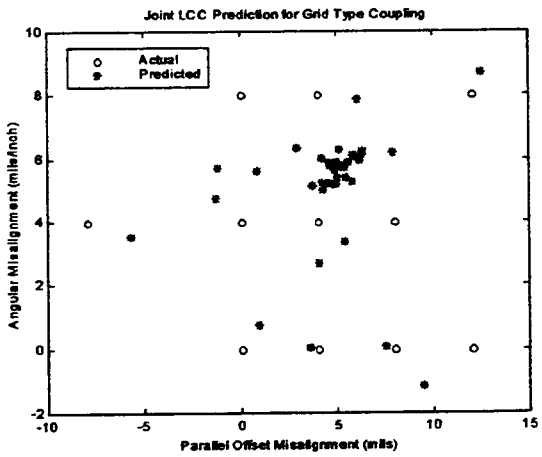


Figure A.36 Prediction for the joint misalignment ANN.

GRAPH OF RESULTS FROM PRINCIPLE COMPONENT NEURAL NETWORK

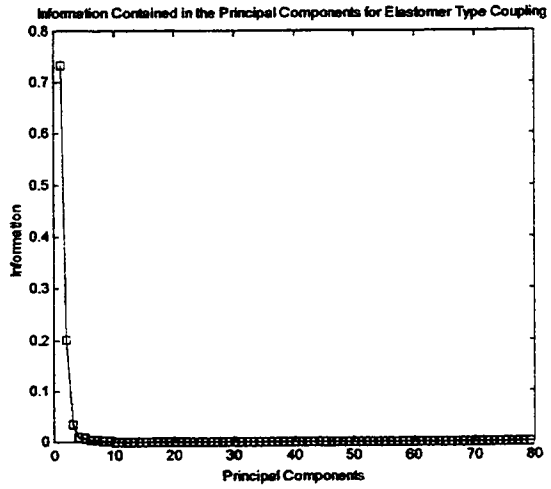


Figure A.37 Information contained in each PC.

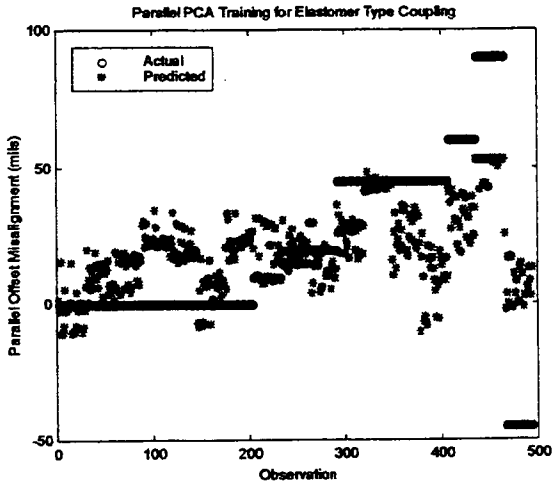


Figure A.38 Training for the parallel offset misalignment network.

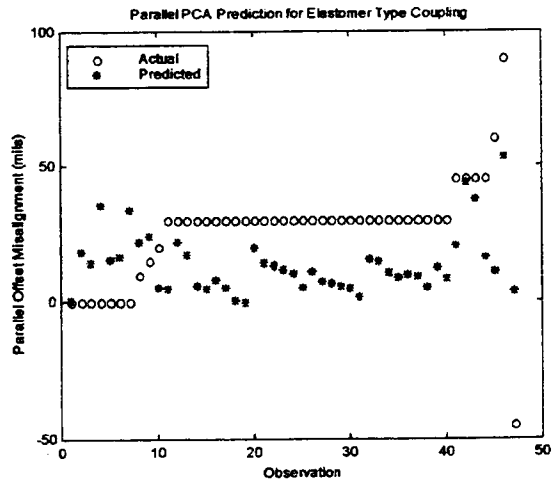


Figure A.39 Prediction for the parallel offset misalignment network.

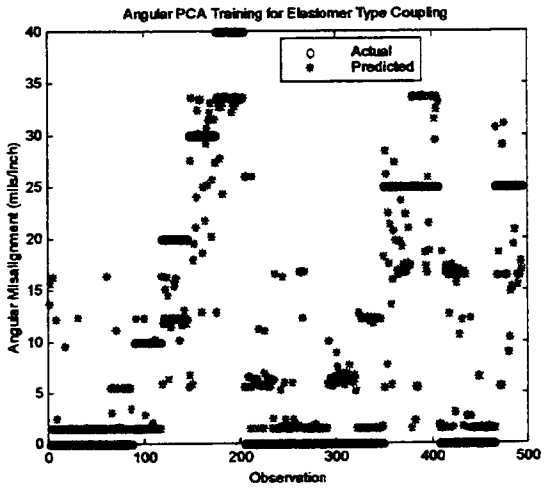


Figure A.40 Training for the angular misalignment ANN.

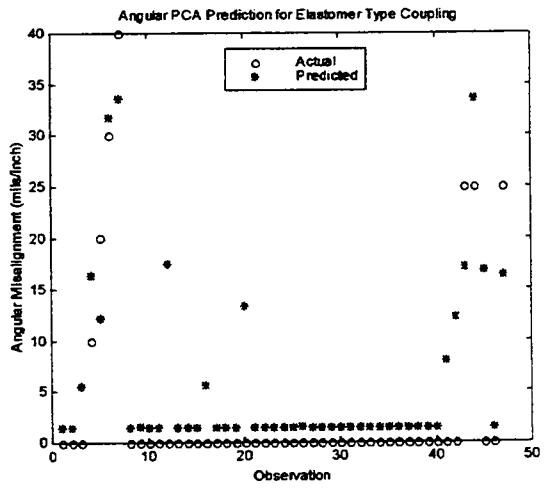


Figure A.41 Prediction for the angular misalignment ANN.

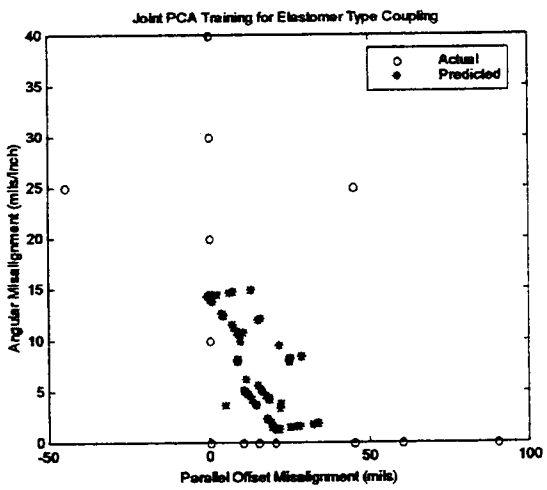


Figure A.42 Training for the joint misalignment ANN.

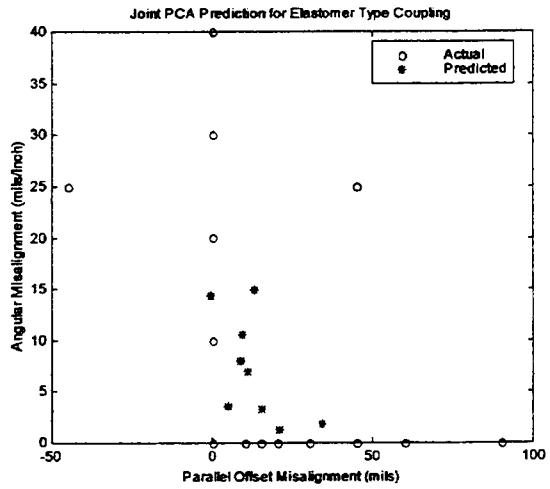


Figure A.43 Prediction for the joint misalignment ANN.

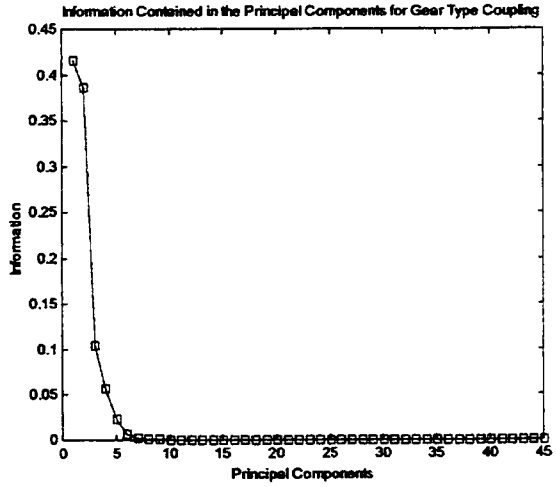


Figure A.44 Information contained in each PC.

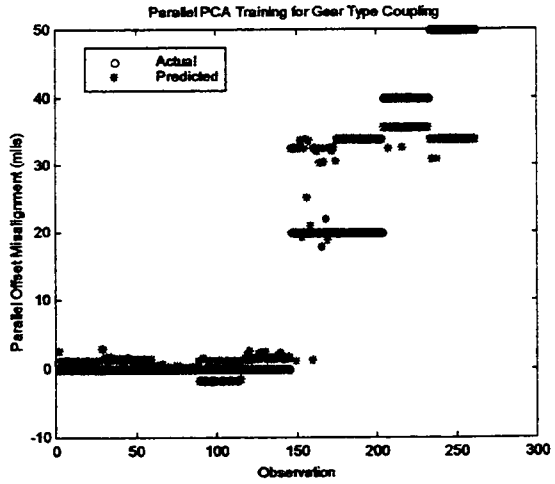


Figure A.45 Training for the parallel offset misalignment network.

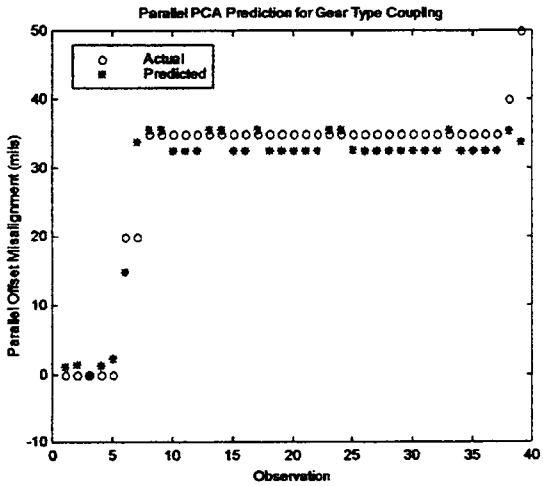


Figure A.46 Prediction for the parallel offset misalignment network.

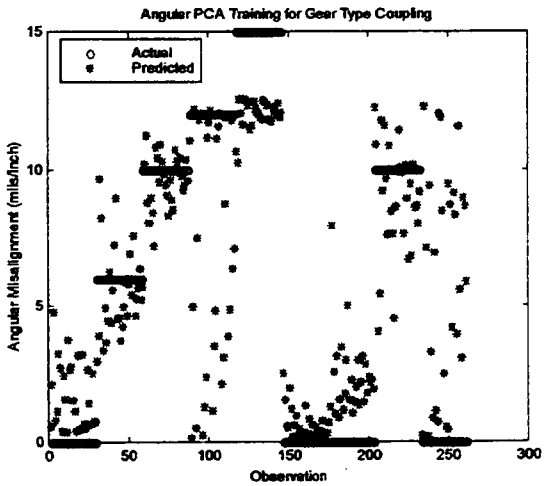


Figure A.47 Training for the angular misalignment ANN.

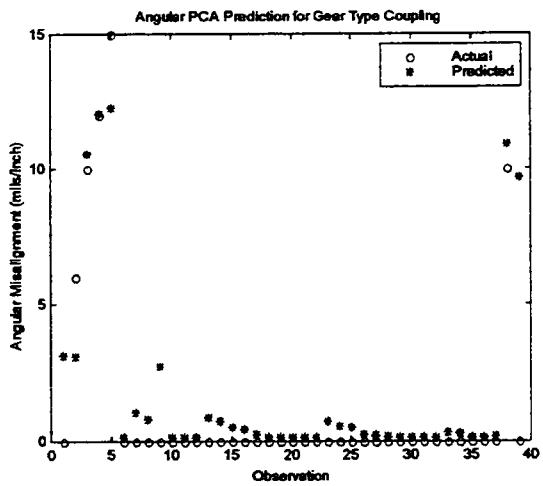


Figure A.48 Prediction for the angular misalignment ANN.

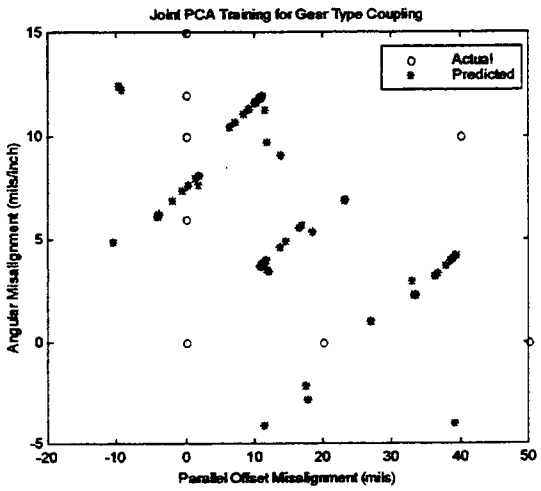


Figure A.49 Training for the joint misalignment ANN.

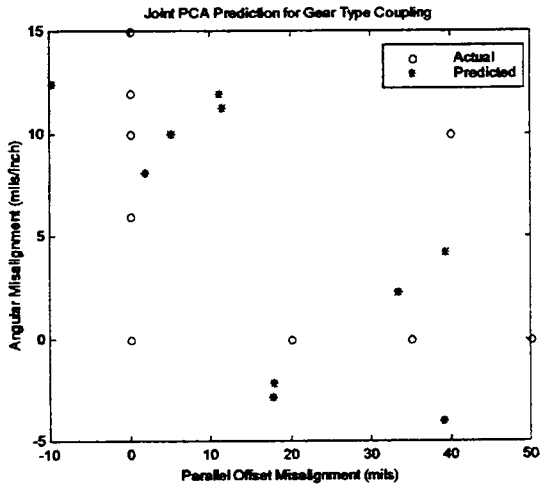


Figure A.50 Prediction for the joint misalignment ANN.

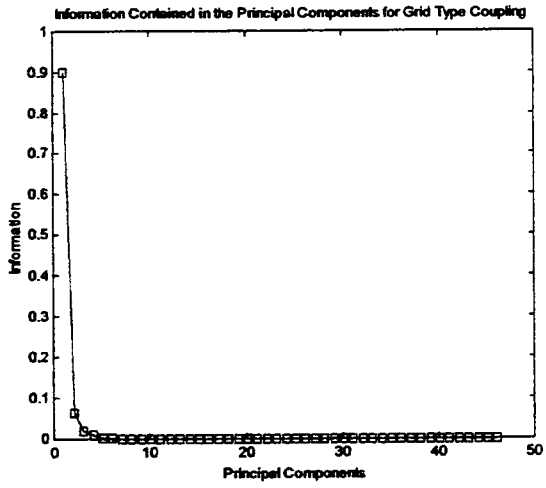


Figure A.51 Information contained in each PC.

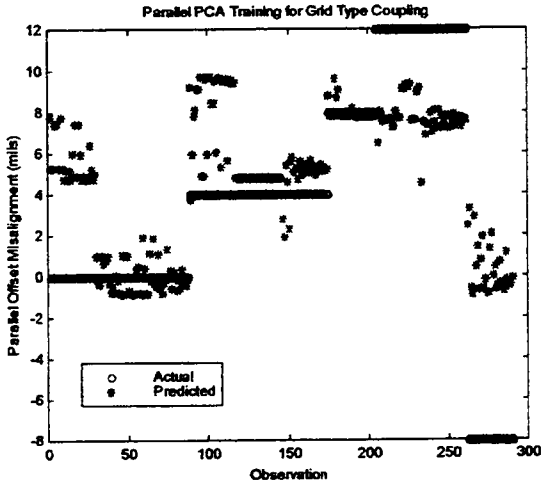


Figure A.52 Training for the parallel offset misalignment network.

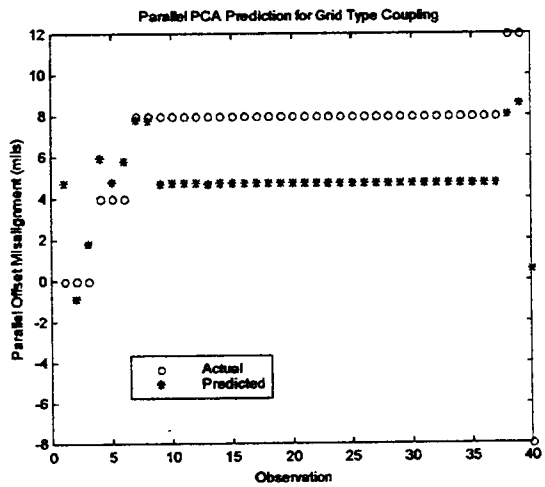


Figure A.53 Prediction for the parallel offset misalignment network.

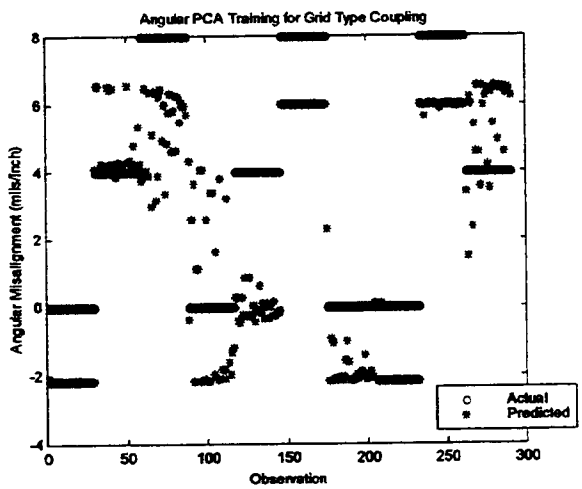


Figure A.54 Training for the angular misalignment ANN.

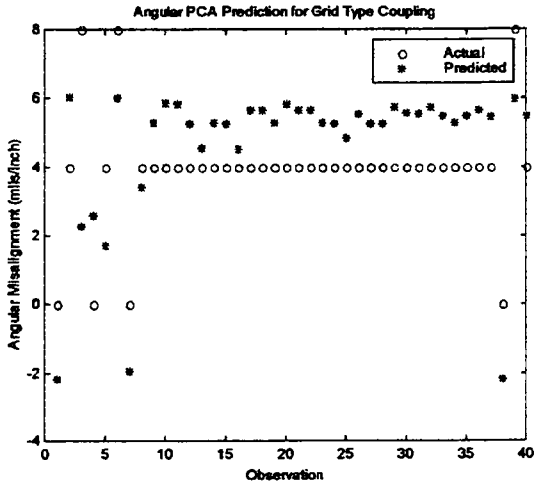


Figure A.55 Prediction for the angular misalignment ANN.

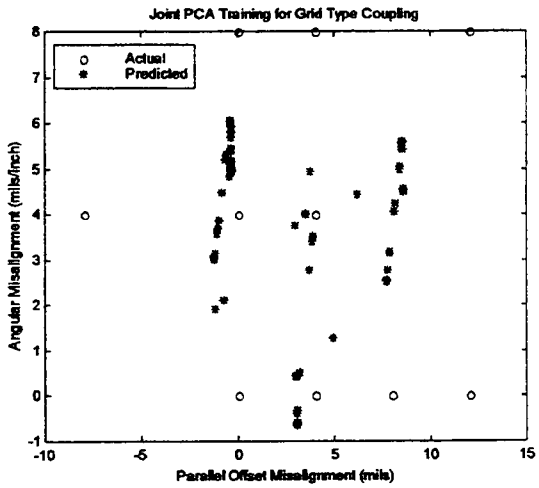


Figure A.56 Training for the joint misalignment ANN.

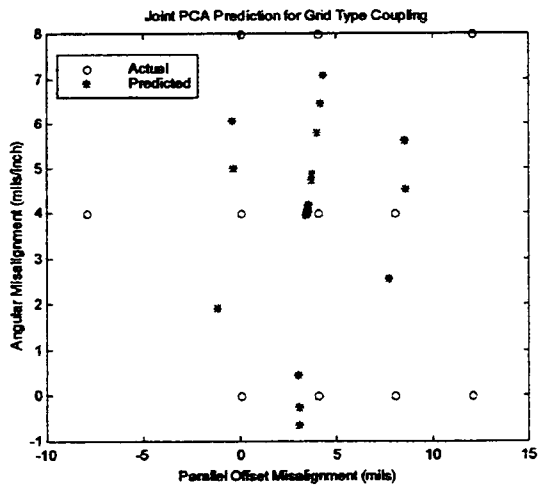


Figure A.57 Prediction for the joint misalignment ANN.

GRAPH OF RESULTS FROM PARTIAL LEAST SQUARES LINEAR MODEL

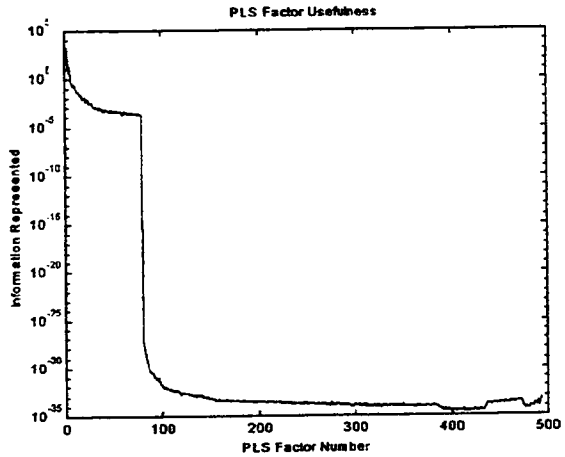


Figure A.58 Amount of information contained in each of the PLS factors.

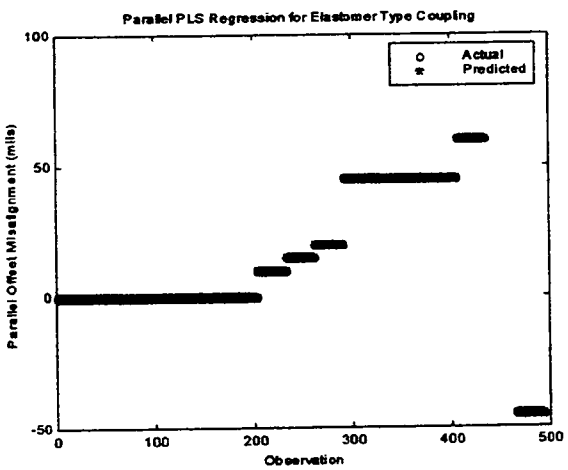


Figure A.59 Training for the parallel offset misalignment model.

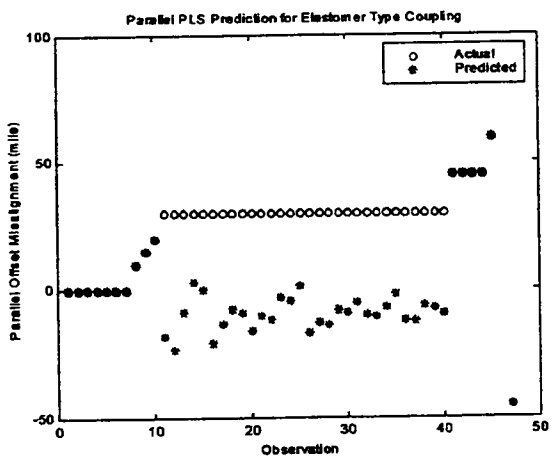


Figure A.60 Prediction for the parallel offset misalignment model.

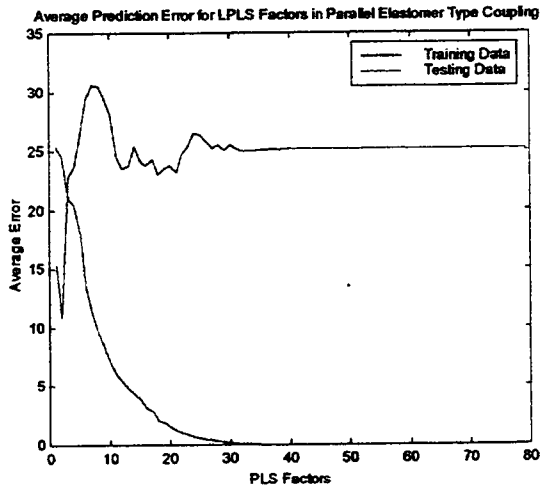


Figure A.61 Prediction error associated with each PLS factor.

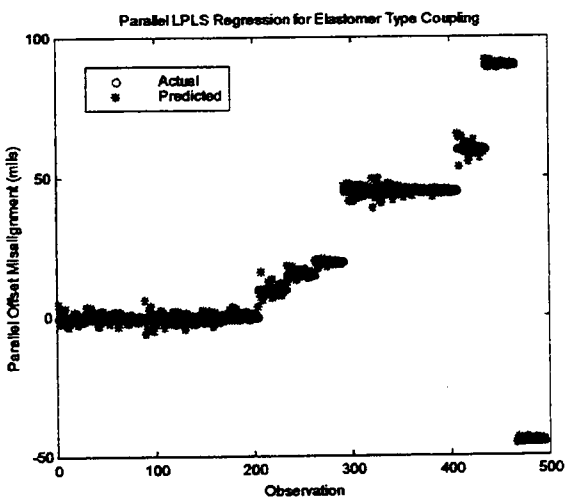


Figure A.62 Training for the reduced parallel offset model.

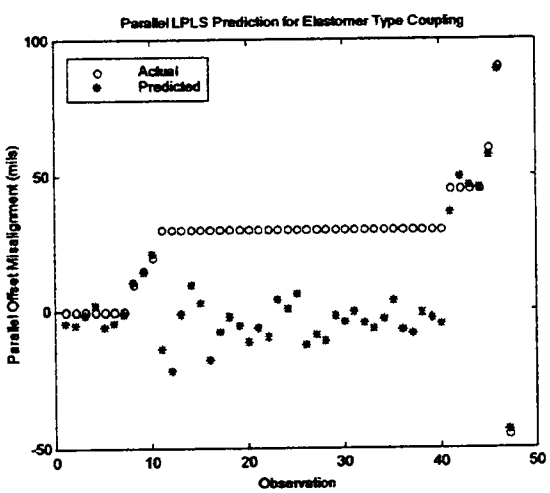


Figure A.63 Prediction for the parallel offset misalignment model.

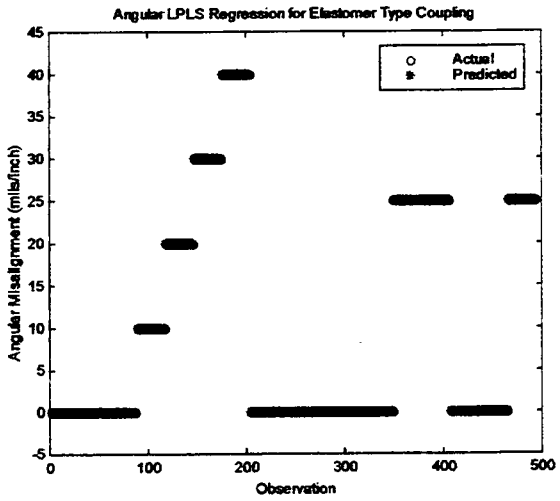


Figure A.64 Training for the angular misalignment model.

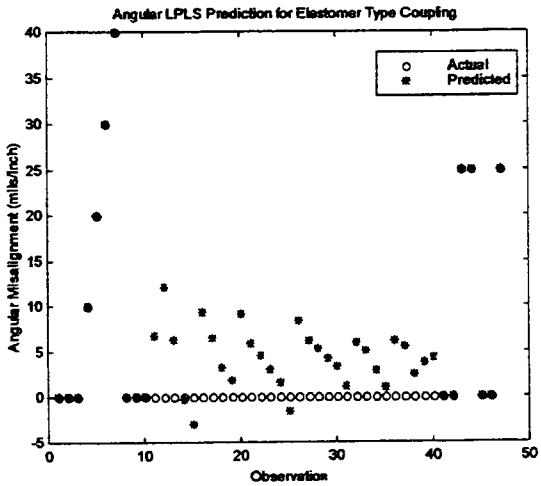


Figure A.65 Prediction for the parallel offset misalignment model.

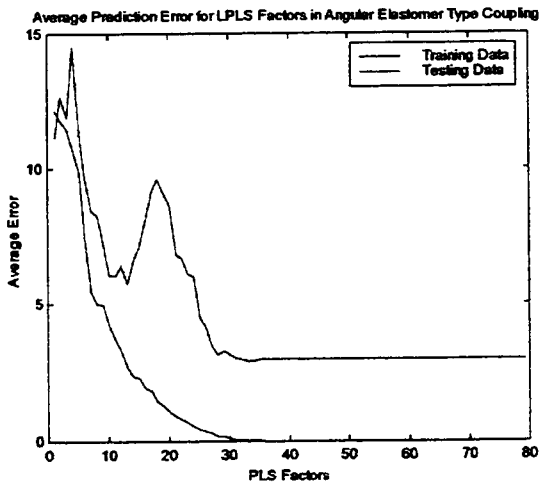


Figure A.66 Prediction error associated with each PLS factor.

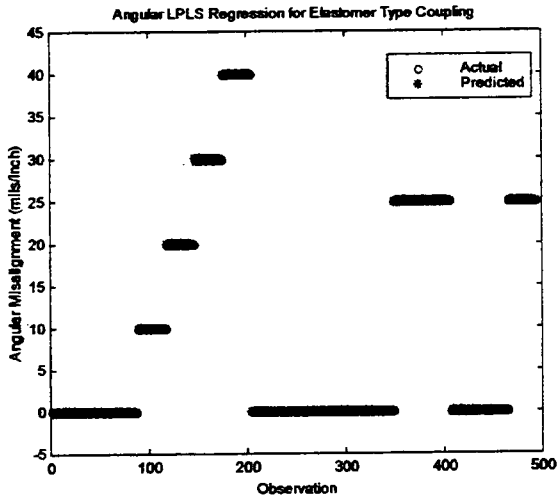


Figure A.67 Training for the reduced angular model.

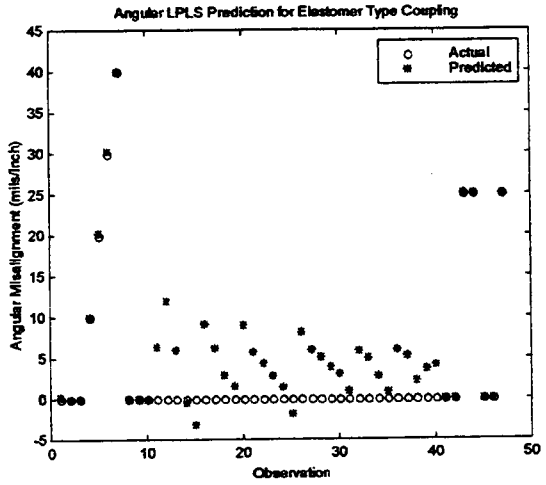


Figure A.68 Prediction for the reduced angular model.

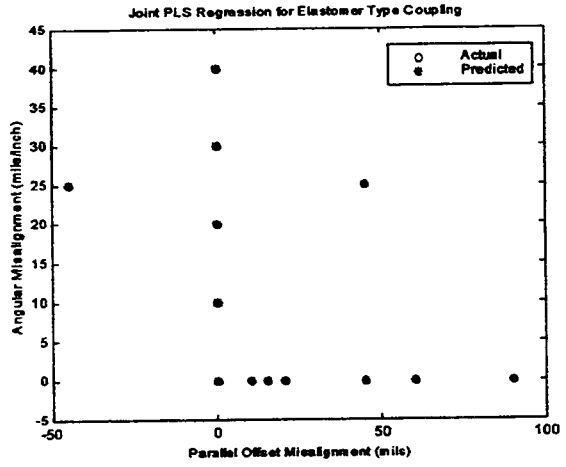


Figure A.69 Training for the joint misalignment model.

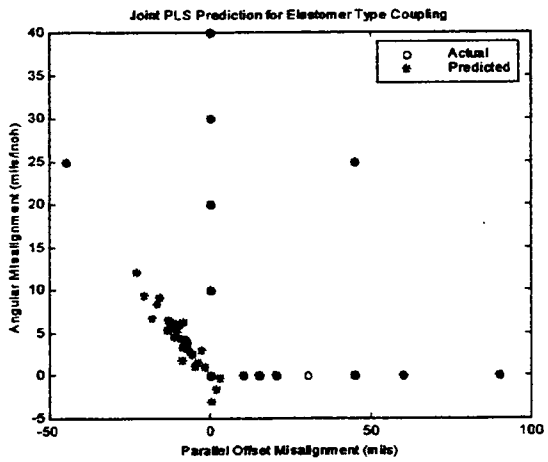


Figure A.70 Prediction for the joint misalignment model.

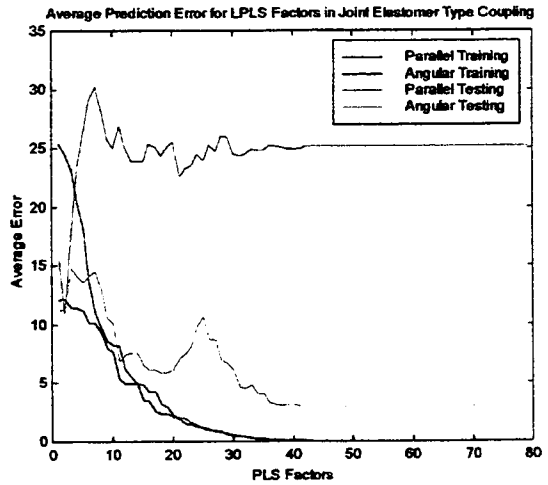


Figure A.71 Prediction error associated with each PLS factor.

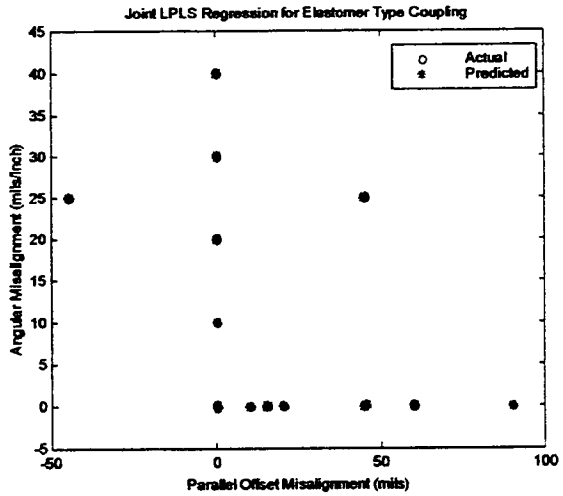


Figure A.72 Training for the reduced joint model.

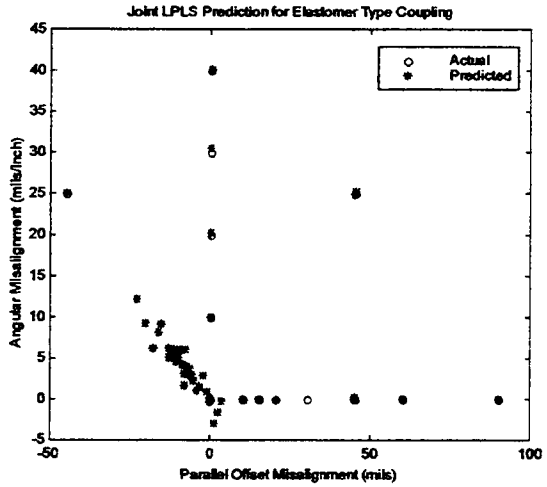


Figure A.73 Prediction for the reduced joint misalignment model.

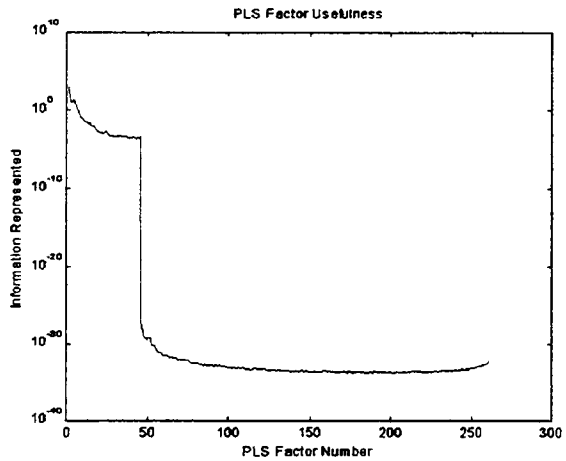


Figure A.74 Amount of information contained in each of the PLS factors.

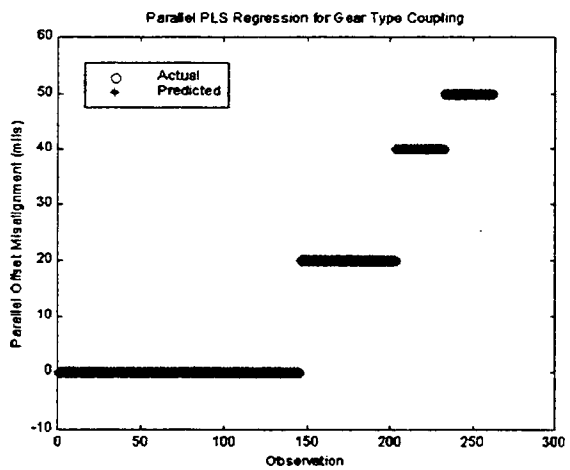


Figure A.75 Training for the parallel offset misalignment model.

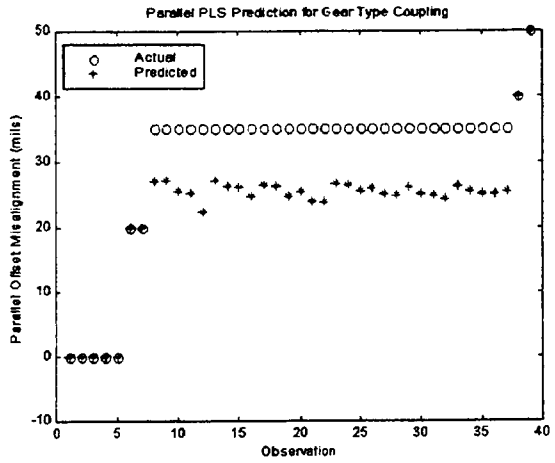


Figure A.76 Prediction for the parallel offset misalignment model.

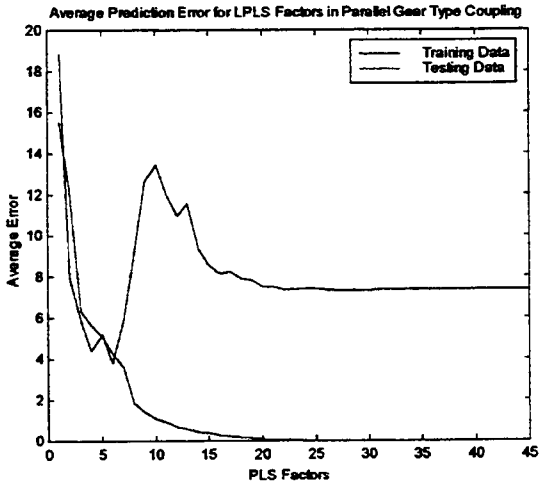


Figure A.77 Prediction error associated with each PLS factor.

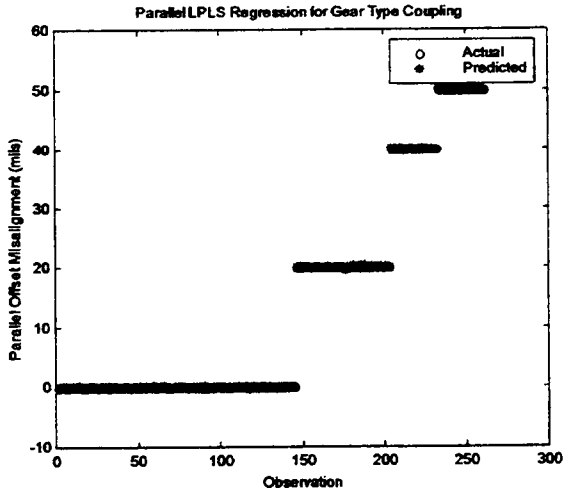


Figure A.78 Training for the reduced parallel offset model.

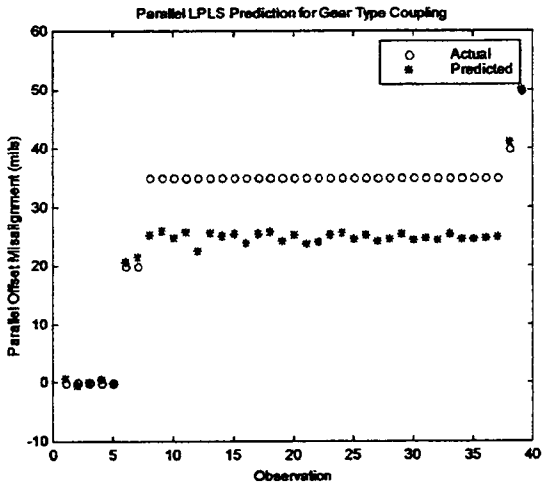


Figure A.79 Prediction for the parallel offset misalignment model.

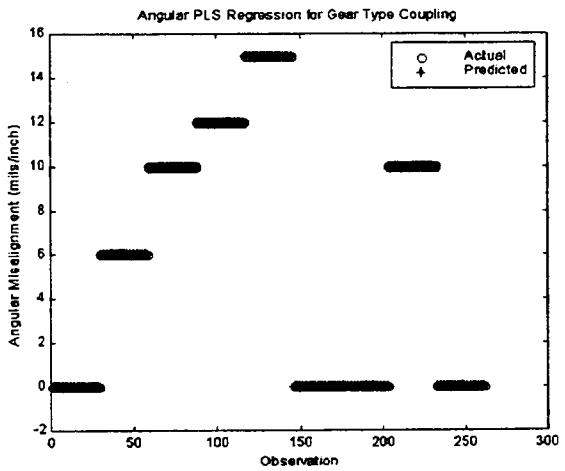


Figure A.80 Training for the angular misalignment model.

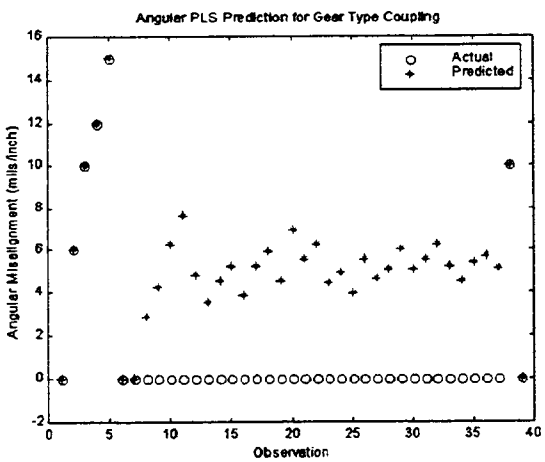


Figure A.81 Prediction for the parallel offset misalignment model.

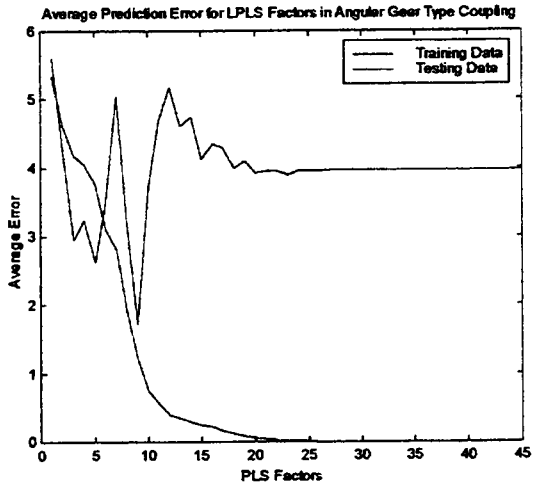


Figure A.82 Prediction error associated with each PLS factor.

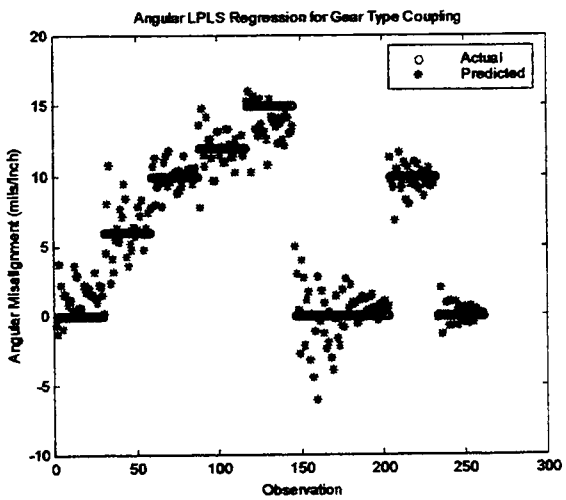


Figure A.83 Training for the reduced angular model.

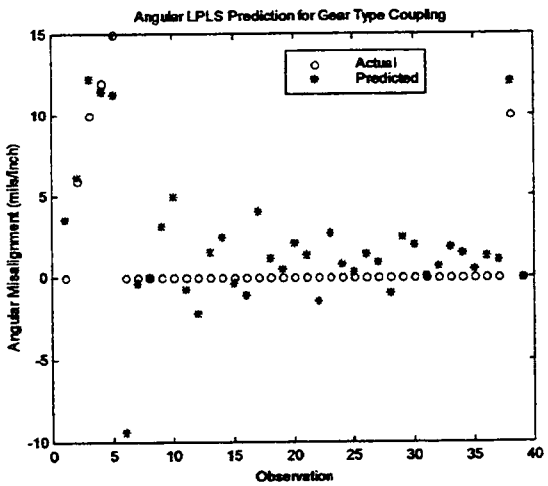


Figure A.84 Prediction for the reduced angular model.

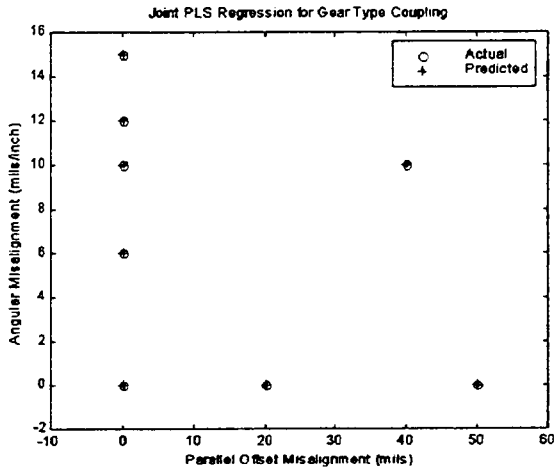


Figure A.85 Training for the joint misalignment model.

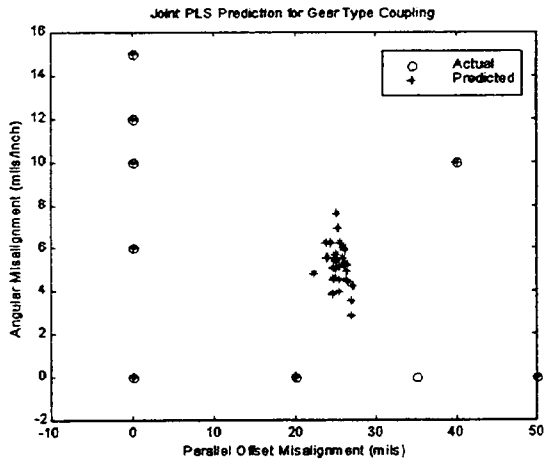


Figure A.86 Prediction for the joint misalignment model.

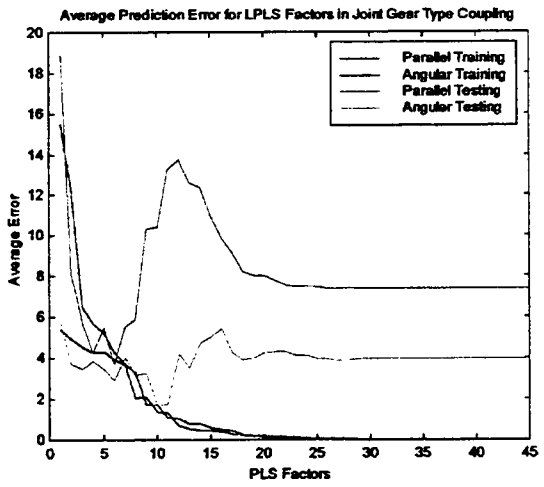


Figure A.87 Prediction error associated with each PLS factor.

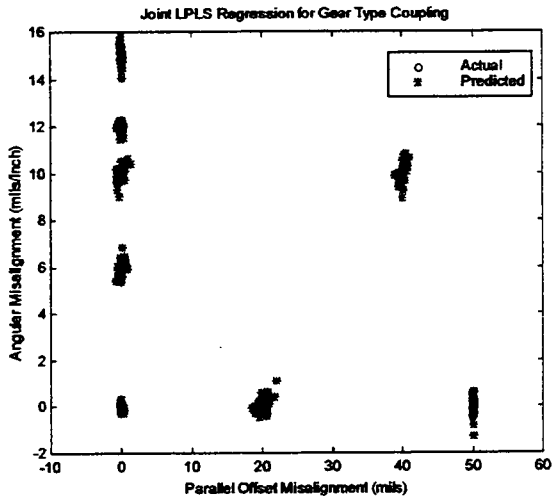


Figure A.88 Training for the reduced joint model.

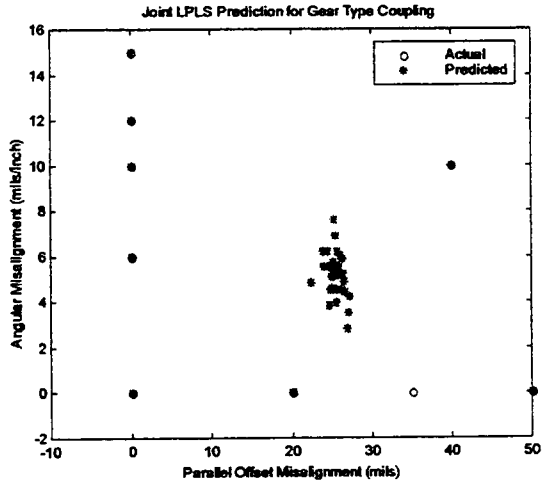


Figure A.89 Prediction for the reduced joint misalignment model.

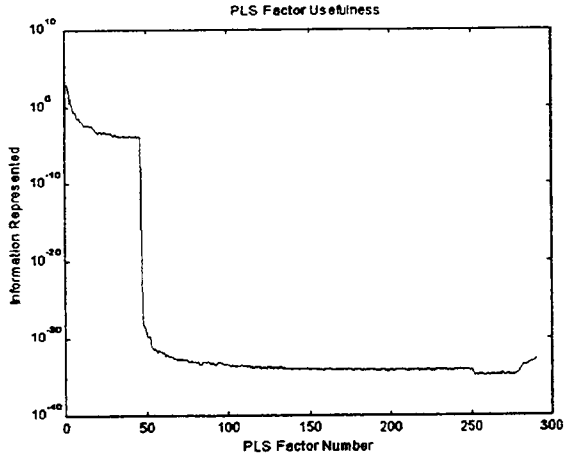


Figure A.90 Amount of information contained in each of the PLS factors.

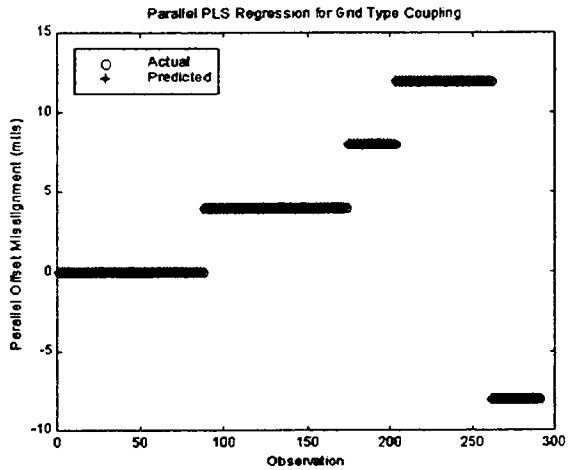


Figure A.91 Training for the parallel offset misalignment model.

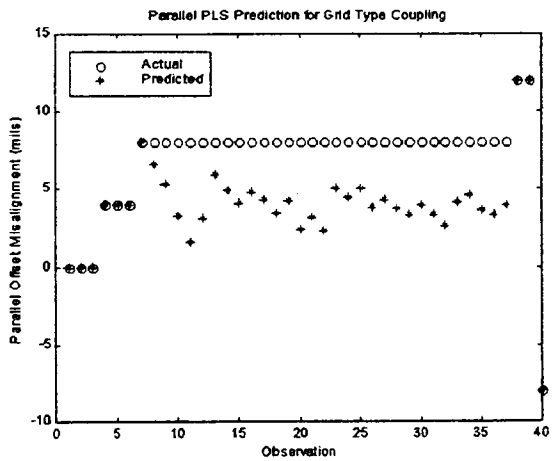


Figure A.92 Prediction for the parallel offset misalignment model.

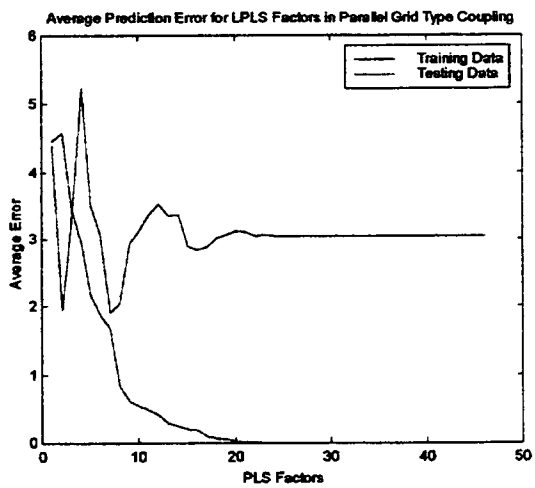


Figure A.93 Prediction error associated with each PLS factor.

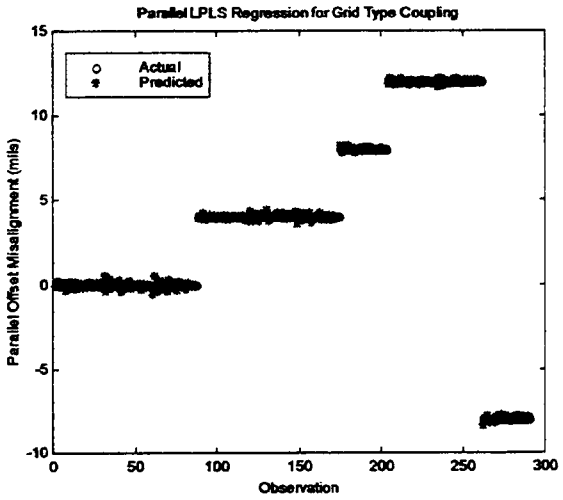


Figure A.94 Training for the reduced parallel offset model.

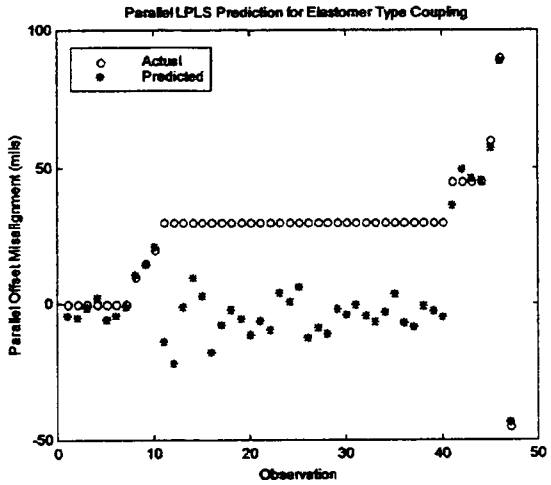


Figure A.95 Prediction for the parallel offset misalignment model.

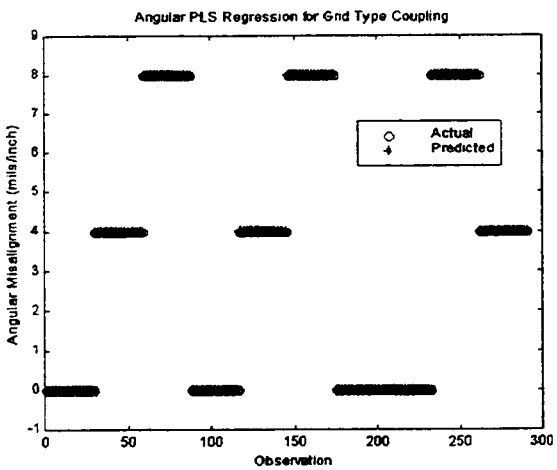


Figure A.96 Training for the angular misalignment model.

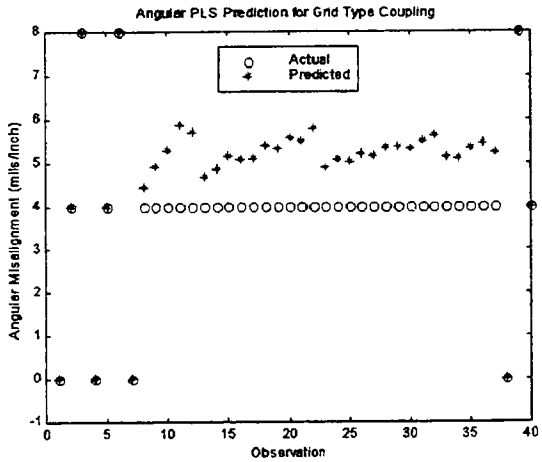


Figure A.97 Prediction for the parallel offset misalignment model.

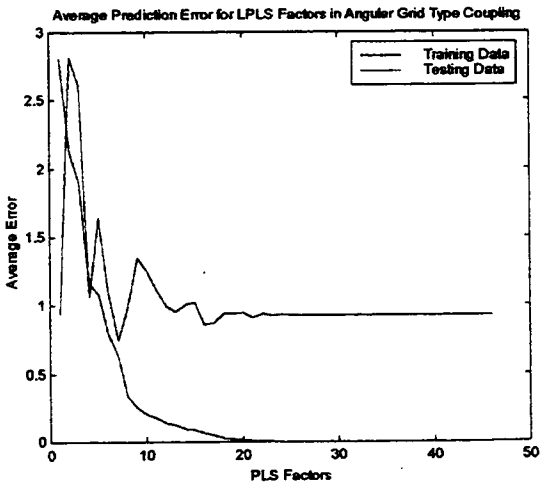


Figure A.98 Prediction error associated with each PLS factor.

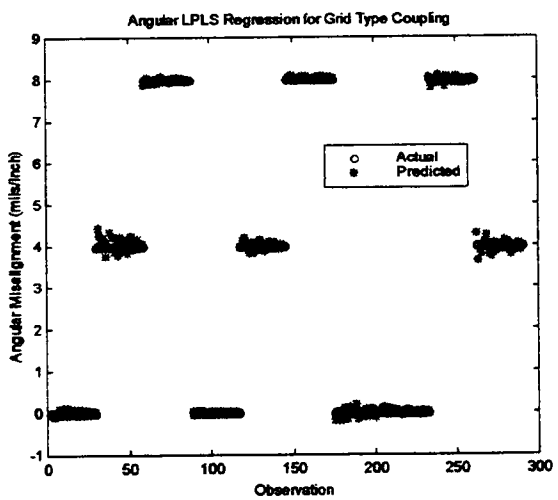


Figure A.99 Training for the reduced angular model.

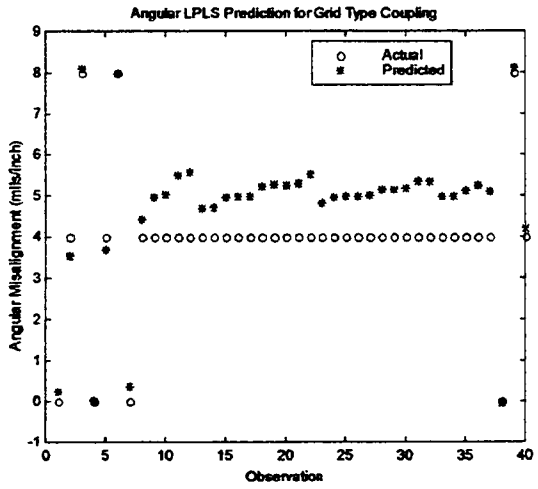


Figure A.100 Prediction for the reduced angular model.

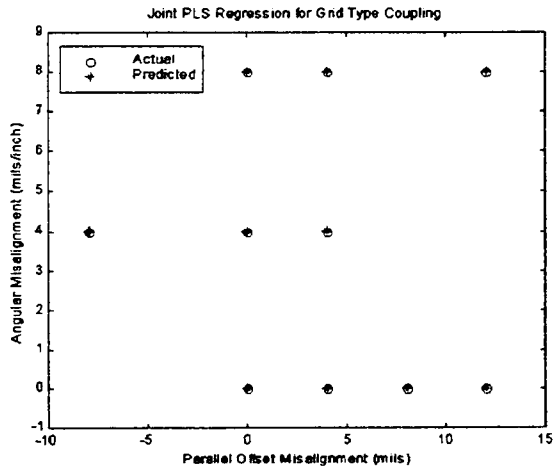


Figure A.101 Training for the joint misalignment model.

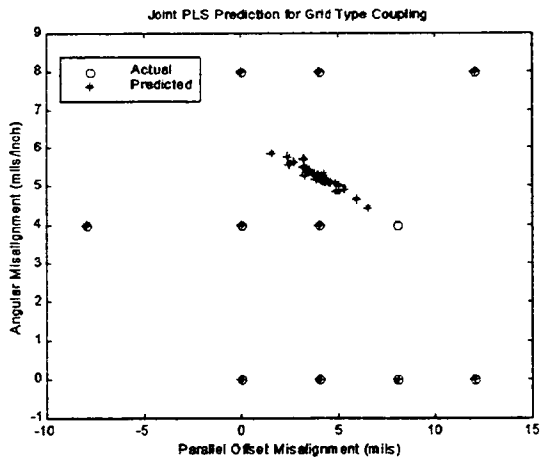


Figure A.102 Prediction for the joint misalignment model.

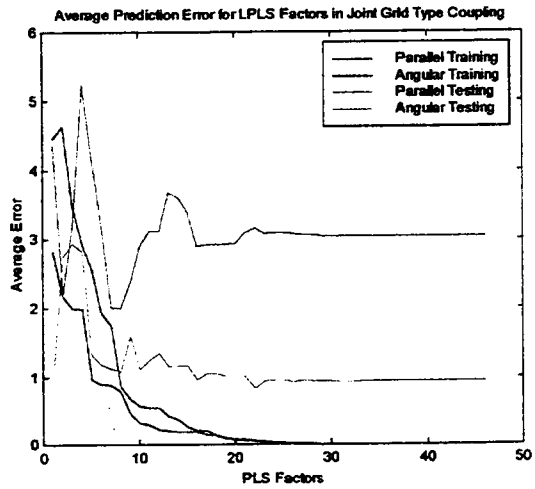


Figure A.103 Prediction error associated with each PLS factor.

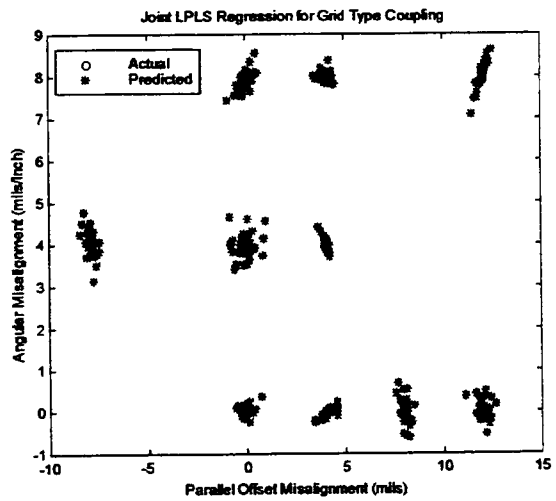


Figure A.104 Training for the reduced joint model.

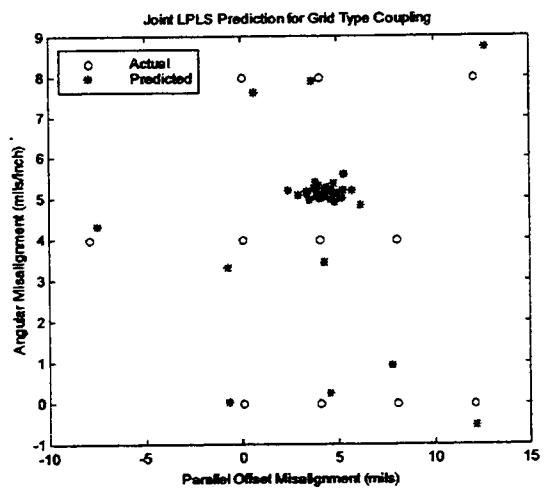
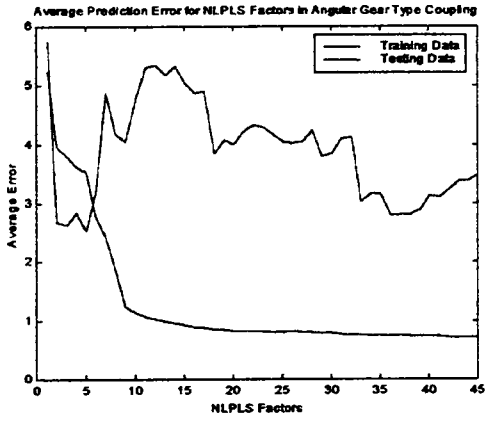
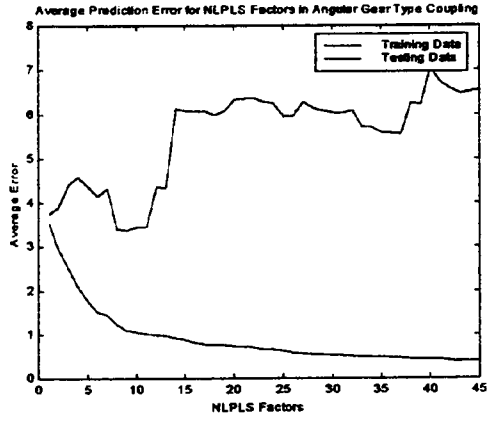


Figure A.105 Prediction for the reduced joint misalignment model.

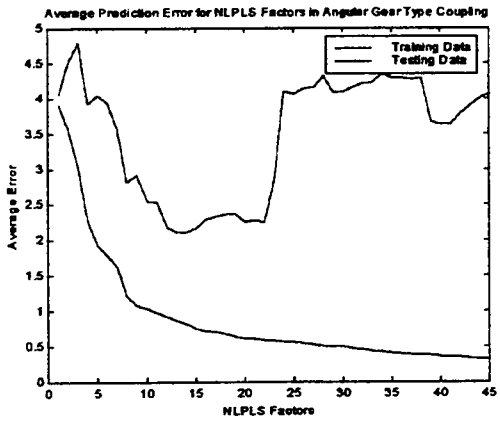
GRAPHS OF RESULTS FROM NON-LINEAR PARTIAL LEAST SQUARES MODELS



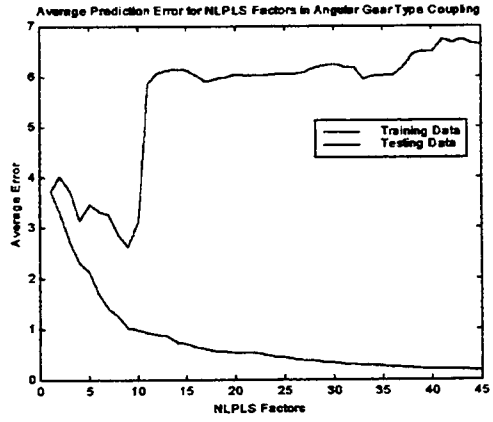
a) 3 Hidden Neurons



b) 10 Hidden Neurons



c) 15 Hidden Neurons



d) 20 Hidden Neurons

Figure A.106 Prediction Errors for different NLPLS Network Architectures.

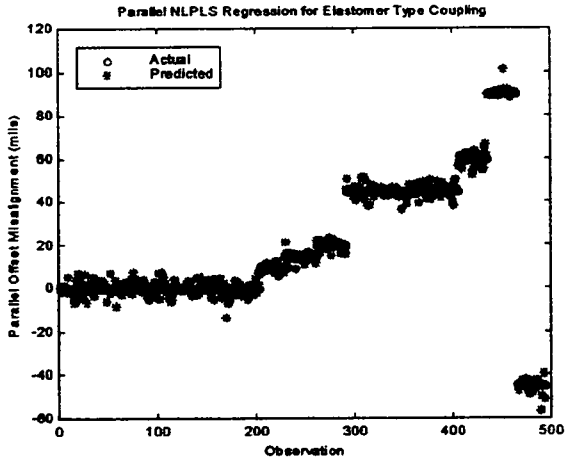


Figure A.107 Training for the parallel offset misalignment model.

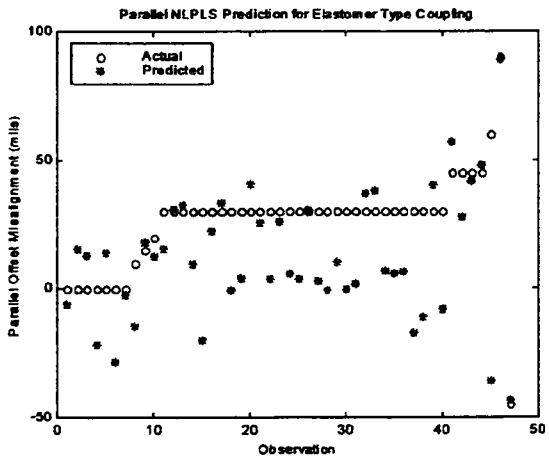


Figure A.108 Prediction for the parallel offset misalignment model.

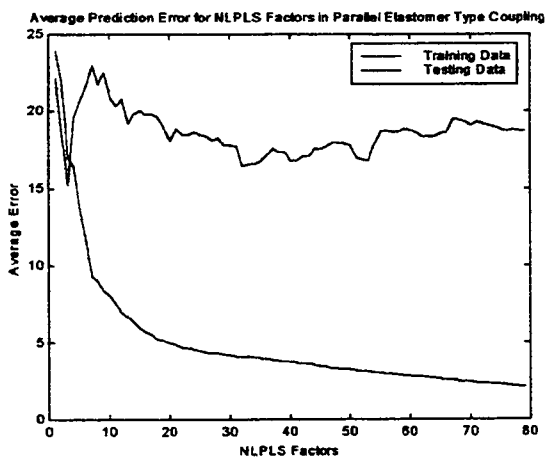


Figure A.109 Prediction error associated with each NLPLS factor.

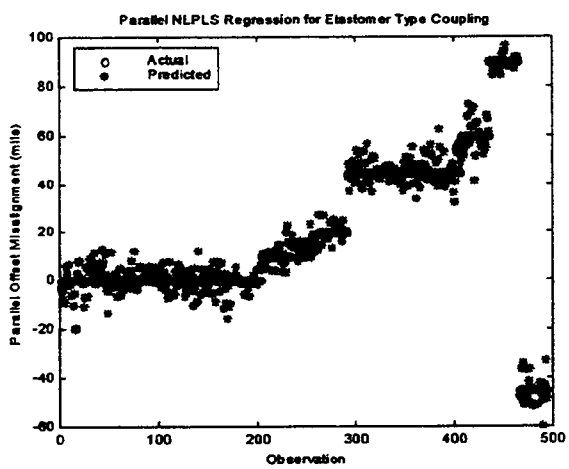


Figure A.110 Training for the reduced parallel offset model.

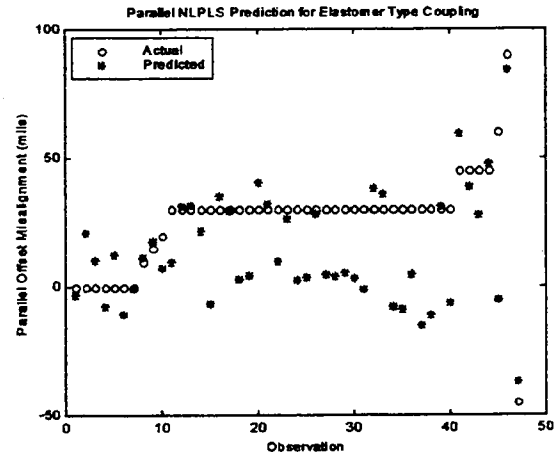


Figure A.111 Prediction for the parallel offset misalignment model.

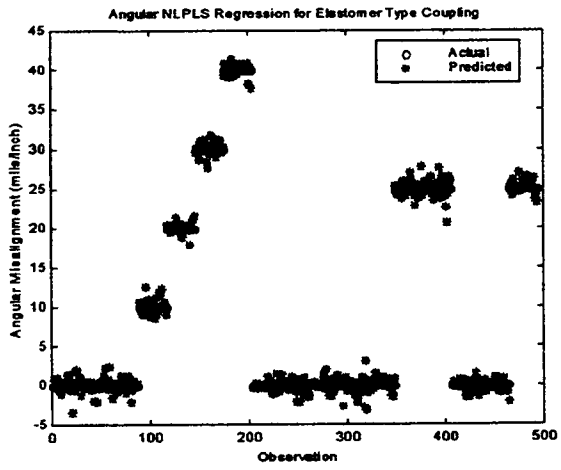


Figure A.112 Training for the angular misalignment model.

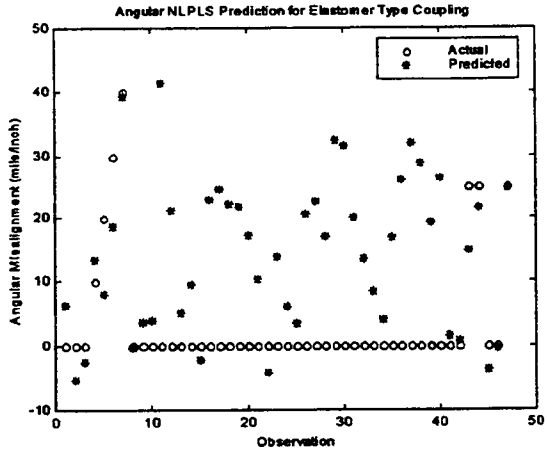


Figure A.113 Prediction for the parallel offset misalignment model.

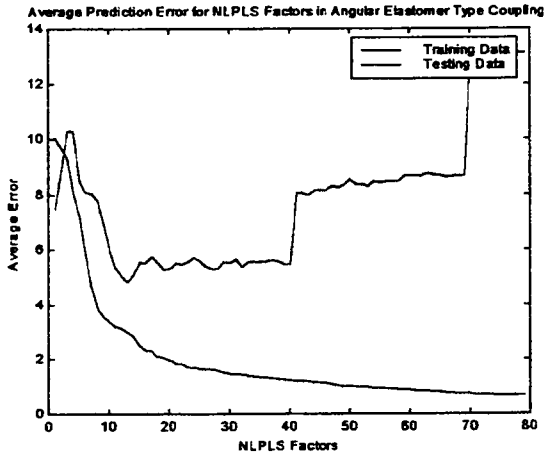


Figure A.114 Prediction error associated with each NLPLS factor.

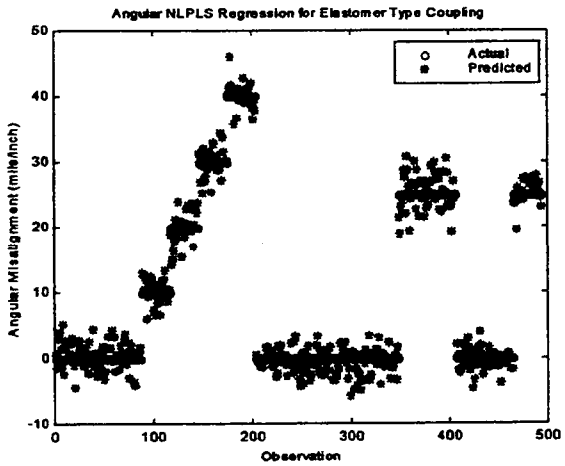


Figure A.115 Training for the reduced angular model.

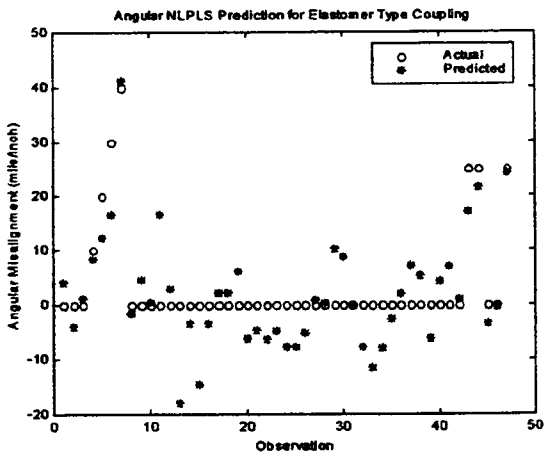


Figure A.116 Prediction for the reduced angular model.

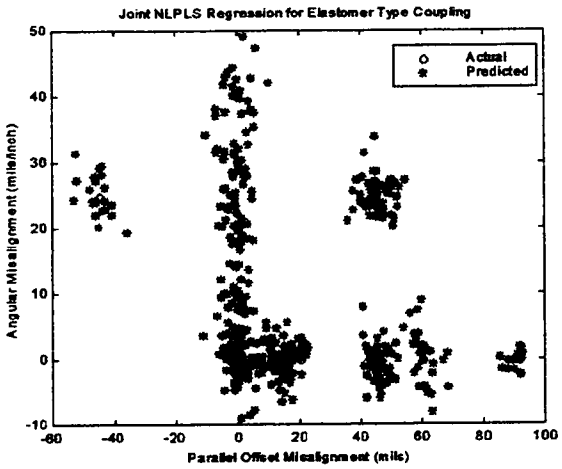


Figure A.117 Training for the joint misalignment model.

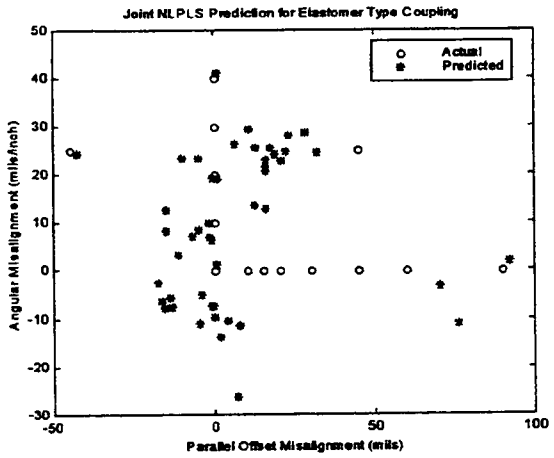


Figure A.118 Prediction for the joint misalignment model.

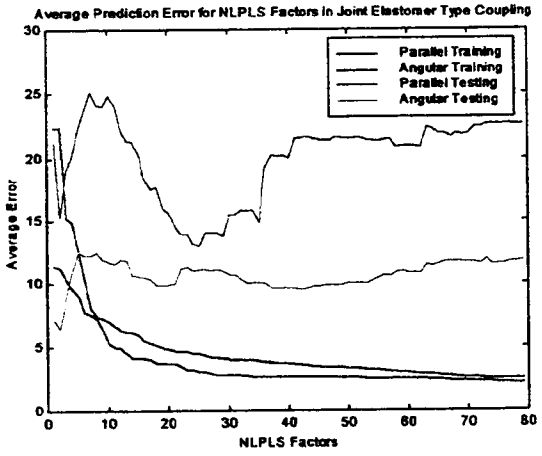


Figure A.119 Prediction error associated with each NLPLS factor.

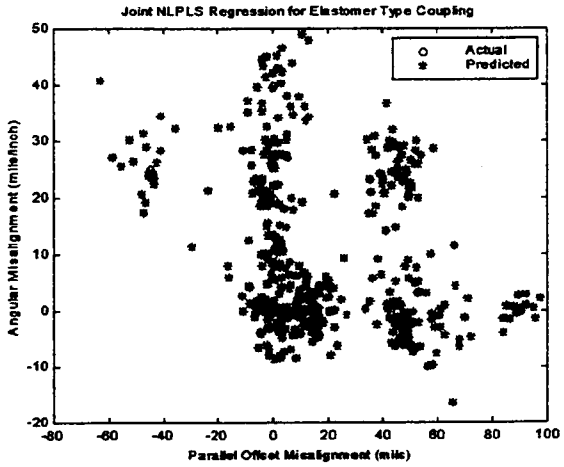


Figure A.120 Training for the reduced joint model.

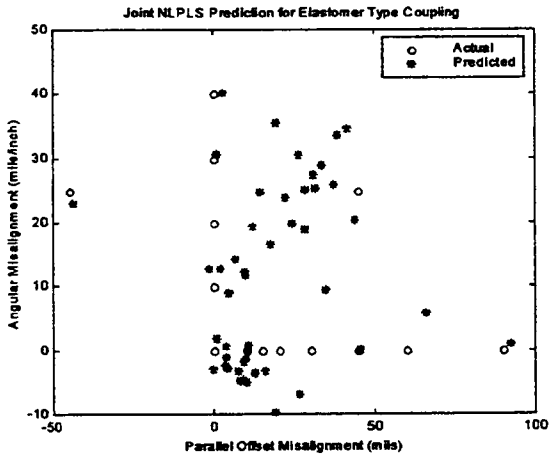


Figure A.121 Prediction for the reduced joint misalignment model.

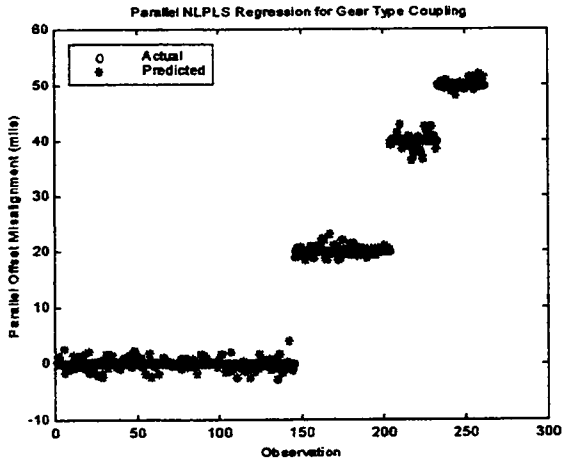


Figure A.122 Training for the parallel offset misalignment model.

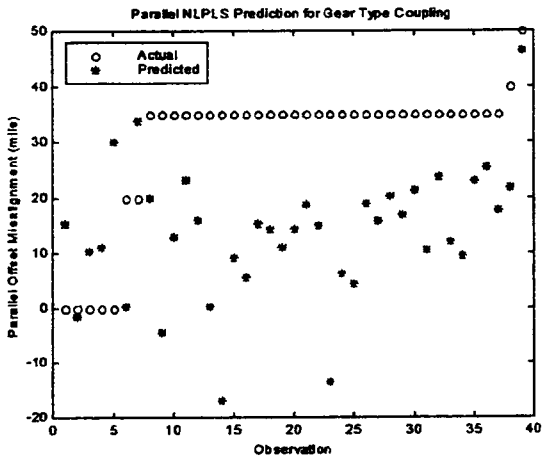


Figure A.123 Prediction for the parallel offset misalignment model.

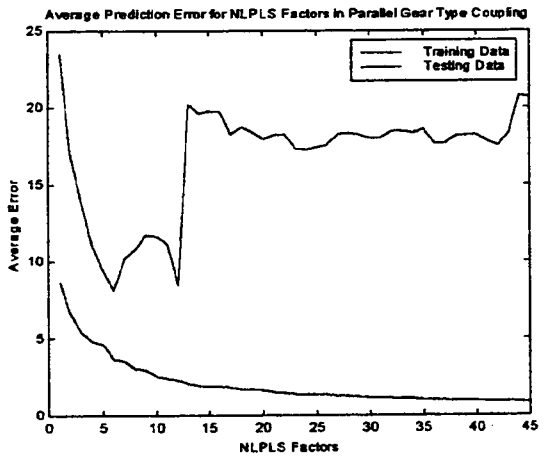


Figure A.124 Prediction error associated with each NLPLS factor.

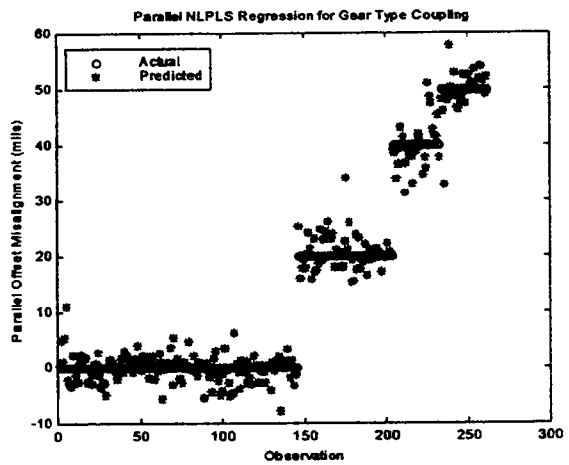


Figure A.125 Training for the reduced parallel offset model.

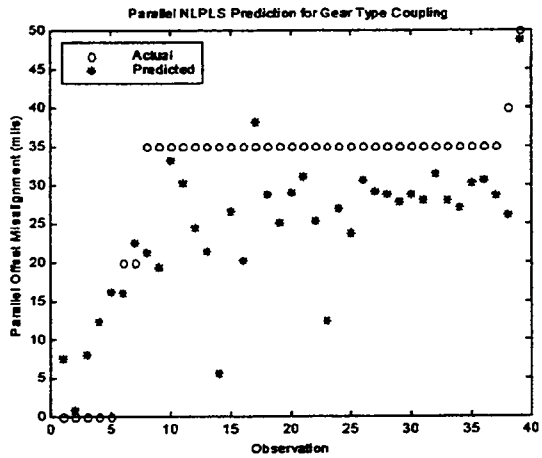


Figure A.126 Prediction for the parallel offset misalignment model.

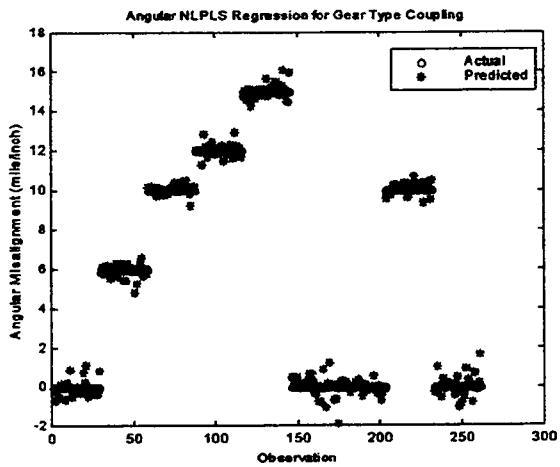


Figure A.127 Training for the angular misalignment model.

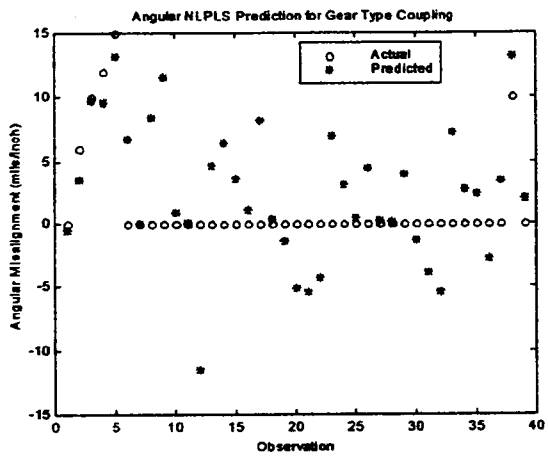


Figure A.128 Prediction for the parallel offset misalignment model.

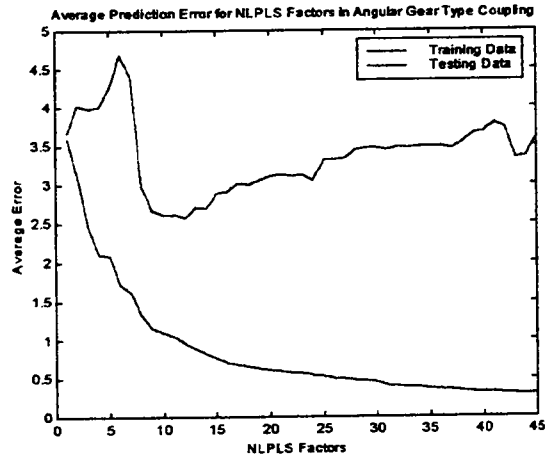


Figure A.129 Prediction error associated with each NLPLS factor.

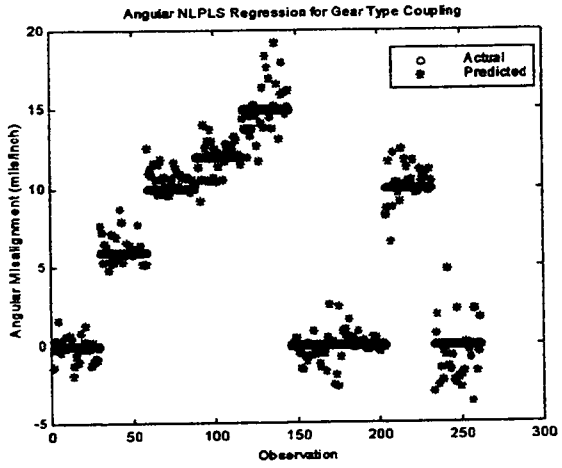


Figure A.130 Training for the reduced angular model.

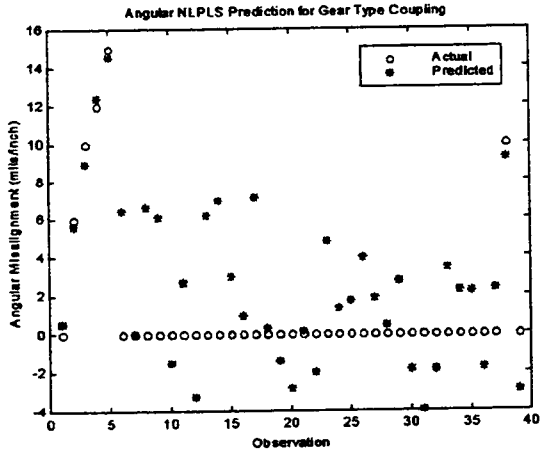


Figure A.131 Prediction for the reduced angular model.

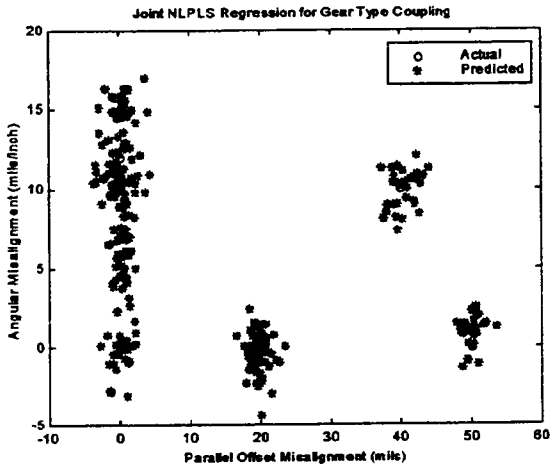


Figure A.132 Training for the joint misalignment model.

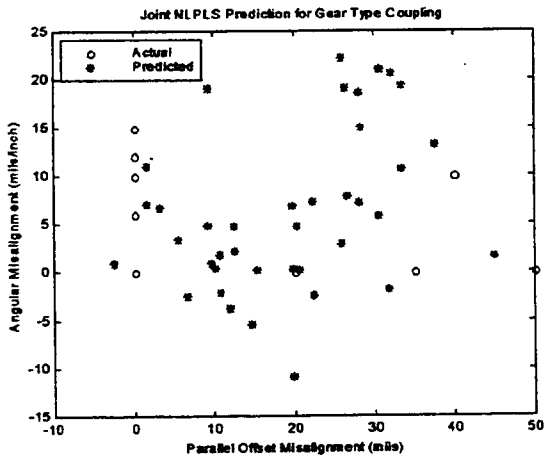


Figure A.133 Prediction for the joint misalignment model.

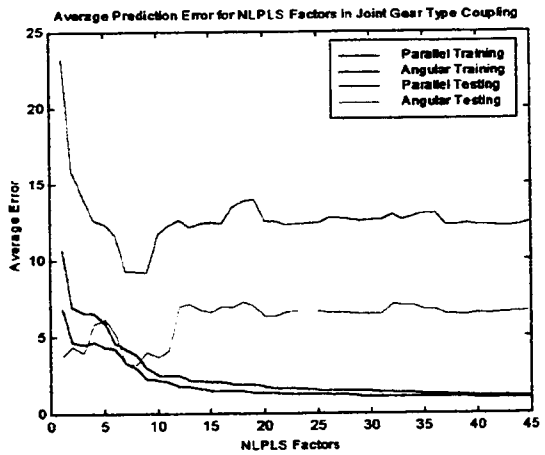


Figure A.134 Prediction error associated with each NLPLS factor.

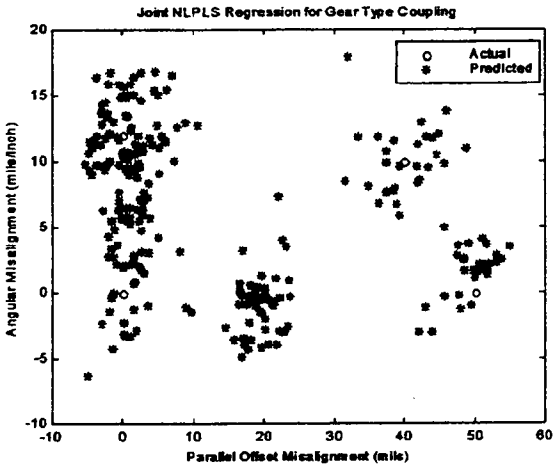


Figure A.135 Training for the reduced joint model.

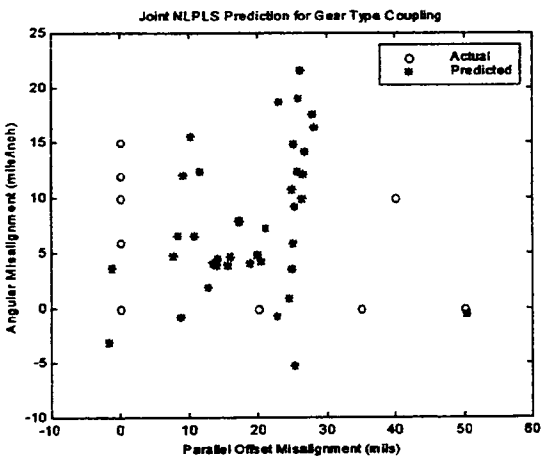


Figure A.136 Prediction for the reduced joint misalignment model.

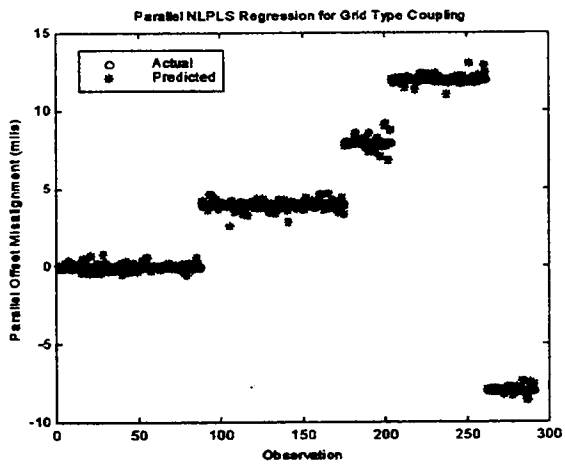


Figure A.137 Training for the parallel offset misalignment model.

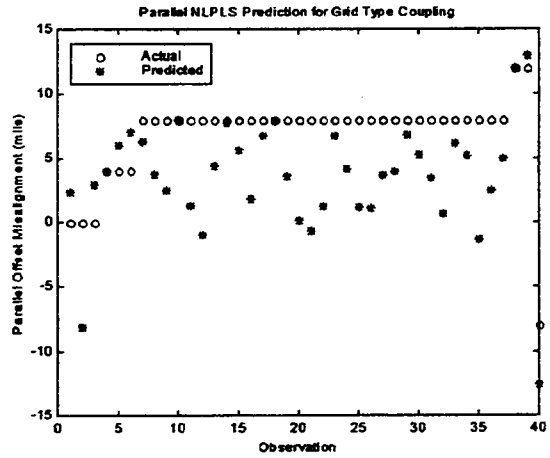


Figure A.138 Prediction for the parallel offset misalignment model.

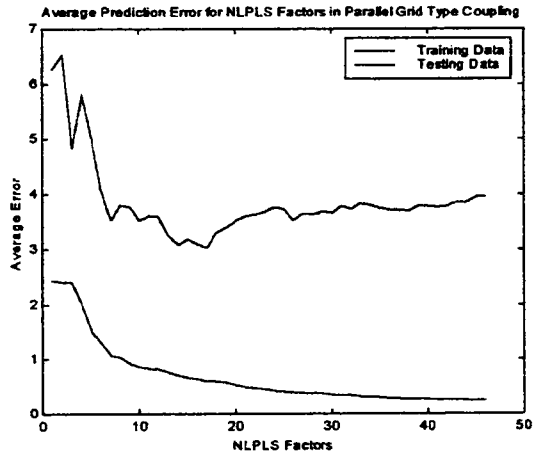


Figure A.139 Prediction error associated with each NLPLS factor.

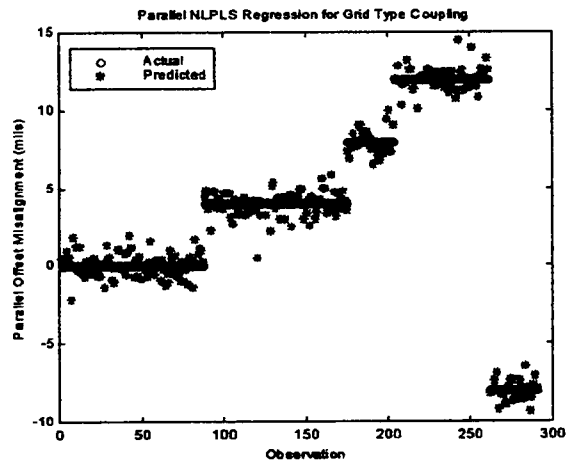


Figure A.140 Training for the reduced parallel offset model.

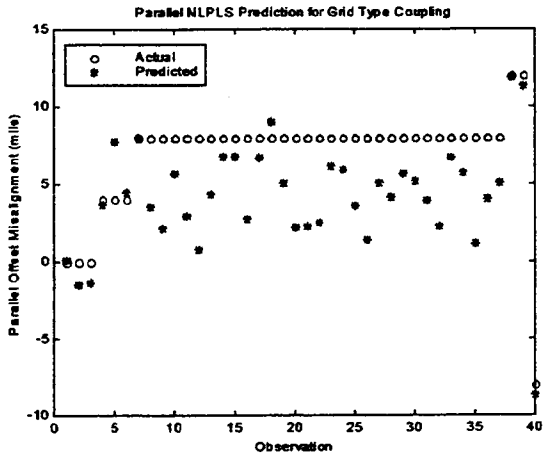


Figure A.141 Prediction for the parallel offset misalignment model.

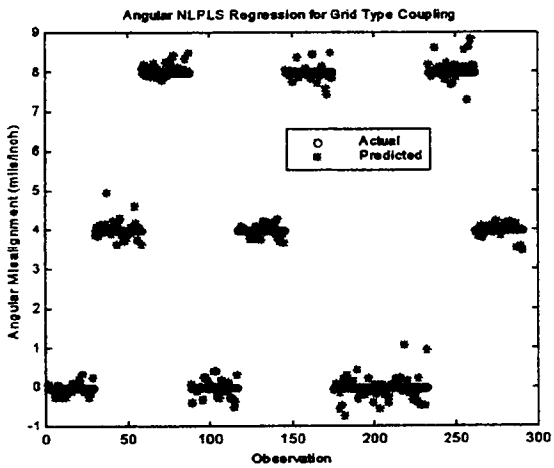


Figure A.142 Training for the angular misalignment model.

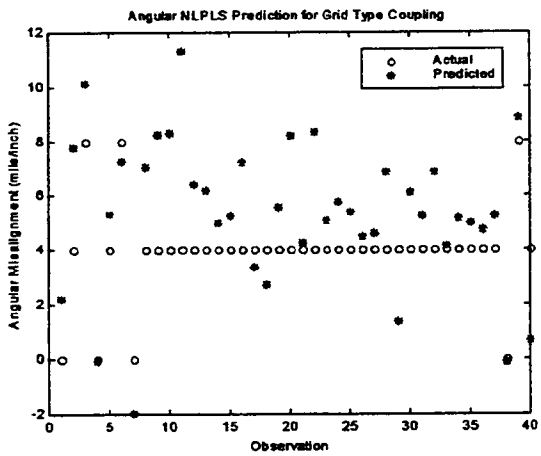


Figure A.143 Prediction for the parallel offset misalignment model.

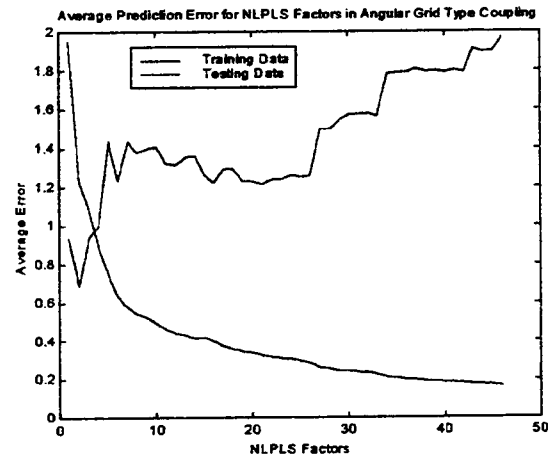


Figure A.144 Prediction error associated with each NLPLS factor.

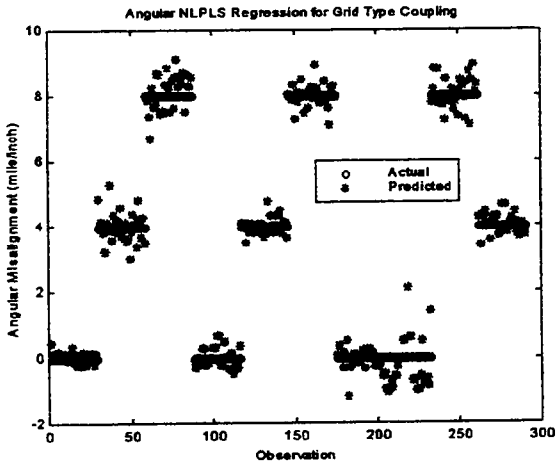


Figure A.145 Training for the reduced angular model.

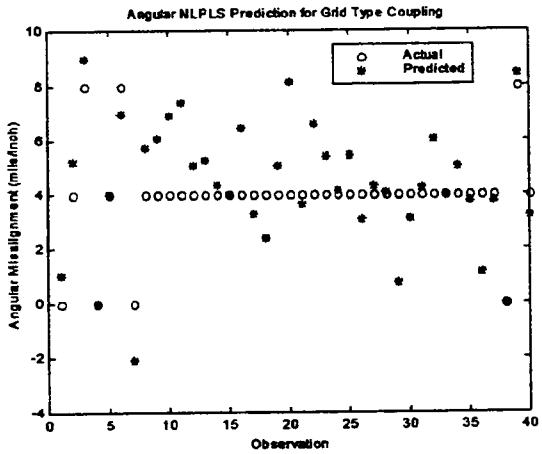


Figure A.146 Prediction for the reduced angular model.

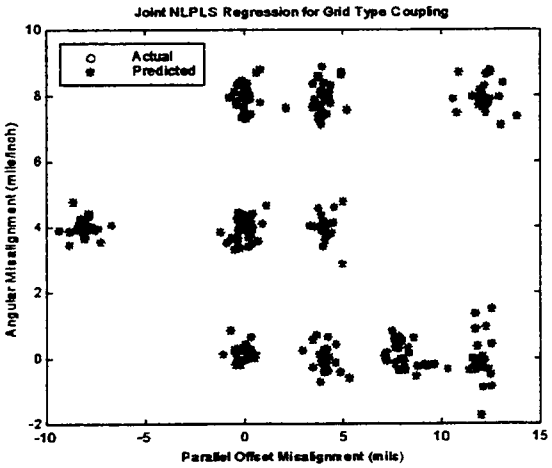


Figure A.147 Training for the joint misalignment model.

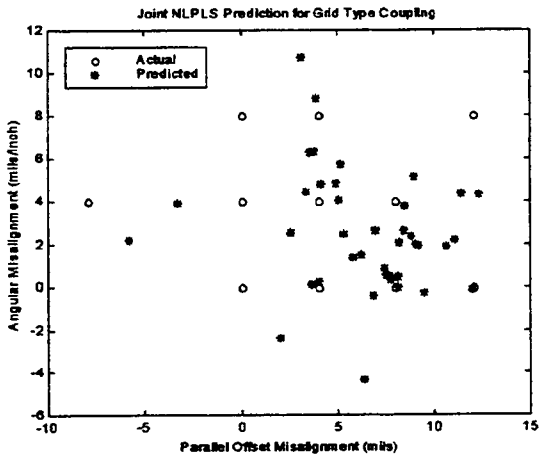


Figure A.148 Prediction for the joint misalignment model.

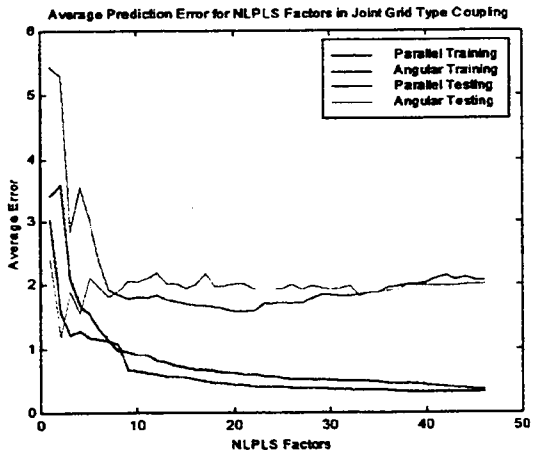


Figure A.149 Prediction error associated with each NLPLS factor.

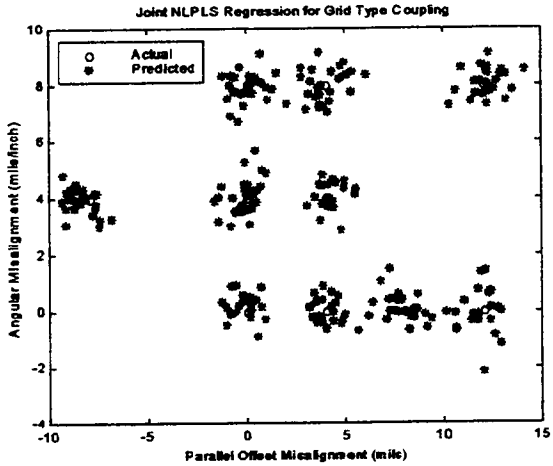


Figure A.150 Training for the reduced joint model.

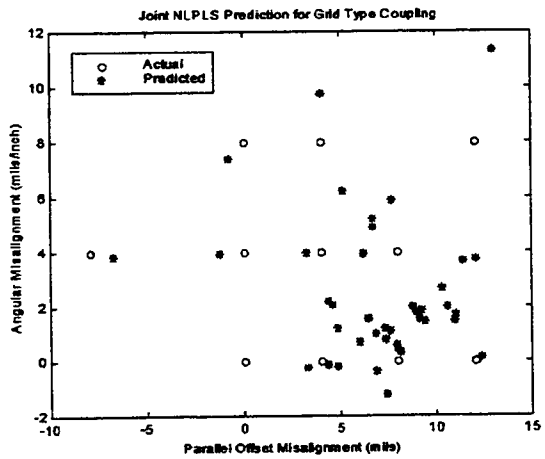


Figure A.151 Prediction for the reduced joint misalignment model.

APPENDIX B

ACTUAL TEST ALIGNMENT CONDITIONS WITH THE PREDICTED ONES.

Reynard

Elastomer Coupling

Actual Par	Actual Ang	MLR Par		LCC Par	LCC Ang	Joint Lcc Par	Joint Lcc Ang	PCA Par
0	0	0.00	0.00	8.31	0.64	14.2296	3.7630	0.31
0	0	0.00	0.00	33.24	1.00	12.5917	4.0759	18.23
0	0	0.00	0.00	32.02	0.64	-11.4864	22.8010	14.17
0	10	0.00	10.00	33.24	27.46	16.5232	17.4603	35.24
0	20	0.00	20.00	31.05	20.83	11.0983	18.4946	15.34
0	30	0.00	30.00	32.21	28.61	16.5229	17.4603	16.32
0	40	0.00	40.00	61.14	28.68	-6.4482	38.4586	33.44
10	0	10.00	0.00	31.87	0.64	54.4259	0.5584	21.91
15	0	15.00	0.00	31.29	0.74	16.5231	17.4602	24.25
20	0	20.00	0.00	10.70	0.64	16.5230	17.4602	5.03
30	0	-18.20	6.69	33.32	0.40	16.5230	17.4594	4.90
30	0	-23.30	12.08	32.96	21.07	16.5058	17.4635	21.91
30	0	-8.69	6.25	32.95	6.90	54.4238	0.5586	17.08
30	0	2.91	-0.29	32.99	0.67	54.4259	0.5584	6.08
30	0	0.23	-2.97	32.90	0.67	54.4259	0.5584	4.97
30	0	-20.75	9.39	33.23	2.18	16.5231	17.4602	7.99
30	0	-13.44	6.47	33.23	1.18	14.2296	3.7630	5.36
30	0	-7.64	3.20	33.23	0.67	14.2296	3.7630	0.60
30	0	-8.98	1.86	33.22	0.67	14.2297	3.7631	-0.24
30	0	-15.99	9.17	32.96	13.75	14.2318	3.7796	19.60
30	0	-10.19	5.90	32.98	2.01	14.2296	3.7630	14.33
30	0	-11.53	4.56	32.93	1.99	14.3856	4.6945	13.22
30	0	-2.89	2.98	32.97	1.10	54.4259	0.5584	11.58
30	0	-4.23	1.64	32.93	1.10	54.4259	0.5584	10.46
30	0	1.57	-1.63	32.95	0.67	54.4259	0.5584	5.04
30	0	-16.73	8.34	33.17	3.21	14.7472	6.8539	11.04
30	0	-12.86	6.16	33.17	1.06	14.2330	3.7829	7.34
30	0	-13.75	5.27	33.16	1.06	16.1064	14.9715	6.63
30	0	-7.99	4.22	33.17	0.84	14.2296	3.7630	5.60
30	0	-8.88	3.32	33.16	0.84	14.2458	3.7617	4.91
30	0	-5.02	1.14	33.16	0.67	36.5691	1.9820	1.68
30	0	-9.69	6.01	32.97	2.98	14.2296	3.7630	15.26
30	0	-10.58	5.12	32.94	2.97	14.2296	3.7630	14.53
30	0	-6.72	2.94	32.96	1.02	14.2296	3.7630	10.81
30	0	-1.85	1.00	32.95	0.82	54.4259	0.5584	8.97
30	0	-11.82	6.18	33.13	1.50	14.2296	3.7630	9.77
30	0	-12.49	5.51	33.12	1.50	14.2299	3.7645	9.22
30	0	-5.93	2.42	33.12	0.76	51.7300	0.7734	5.20
30	0	-7.21	3.77	32.95	1.43	14.2296	3.7630	12.40
30	0	-9.41	4.35	33.10	1.07	14.2296	3.7630	8.58
45	0	45.00	0.00	33.33	18.51	27.3931	18.9012	20.38
45	0	45.00	0.00	32.16	0.64	54.4259	0.5584	43.53
45	25	45.00	25.00	33.29	16.53	16.5231	17.4602	37.36
45	25	45.00	25.00	38.82	26.39	21.6116	20.9499	16.09
60	0	60.00	0.00	36.19	0.85	54.4255	0.5585	11.19
90	0	90.00	0.00	45.24	0.64	54.4259	0.5584	52.99

-45 25 -45.00 25.00 31.42 24.43 -21.1374
10.5068 3.82

Actual		Joint PCA		LPLS		Joint LPLS		NLPLS	
Par	Ang	Par	Ang	Par	Ang	Par	Ang	Par	Ang
0	0	12.7578	14.9556	-4.26	0.27	-0.2709	0.3031	-3.32	4.04
0	0	15.1581	3.3118	-4.89	-0.09	-0.2961	-0.3927	20.96	-3.93
0	0	9.1988	10.5420	-1.50	0.00	-0.0867	0.1051	10.19	1.15
0	10	34.0757	1.8655	2.20	9.99	-0.2196	9.9878	-7.50	8.35
0	20	10.9416	7.0145	-5.80	20.19	0.0443	20.1993	12.47	12.27
0	30	12.7578	14.9556	-4.39	30.26	-0.0769	30.4530	-10.33	16.56
0	40	20.5582	1.2515	-1.15	40.02	0.0851	40.0960	-0.69	41.20
10	0	-0.7597	14.3415	10.89	0.03	10.0554	0.0434	11.62	-1.63
15	0	8.4144	8.0066	14.26	0.06	15.0388	-0.0478	17.59	4.57
20	0	-0.7597	14.3415	20.83	-0.12	20.2439	-0.0838	7.46	0.50
30	0	34.0757	1.8655	-13.93	6.34	-18.1547	6.2788	9.56	16.54
30	0	20.5582	1.2515	-21.66	12.01	-23.0603	12.1885	31.10	2.86
30	0	20.5582	1.2515	-1.13	5.99	-8.2954	6.0802	31.76	-18.02
30	0	9.1990	10.5419	9.69	-0.44	3.4719	-0.2238	21.85	-3.50
30	0	9.1983	10.5422	3.03	-3.16	1.0576	-2.9417	-6.54	-14.54
30	0	34.0757	1.8655	-17.80	9.18	-20.6075	9.2337	35.15	-3.40
30	0	20.5582	1.2515	-7.53	6.17	-13.2251	6.1795	29.51	2.20
30	0	20.5582	1.2515	-2.12	2.95	-7.3414	3.0275	3.09	2.13
30	0	34.0757	1.8655	-5.45	1.59	-8.5486	1.6685	4.45	6.08
30	0	20.5582	1.2515	-11.39	9.00	-15.6779	9.1343	40.49	-6.25
30	0	20.5582	1.2515	-5.99	5.78	-9.7942	5.9824	32.18	-4.69
30	0	20.5582	1.2515	-9.32	4.43	-11.0014	4.6234	10.12	-6.31
30	0	4.8556	3.5929	4.28	2.77	-2.4118	2.9282	26.61	-4.74
30	0	4.8556	3.5929	0.95	1.42	-3.6189	1.5692	2.81	-7.68
30	0	9.1990	10.5419	6.36	-1.80	2.2647	-1.5827	3.86	-7.72
30	0	20.5582	1.2515	-12.24	8.11	-16.5035	8.1825	28.18	-5.09
30	0	20.5582	1.2515	-8.64	5.97	-12.5811	6.0812	5.05	0.89
30	0	20.5582	1.2515	-10.86	5.07	-13.3858	5.1752	4.32	0.24
30	0	20.5582	1.2515	-1.79	3.96	-7.6594	4.0451	5.63	10.26
30	0	20.5582	1.2515	-4.01	3.06	-8.4642	3.1391	3.39	8.65
30	0	20.5582	1.2515	-0.41	0.92	-4.5418	1.0378	-1.13	-0.18
30	0	20.5582	1.2515	-4.37	5.85	-9.2946	6.0150	38.18	-7.68
30	0	20.5582	1.2515	-6.59	4.95	-10.0994	5.1090	35.91	-11.53
30	0	4.8556	3.5929	-2.98	2.80	-6.1770	3.0077	-7.71	-7.85
30	0	4.8607	3.6010	3.86	0.80	-1.2553	0.9716	-8.63	-2.52
30	0	20.5582	1.2515	-6.76	5.97	-11.5096	6.0809	4.91	2.06
30	0	20.5582	1.2515	-8.42	5.30	-12.1132	5.4014	-14.95	7.16
30	0	20.5582	1.2515	-0.59	2.18	-5.4802	2.2984	-10.95	5.34
30	0	4.8556	3.5929	-2.52	3.60	-6.7066	3.7758	31.05	-6.23
30	0	20.5582	1.2515	-4.80	4.15	-8.9962	4.2764	-6.02	4.21
45	0	34.0757	1.8655	36.51	0.00	44.8824	-0.0145	59.30	6.89
45	0	20.5582	1.2515	49.40	0.04	44.9167	0.2453	39.00	1.03
45	25	20.5520	1.2539	46.09	25.13	45.1795	25.2481	27.95	17.02
45	25	12.7578	14.9555	45.64	25.01	44.9412	24.8346	47.82	21.50
60	0	12.7578	14.9556	57.18	-0.06	60.0469	0.0421	-4.89	-3.52
90	0	34.0757	1.8655	89.02	-0.04	90.0256	0.0044	84.36	-0.31

-45	25	-0.7597	14.3415	-43.57	25.05	-45.0461	24.9997	-36.67	24.26

Actual		~~Joint~~ NLPLS		PCA
Par	Ang	Par	Ang	Ang
0	0	-0.4830	-3.0472	1.46
0	0	18.8934	-9.6719	1.47
0	0	9.2290	-1.7780	5.51
0	10	-1.5795	12.8151	16.35
0	20	12.0555	19.3641	12.18
0	30	26.2099	30.5276	31.73
0	40	2.7438	40.2292	33.61
10	0	3.7892	0.6272	1.46
15	0	4.4154	8.9534	1.53
20	0	10.7123	0.8796	1.46
30	0	9.5398	12.4340	1.46
30	0	1.9197	12.8698	17.42
30	0	26.5214	-6.8875	1.47
30	0	8.7231	-4.5808	1.46
30	0	15.7482	-3.2467	1.46
30	0	19.0894	35.5277	5.59
30	0	36.9732	25.9933	1.47
30	0	22.0645	23.9251	1.46
30	0	0.8684	30.6551	1.46
30	0	6.5571	14.3226	13.32
30	0	0.6826	1.8485	1.46
30	0	3.5424	-1.0546	1.46
30	0	9.8908	-5.0416	1.46
30	0	8.0764	-4.7602	1.46
30	0	10.1478	-0.0587	1.46
30	0	41.2982	34.6078	1.51
30	0	38.2703	33.6015	1.46
30	0	30.7289	27.5125	1.46
30	0	31.2849	25.4244	1.46
30	0	28.1420	25.1278	1.46
30	0	17.4468	16.6914	1.46
30	0	9.6467	-1.3937	1.46
30	0	12.5116	-3.4901	1.46
30	0	3.2880	-2.4090	1.46
30	0	4.0575	-2.7670	1.46
30	0	14.4640	24.8929	1.46
30	0	33.4166	28.9971	1.46
30	0	28.1219	19.0284	1.46
30	0	7.3663	-3.2666	1.46
30	0	9.7764	11.7833	1.46
45	0	24.2294	19.8537	8.04
45	0	45.5235	0.1110	12.30
45	25	34.4630	9.4663	17.13
45	25	43.6808	20.4893	33.62
60	0	66.0703	5.8627	16.81
90	0	92.0931	1.0469	1.46
-45	25	-43.9521	23.0646	16.35

Gear Coupling

Actual Par	Actual Ang	MLR Par	MLR Ang	LCC Par	LCC Ang	Joint Lcc Par	Joint Lcc Ang	PCA Par
0	0	0.00	0.00	2.65	0.05	4.4604	1.8410	1.19
0	6	0.00	6.00	2.65	6.71	1.5727	5.5707	1.35
0	10	0.00	10.00	2.65	10.19	8.6642	5.6155	-0.14
0	12	0.00	12.00	2.65	11.99	-0.3604	16.2096	1.20
0	15	0.00	15.00	2.65	15.05	11.6780	7.4418	2.27
20	0	20.00	0.00	37.65	0.05	23.2054	-0.1918	14.81
20	0	20.00	0.00	36.89	1.29	17.5187	1.2091	33.78
35	0	26.96	2.84	38.54	1.30	20.7077	9.2763	35.45
35	0	27.15	4.23	38.54	0.05	35.0423	6.2341	35.45
35	0	25.61	6.23	38.54	0.05	33.2139	-1.2718	32.41
35	0	25.20	7.60	38.54	0.05	32.3004	-0.7074	32.45
35	0	22.35	4.83	35.92	0.05	32.2777	-0.7076	32.45
35	0	27.05	3.54	38.54	0.05	26.8643	6.7611	35.45
35	0	26.28	4.54	38.54	0.06	35.6762	-0.5732	35.44
35	0	26.08	5.22	38.54	0.05	34.5104	-0.5637	32.45
35	0	24.65	3.84	38.54	0.07	31.8672	-0.4445	32.45
35	0	26.38	5.23	38.54	0.05	37.7347	-0.4901	35.44
35	0	26.17	5.91	38.54	0.05	37.6632	-0.4931	32.45
35	0	24.75	4.53	38.54	0.05	32.2777	-0.7081	32.45
35	0	25.40	6.91	38.54	0.05	32.3107	-0.7069	32.44
35	0	23.98	5.53	38.54	0.05	32.2775	-0.7081	32.45
35	0	23.77	6.22	38.54	0.05	32.2774	-0.7081	32.45
35	0	26.57	4.43	38.54	0.05	37.8168	-0.4740	35.45
35	0	26.44	4.89	38.54	0.05	37.8040	-0.4859	35.45
35	0	25.49	3.97	38.54	0.05	32.3270	-0.7051	32.55
35	0	25.92	5.56	38.54	0.05	33.2756	-0.6681	32.45
35	0	24.97	4.64	38.54	0.05	32.2772	-0.7080	32.45
35	0	24.84	5.09	38.54	0.05	32.2481	-0.7070	32.45
35	0	25.99	6.02	38.54	0.05	35.7221	-0.5704	32.45
35	0	25.03	5.10	38.54	0.05	32.2790	-0.7080	32.45
35	0	24.90	5.55	38.54	0.05	32.2787	-0.7080	32.45
35	0	24.38	6.22	38.54	0.05	32.2775	-0.7081	32.45
35	0	26.23	5.23	38.54	0.05	37.0822	-0.5160	35.45
35	0	25.52	4.53	38.54	0.05	32.3268	-0.7061	32.45
35	0	25.03	5.38	38.54	0.05	32.2780	-0.7081	32.45
35	0	25.08	5.72	38.54	0.05	32.2805	-0.7080	32.45
35	0	25.45	5.15	38.54	0.05	32.3200	-0.7064	32.45
40	10	40.00	10.00	38.54	10.13	38.2631	9.9869	35.42
50	0	50.00	0.00	38.54	0.05	34.2894	-1.1862	33.78

Actual Par	Actual Ang	Joint PCA Par	Joint PCA Ang	LPLS Par	LPLS Ang	Joint LPLS Par	Joint LPLS Ang	NLPLS Par	NLPLS Ang
0	0	1.9074	8.0844	0.77	3.52	-0.0000	-0.0000	7.62	0.55
0	6	11.0617	11.9161	-0.46	6.14	0.0000	6.0000	0.88	5.61
0	10	-9.8210	12.3977	0.03	12.24	-0.0000	10.0000	7.99	8.99
0	12	1.9052	8.0837	0.61	11.50	0.0000	12.0000	12.36	12.38
0	15	11.1143	11.9332	-0.11	11.34	0.0000	15.0000	16.17	14.53
20	0	17.7541	-2.1698	20.79	-9.36	20.0000	-0.0000	16.04	6.42

20	0	33.3393	2.2680	21.66	-0.36	20.0000	-0.0000	22.55	0.02
35	0	5.0908	9.9739	25.35	0.00	26.9612	2.8435	21.40	6.63
35	0	11.4857	11.2375	26.03	3.11	27.1484	4.2302	19.34	6.11
35	0	17.7375	-2.8443	24.84	4.93	25.6066	6.2293	33.15	-1.49
35	0	17.7375	-2.8443	25.79	-0.76	25.1999	7.5990	30.28	2.70
35	0	17.7375	-2.8443	22.65	-2.19	22.3478	4.8336	24.55	-3.28
35	0	5.0908	9.9739	25.69	1.55	27.0548	3.5368	21.48	6.22
35	0	33.3393	2.2680	25.09	2.47	26.2839	4.5364	5.62	6.96
35	0	39.0443	-4.0046	25.57	-0.38	26.0805	5.2212	26.58	2.99
35	0	17.7375	-2.8443	24.00	-1.10	24.6545	3.8385	20.22	0.94
35	0	33.3393	2.2680	25.43	4.02	26.3775	5.2297	38.18	7.12
35	0	17.7375	-2.8443	25.91	1.18	26.1741	5.9146	28.72	0.32
35	0	17.7375	-2.8443	24.34	0.46	24.7481	4.5319	25.07	-1.43
35	0	17.7375	-2.8443	25.31	2.09	25.4032	6.9141	29.00	-2.84
35	0	17.7375	-2.8443	23.74	1.37	23.9772	5.5314	31.08	0.13
35	0	17.7375	-2.8443	24.22	-1.48	23.7739	6.2163	25.33	-2.02
35	0	33.3393	2.2680	25.41	2.68	26.5721	4.4343	12.42	4.84
35	0	39.0443	-4.0046	25.72	0.78	26.4365	4.8909	26.95	1.34
35	0	39.0443	-4.0046	24.68	0.30	25.4858	3.9691	23.74	1.70
35	0	17.7375	-2.8443	25.32	1.39	25.9226	5.5573	30.64	3.94
35	0	17.7375	-2.8443	24.28	0.91	24.9719	4.6355	29.10	1.86
35	0	17.7375	-2.8443	24.60	-0.98	24.8363	5.0920	28.75	0.44
35	0	17.7375	-2.8443	25.55	2.43	25.9850	6.0195	27.86	2.75
35	0	17.7375	-2.8443	24.51	1.95	25.0343	5.0977	28.82	-1.87
35	0	17.7375	-2.8443	24.83	0.05	24.8987	5.5542	28.03	-3.96
35	0	17.7375	-2.8443	24.43	0.66	24.3848	6.2206	31.48	-1.84
35	0	39.0443	-4.0046	25.50	1.82	26.2290	5.2255	27.99	3.41
35	0	39.0443	-4.0046	24.72	1.46	25.5160	4.5341	27.07	2.25
35	0	17.7375	-2.8443	24.66	0.50	25.0289	5.3763	30.25	2.19
35	0	17.7375	-2.8443	24.83	1.27	25.0757	5.7230	30.62	-1.74
35	0	17.7375	-2.8443	24.93	1.02	25.4528	5.1471	28.63	2.32
40	10	11.4839	11.2371	41.14	12.05	40.0000	10.0000	26.15	9.27
50	0	39.3120	4.2108	50.08	-0.09	50.0000	0.0000	48.84	-2.92

Actual		Joint NLPLS		PCA
Par	Ang	Par	Ang	Ang
0	0	-4.64		3.13
0	6	-1.1832	3.6830	3.10
0	10	11.5624	12.3514	10.55
0	12	9.0864	12.0272	12.07
0	15	10.2452	15.5424	12.29
20	0	19.9287	4.8520	0.15
20	0	18.8618	4.0702	1.06
35	0	14.0999	4.4840	0.82
35	0	22.6726	-0.6989	2.76
35	0	8.2796	6.5859	0.16
35	0	27.7819	17.5827	0.15
35	0	22.9882	18.7128	0.15
35	0	25.2173	-5.1900	0.87
35	0	13.9896	3.9507	0.73
35	0	24.8990	10.7659	0.51

35	0	25.6530	12.3924	0.43
35	0	20.3743	4.2850	0.26
35	0	24.8056	3.5975	0.16
35	0	24.5280	0.9547	0.15
35	0	26.4326	12.1211	0.15
35	0	26.7132	14.1626	0.15
35	0	26.1192	21.5572	0.15
35	0	13.4451	4.0520	0.73
35	0	10.6714	6.5686	0.55
35	0	12.7084	1.9194	0.51
35	0	17.2481	7.9258	0.26
35	0	17.2632	7.8440	0.23
35	0	25.1730	14.8480	0.17
35	0	7.6623	4.8039	0.16
35	0	8.7393	-0.7890	0.15
35	0	28.1454	16.4184	0.15
35	0	25.8735	19.0580	0.15
35	0	15.5302	3.9362	0.34
35	0	15.9411	4.7200	0.31
35	0	25.2371	9.2355	0.16
35	0	25.0491	5.8593	0.15
35	0	21.0512	7.2078	0.19
40	10	26.3991	9.9161	10.92
50	0	50.2853	-0.5273	9.66

Dodge Grid Coupling

Actual		MLR		LCC		Joint Lcc		PCA
Par	Ang	Par	Ang	Par	Ang	Par	Ang	Par
0	0 ✓	0.00	0.00	3.00	1.47	0.9254	0.7493	4.72
0	4 ✓	0.00	4.00	-3.85	3.08	5.4026	3.3561	-0.90
0	8 ✓	0.00	8.00	1.56	7.71	-1.1936	5.7144	1.82
4	0 ✓	4.00	0.00	2.63	1.05	3.5511	0.0534	5.97
4	4 ✓	4.00	4.00	4.99	5.63	4.0563	2.6758	4.76
4	8 ✓	4.00	8.00	4.71	7.81	6.0584	7.8624	5.78
8	0 ✓	8.00	0.00	6.83	0.68	7.4938	0.0735	7.79
8	4 ✓	6.53	4.43	1.22	3.85	5.9782	6.0825	7.74
8	4	5.31	4.91	9.98	3.85	4.9698	5.1920	4.71
8	4	3.23	5.29	7.82	3.85	7.9016	6.1896	4.73
8	4	1.55	5.86	3.69	3.85	-1.2938	4.7425	4.73
8	4	3.14	5.71	7.32	3.08	2.9086	6.3341	4.73
8	4	5.92	4.67	5.67	3.85	4.2889	4.9808	4.70
8	4	4.88	4.86	4.50	3.85	6.3086	6.2532	4.71
8	4	4.04	5.15	2.83	3.85	3.6940	5.1289	4.72
8	4	4.84	5.07	4.77	3.85	5.0844	6.2740	4.72
8	4	4.27	5.10	9.34	3.85	5.7572	5.3021	4.72
8	4	3.43	5.39	6.98	3.85	4.8415	5.6723	4.72
8	4	4.23	5.31	9.28	3.85	5.4075	5.7592	4.72
8	4	2.39	5.57	5.51	3.85	4.7403	5.2043	4.73
8	4	3.19	5.50	7.60	3.85	6.2659	6.1491	4.73
8	4	2.35	5.79	5.45	3.85	0.8319	5.6329	4.73
8	4	5.03	4.88	6.62	3.85	5.0019	5.4310	4.71

8	4	4.47	5.07	4.91	3.85	4.2161	5.2695	4.71
8	4	5.00	5.02	6.63	3.85	4.9700	5.8998	4.72
8	4	3.77	5.19	4.38	3.85	4.5055	5.2209	4.72
8	4	4.30	5.14	5.76	3.85	5.8134	6.1041	4.72
8	4	3.74	5.34	4.54	3.85	4.1669	6.0287	4.72
8	4	3.37	5.35	7.31	3.85	5.4218	5.4342	4.72
8	4	3.90	5.30	8.85	3.85	6.1453	5.9544	4.72
8	4	3.33	5.50	7.19	3.85	4.5716	5.8712	4.72
8	4	2.64	5.62	6.15	3.85	4.6686	5.8130	4.73
8	4	4.16	5.12	5.74	3.85	4.5931	5.2434	4.72
8	4	4.56	5.09	7.01	3.85	5.3943	5.8092	4.72
8	4	3.62	5.32	5.26	3.85	5.0854	5.8115	4.72
8	4	3.31	5.44	7.37	3.85	5.5660	5.9092	4.72
8	4	3.95	5.24	6.21	3.85	5.1700	5.7639	4.72
12	0	12.00	0.00	10.22	0.62	9.4791	-1.1484	8.03
12	8	12.00	8.00	10.87	7.78	12.5000	8.7094	8.58
-8	4	-8.00	4.00	-7.48	3.87	-5.7271	3.5261	0.52

Actual		Joint PCA		LPLS		Joint LPLS		NLPLS	
Par	Ang	Par	Ang	Par	Ang	Par	Ang	Par	Ang
0	0	3.0393	-0.6513	-0.54	0.24	-0.7088	0.0194	0.10	1.03
0	4	-0.3746	4.9915	-0.35	3.53	-0.7458	3.3253	-1.49	5.25
0	8	-0.4127	6.0780	0.07	8.11	0.6186	7.6276	-1.33	8.98
4	0	3.0010	0.4419	3.89	0.03	4.5141	0.2445	3.68	0.00
4	4	-1.2139	1.9134	4.44	3.68	4.2307	3.4457	7.74	3.99
4	8	8.5131	5.6133	3.71	7.99	3.5989	7.8925	4.47	6.97
8	0	3.0252	-0.2464	7.80	0.37	7.7218	0.9385	8.01	-2.10
8	4	4.2982	7.0847	6.74	4.41	6.1370	4.8302	3.52	5.72
8	4	4.2969	7.0803	5.55	4.96	5.2891	5.5776	2.11	6.06
8	4	3.4586	4.0133	3.53	5.02	3.4666	4.9504	5.68	6.90
8	4	3.3605	3.9692	1.99	5.49	2.3319	5.1976	2.95	7.38
8	4	3.4586	4.0133	3.48	5.56	4.2599	5.1660	0.78	5.07
8	4	4.2981	7.0845	6.14	4.68	5.7131	5.2039	4.31	5.29
8	4	3.5064	4.1882	5.14	4.71	4.8018	4.8903	6.74	4.32
8	4	3.4661	4.0408	4.36	4.95	4.2345	5.0139	6.78	3.99
8	4	3.6515	4.7190	5.11	4.98	5.1985	4.9981	2.76	6.45
8	4	3.4610	4.0221	4.54	4.99	4.3778	5.2640	6.71	3.27
8	4	3.4590	4.0146	3.77	5.22	3.8105	5.3876	9.05	2.39
8	4	3.4704	4.0565	4.52	5.26	4.7745	5.3718	5.08	5.07
8	4	3.4582	4.0131	2.76	5.25	2.8993	5.0740	2.22	8.11
8	4	3.4586	4.0133	3.51	5.29	3.8632	5.0582	2.23	3.66
8	4	3.4586	4.0133	2.73	5.52	3.2959	5.1818	2.48	6.60
8	4	3.9421	5.7820	5.27	4.80	4.9642	5.1194	6.17	5.43
8	4	3.6912	4.8644	4.76	4.95	4.5860	5.2018	5.92	4.13
8	4	4.1281	6.4627	5.26	4.97	5.2287	5.1913	3.57	5.47
8	4	3.4587	4.0136	4.09	4.97	3.9785	4.9927	1.43	3.09
8	4	3.4595	4.0164	4.58	4.99	4.6212	4.9822	5.07	4.31
8	4	3.4588	4.0142	4.07	5.15	4.2430	5.0646	4.13	4.05
8	4	3.4586	4.0133	3.69	5.15	3.6959	5.2419	5.69	0.73
8	4	3.4587	4.0137	4.19	5.18	4.3385	5.2313	5.21	3.11
8	4	3.4586	4.0134	3.67	5.33	3.9603	5.3137	3.92	4.24

8	4	3.4586	4.0133	3.00	5.35	3.3528	5.1047	2.23	6.05
8	4	3.4629	4.0289	4.45	4.97	4.3062	5.1390	6.74	4.00
8	4	3.4825	4.1009	4.83	4.99	4.7882	5.1310	5.70	5.04
8	4	3.4586	4.0133	3.94	5.12	4.0489	5.0360	1.17	3.76
8	4	3.4586	4.0133	3.64	5.25	3.8369	5.2229	4.05	1.11
8	4	3.4592	4.0155	4.26	5.09	4.2969	5.1444	5.05	3.74
12	0	7.6752	2.5480	11.83	-0.05	12.0970	-0.5267	11.87	-0.01
12	8	8.5508	4.5374	12.10	8.13	12.6260	8.7216	11.32	8.43
-8	4	-0.3747	4.9951	-7.67	4.18	-7.5523	4.3130	-8.67	3.20

Actual		Joint NLPLS		PCA
Par	Ang	Par	Ang	Ang
0	0	4.3104	-0.1379	-2.18
0	4	-1.2459	3.9264	6.05
0	8	-0.7557	7.3733	2.25
4	0	3.2893	-0.2145	2.57
4	4	3.2038	3.9788	1.70
4	8	3.9701	9.7530	6.01
8	0	4.8712	-0.1870	-1.95
8	4	6.6799	4.8877	3.41
8	4	7.7119	5.8796	5.28
8	4	4.8453	1.1933	5.85
8	4	4.3538	2.1964	5.84
8	4	7.3845	-1.2247	5.25
8	4	5.1576	6.2369	4.55
8	4	10.2863	2.6724	5.26
8	4	9.2329	1.8617	5.24
8	4	6.1804	3.9362	4.52
8	4	9.1334	1.5605	5.66
8	4	10.9861	1.7371	5.65
8	4	10.9376	1.4726	5.27
8	4	4.5536	2.0623	5.85
8	4	6.8406	1.0078	5.66
8	4	6.0158	0.7083	5.65
8	4	11.3994	3.6826	5.27
8	4	12.0664	3.7317	5.25
8	4	6.6750	5.2179	4.82
8	4	7.3081	1.2034	5.55
8	4	9.4423	1.4529	5.26
8	4	7.9764	0.4646	5.25
8	4	8.7392	1.9827	5.74
8	4	7.3588	0.8097	5.56
8	4	7.9273	0.5977	5.55
8	4	6.4353	1.5363	5.73
8	4	8.9328	1.7981	5.49
8	4	10.5883	1.9894	5.27
8	4	6.8577	-0.3611	5.49
8	4	8.1449	0.3287	5.66
8	4	7.5800	1.0939	5.45
12	0	12.3334	0.1449	-2.18
12	-8	12.9922	11.3195	5.99

APPENDIX C

NON-LINEAR PARTIAL LEAST SQUARES MATLAB SCRIPTS

```
function [p,q,w,b,t,u,x,y] = nlpls(a,c,maxrank);
% nlpls.m
% Non Linear Partial Least Squares in latent variables.
%   Uses the Matlab's SVD routine on the smallest
%   covariance matrix for computational efficiency.
%  Calls the function plsnet to determine the
%  PLS Factor's Relationships.
%
%   [P, Q, W, B] = PLS(A, C, MAXRANK)    or,
%
%   [P, Q, W, B, T, U, X, Y] = PLS(A, C, MAXRANK)
%
%   Where:
%
%   P       is the matrix of spectral factors
%   Q       is the matrix of concentration factors
%   W       is the matrix of weights
%   B       is the vector containing ANN Architectures
%   T       is the matrix of spectral scores
%   U       is the matrix of concentration scores
%   X       is the matrix of spectral residuals
%   Y       is the matrix of concentration residuals
%   A       is the training set absorbance matrix
%   C       is the training set concentration matrix
%   MAXRANK  is optional limit to the number of factors calculated
%
% By: Dax Jolly
%     University of Tennessee, Knoxville
%     Department of Nuclear Engineering
%     July 22, 1998
%
[m,n] = size(a);
[m,l] = size(c);
if nargin == 3
  i = min([n, m, maxrank]);
else
  i = min([n m]);
end
%
x = a;
y = c;
%
% First run
%
xy = x' * y;
[pt,s,qt] = svd(xy'*xy,0);
q(1,:) = qt(:,1)';
w(:,1) = (xy * qt(:,1)) / sqrt(s(1,1));
t(:,1) = x * w(:,1);
tsqr = t(:,1)' * t(:,1);
```

```
u(:,1) = y * qt(:,1);
p(1,:) = t(:,1)' * x / tsqr;
b = plsnet(t(:,1),u(:,1));
x = x - (t(:,1) * p(1,:));
y = y - (sim(b,t(:,1)')' * q(1,:));
for h = 2:i,
  xy = x' * y;
  [pt,s,qt] = svd(xy'*xy,0);
  q(h,:) = qt(:,1)';
  w(:,h) = (xy * qt(:,1)) / sqrt(s(1,1));
  t(:,h) = x * w(:,h);
  tsqr = t(:,h)' * t(:,h);
  u(:,h) = y * qt(:,1);
  p(h,:) = t(:,h)' * x / tsqr;
  eval([sprintf('b%0.0f=plsnet(t(:,h),u(:,h));',h)]);
  b = [b eval([sprintf('b%0.0f',h)])];
  x = x - (t(:,h) * p(h,:));
  up=sim(b(h),t(:,h)');
  y = y - (up'*q(h,:));

end

function [net] = plsnet(xn,yn);
% plsnet.m
%
% This function takes the inner relationship
%   in a LPLS model and fits an ANN to it.
%
% xn    is the vextor of spectral scores
% yn    is the matrix of concentration scores
% net   is the network model for the PLS factor
%
% By: Dax Jolly
%   University of Tennessee, Knoxville
%   Department of Nuclear Engineering
%   July 22, 1998
%
F1 = 'tansig';                  % Tansig hidden neurons
F2 = 'purelin';             % Linear output neurons
numhid=3;                       % Three hidden neurons
[nov1, numin] = size(xn);
[nov2,numout] = size(yn);
net=newff(minmax(xn'),[numhid numout] ,{F1 F2},'trainlm');
net.trainParam.goal   = .01; % Mean Square Error Goal;
net.trainParam.show   = 100;     % Errors not plotted;
net.trainParam.epochs = 10;   % 100 Training Epochs;
net=train(net,xn',yn');
% End
function [c,x] = nlplsprd(a,p,q,w,b,n,amean,cmean,ascal,cscal);
% nlplsprd.m
```

```
% Predicts unknown concentrations using NLPLS.
%
%  c  is the matrix of the unknown's concentrations
%  x  is the matrix of spectral residuals after decomposition
%  a  is the unknown spectrum (or spectra)
%  p  is the matrix of spectral factors
%  q  is the matrix of concentration factors
%  w  is the matrix of weights
%  b  is the vector containing the network architectures
%  n  is the number of factors to use
%
%  optional arguments:
%
%  amean   vector of means of mean-centered calibration spectra
%  cmean   vector of means of mean-centered calibration concentrations
%  ascal   vector of scaling factors of scaled calibration spectra
%  scal    vector of scaling factors of scaled calibration concentrations
%
%  Specify 0 for amean, cmean, ascal, cscal if no scaling or centering
%
% By: Dax Jolly
%    University of Tennessee, Knoxville
%    Department of Nuclear Engineering
%    July 22, 1998
%
[maxrank, h] = size(p);
if nargin > 5
  maxrank = min([n, maxrank]);
end
c=0;
[j, i] = size(a);
if nargin > 6
    if amean ~= 0
        a = a - amean * ones(1, j);
    end
    if nargin > 8
        if ascal ~= 0
            a = a ./ (ascal * ones(1, j));
        end
    end
end

x = a;
for h=1:maxrank
    t(:,h) = x * w(:,h);
  x = x - t(:,h) * p(h,:);
  c = c + (sim(b(h),t(:,h)')' * q(h,:));
end

[l, k] = size(c);
```

```
if nargin > 9
    if cscal ~= 0
        c = c .* (cscal * ones(1,l));
    end
end

if nargin > 7
    if cmean ~=0
        c = c + cmean * ones(1,l);
    end
end
```

VITA

Dax D. Jolly was born in Clarksville, Tennessee on May 11, 1972. He received an Honors Diploma from The Clarksville Academy in Clarksville Tennessee in May 1990. The following August he entered the Architecture program at the University of Tennessee, Knoxville on an Alumni Memorial Scholarship. After two years he decided to change majors and entered the Nuclear Engineering program at the University of Tennessee. After a one and a half-year break in 1995 to 1996 Dax received a Bachelor of Science Degree in Nuclear Engineering in May 1997.

In August 1997 Dax accepted a Graduate Research Assistantship from the University of Tennessee, Knoxville Department of Nuclear Engineering to work in the application of Advanced Maintenance and Reliability Technology and began study towards a Master of Science Degree in Nuclear Engineering. Dax's studies and thesis were finished in August 1998. This degree is to be awarded in December 1998 with the University of Tennessee Maintenance and Reliability Center Certification.

Dax is planning to work in the Nuclear Industry and the Maintenance and Reliability Field using his education to broaden his technical experience.